Implementation of a high throughput screening assay to identify and characterize insecticides acting on ion channels

Dissertation

zur

Erlangung des Doktorgrades (Dr. rer. nat.)

der

Mathematisch-Naturwissenschaftlichen Fakultät

der

Rheinischen Friedrich-Wilhelms-Universität Bonn

vorgelegt von

Andreas Brockmann

aus

Bergheim

Bonn 2023

Angefertigt mit Genehmigung der Mathematisch-Naturwissenschaftlichen Fakultät
der Rheinischen Friedrich-Wilhelms-Universität Bonn und der Bayer AG

Gutachter*in: PD Dr. Anke Schiedel
Gutachter*in: Prof. Dr. Gerd Bendas

Tag der Promotion: 23.08.2023
Erscheinungsjahr: 2023

The presented work was carried out from September 2019 to March 2023 in cooperation between the Pharmaceutical Institute of the Rheinische Friedrichs Wilhelms Universität Bonn and the Bayer AG in Monheim under the direction and supervision of PD. Dr. Anke Schiedel (University Bonn) and Dr. Ulrich Ebbinghaus-Kintscher. (Bayer AG)

Agenda

1. Abstract

With 800 million people suffering from hunger, new innovative crop protection products are required to ensure food supply and stop hunger.

The voltage-sensitive sodium channel (VSSC) was shown to be a safe and effective insecticidal target in over 40 years of intensive use of pyrethroids. Arising pyrethroid-resistances, however, require the development of new resistance-breaking VSSC modulators. For this purpose, a new high throughput screening assay was developed to screen over 1.000.000 compounds. Channelrhodopsin 2 (ChR2), a light-activated ion channel, was implemented to activate the sodium channel. Optimizing light pulse protocols facilitated the identification of weak and state-dependent modulators.

After performing the screen, the potential hits were biochemically characterized. Automated patch clamp technology was used to validate 2000 potential HTS hits. A tailor-made pulse protocol enabled the detection of true VSSC modulators. Subsequently, purified hits and close analogs were characterized using fluorescent and electrophysiological readouts. Two different cell lines were used to identify resistance-breaking potential and selectivity to one human analog. An injection assay monitored potential *in vivo* efficacy on pest-relevant caterpillars (*Spodoptera frugiperda*). Finally, one hit class was found, showing the following required properties: high selectivity towards the human channel $Na_V1.7$, resistance-breaking potential and already strong intrinsic *in vivo* efficacy. Chemical optimization of the hit has started and delivered plausible structure-activity relationships. The *in vitro* activity was thereby matching the *in vivo* activity.

In this thesis, mutagenesis studies were implemented to identify the binding site of a new insect-selective VSSC modulator. A couple of different mutations were created to gain a loss of sensitivity towards the modulator by humanizing the insect VSSC. A significant reduction in the response of the compound was observed, narrowing down the binding site to a small area. Further experiments must be performed to elucidate the binding site.

In the last part of my thesis, the exact binding site of two different Slo-channel modulators was identified in cooperation between the Max Planck Institute Dortmund and Bayer. With the data this thesis provides, we were able to characterize the electrophysiological behavior of emodepside and verruculogen. The resolved cryo-EM structure helped to understand their mechanism of action and explained the interaction between both compounds. Through further mutagenesis studies performed at the Slo channel, we gained more profound insights into the mode of action of verruculogen and highlighted the importance of the gating threonine for the Slo channel.

2. Introduction

2.1 Crop protection and insecticide market

In the last 50 years, the worldwide population almost doubled, while the area used for farming remained stable. Therefore, the efficiency of agriculture had to increase strongly.[1,2] According to Oerke, 35 % of the global crop yield is lost to pests even before harvest, with additional losses during storage.[3,4] The application of innovative crop protection products could help to counteract this trend.[5] Pesticide use worldwide has increased 15 – 20 fold over the last years, showing the market potential of sustainable crop protection products.[3,5] The market value of insecticides in 2022 was 9.12 billion, indicating the market potential of new blockbuster products.[6]

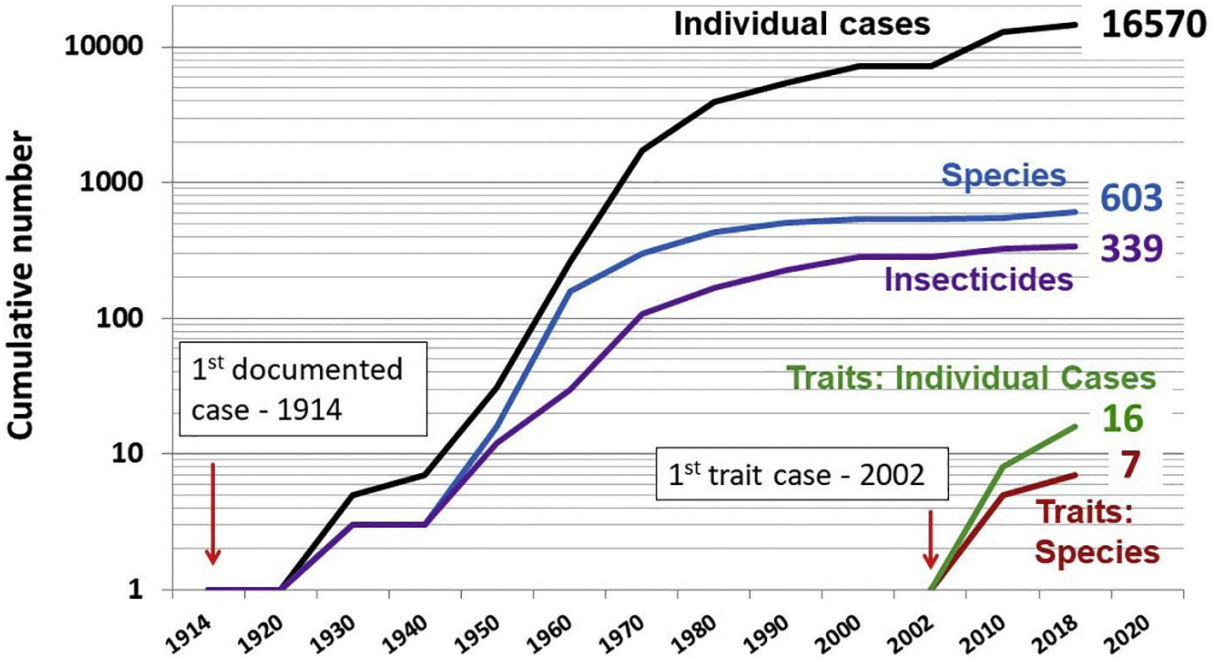

Figure 1 - Development of resistances over the last century[7]

The rising occurrence of insecticide resistance is one of the main reasons for developing new insecticides.[8] In Figure 1 development of resistances among crop protection products is shown for different branches.[8] Insecticidal resistance was first reported by Melander in 2014 to lime sulfur.[9] Since the first application of synthetic insecticides in the 1940s, the number of resistances raised rapidly due to intensive and uncontrolled use. As a response, the insecticides resistance action committee (IRAC) was founded by several agrochemical companies, including Bayer, to monitor resistance and suggest how to use the different agents and modes of actions (MoAs) responsibly. [7,8] Modern crop protection products require a fast response time between application and effect.[10]

Especially insecticides addressing neurological targets have been proven to cause rapid responses due to their devastating effects on the insects' nervous system. The response times mainly depend on the immediate responses of ion channels, leading to fast protection against the crop being eaten.[8] In Figure 2, the market share among the different modes of action (MoA) is shown. It depicts the relevance of neurological targets and in particular ion channels. Seventeen percent of the market share comprises pyrethroids and VSSC blockers (indoxacarb), showing the importance of the voltage-sensitive sodium channel (VSSC) as target.

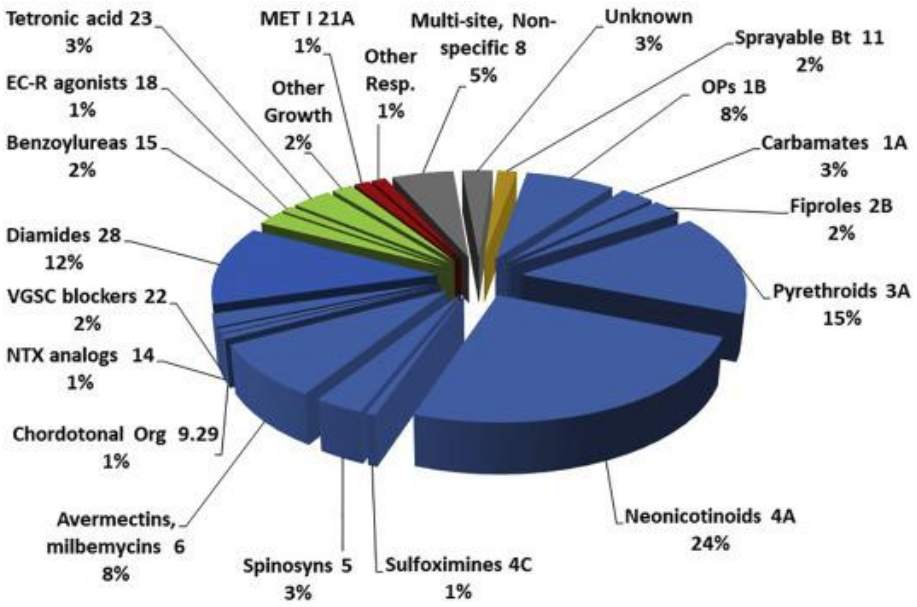

Figure 2 - Market share of MoAs divided by target tissues and compound classes (2020)[7]
Blue: modulators targeting the nerves and muscles, green: modulators targeting growth and development, red: modulators targeting the respiration, yellow: modulators targeting the midgut, gray: mode of action unknown. Pyrethroids and VGSC blockers (indoxacarb) are building 17% market share, showing the importance of the voltage-sensitive sodium channel (VSSC) as target.

2.2 Ion channels

Ion channels are membrane-embedded proteins, forming pores in the membrane. These pores facilitate the passive transport of ions across the phospholipid membrane and increase the permeability, either selective for specific ions or unselective.[11] Ion channels usually consist of different compartments, a funnel, a selectivity filter mediating ion selectivity, a gate and a trigger, which depends on the physiological role. For some ion channels, further compartments might be added.[12] On the intra- or extracellular site, the funnel receives the ions and guides them to the selectivity filter, determining the selectivity for a particular ion species.[13] The trigger reacts to a stimulus, membrane potential, pressure or ligands and induces in response conformational changes, leading to the opening of the gate to facilitate ion flux.[12]

Ion channels can be expressed in all biomembranes, like cell membranes, separating extracellular from the intracellular lumen, but also in membranes of intracellular organelles, like mitochondria and endoplasmic reticula, as described by O'Rourke.[12,14] The transport follows the electrochemical gradient and is driving towards its equilibrium. This gradient is the sum of two driving forces: The chemical gradient, determined by the ion concentrations on both sites of the membrane and the electrical gradient, determined by the distribution of charges separated by the membrane.[15] Typical distribution of ions in cells can be seen in Table 1.[11]

Table 1 - Physiological ion concentrations[11]

	Potassium K^+	**Sodium Na^+**	**Chloride Cl^-**	**Carbonate HCO_3^-**	**Proteins X^-**	**Calcium Ca^{2+}**	**Magnesium Mg^{2+}**
intracellular	139	12	4	12	138	0.1	0.8
Extracellular (blood)	4	145	116	29	9	1.8	1.5

Concentrations [mM]

The membrane potential at which the driving force for one ion is equal to zero is called equilibrium- or reversal potential. The net exchange of ions remains constant at this potential. Thus, for each ion leaving the cell, one ion enters the cell.[16] Considering the ion concentrations, different constants and the temperature, this potential can be calculated based on the Nernst equation. This calculation requires a membrane separating two different ion concentrations from each other and a selective permeability towards the ion of interest.[17] (Figure 3)

$$E_P = \frac{RT}{zF} \ln \frac{[ion]_0}{[ion]_i} \longrightarrow E_P = \frac{58}{z} \ln \frac{[ion]_0}{[ion]_i}$$

E_P	=	Equilibrium potential for permanent ions
R	=	Universal gas constant (8.31 J/mol/K)
T	=	Temperature in Kelvin (room temperature: 293)
F	=	Faraday constant (96 500 c/mol)
z	=	electrical charge of the ion
ln	=	natural log
$[ion]_o$	=	outside concentration of ions
$[ion]_i$	=	inside concentration of ions

Figure 3 - Nernst equation[18]
On the left is the Nernst equation, with variables and constants. On the right site, the simplified equation with all constants applied.

In contrast to the Nernst equation, the Goldman-Hodgkin-Katz equation considers all ions applied to the test system. This equation is an extension of the prior shown Nernst equation.[18] (Figure 4) But it has the disadvantage that permeability values must be determined experimentally in advance.

$$V_m = \frac{RT}{F} \ln \left(\frac{p_K[K^+]_o + p_{Na}[Na^+]_o + p_{Cl}[Cl^-]_i}{p_K[K^+]_i + pN_a[Na^+]_i + pC_l[Cl^-]_o} \right)$$

V_m	=	Membrane potential
R	=	Universal gas constant (8.31 J/mol/K)
T	=	Temperature in Kelvin (room temperature: 293)
F	=	Faraday constant (96 500 c/mol)
p_{ion}	=	Relative permeability (relative to p_K)
ln	=	natural log
$[ion]_o$	=	outside concentration of ions
$[ion]_i$	=	inside concentration of ions

Figure 4 - Goldman-Hodgkin-Katz equation[19,20]

Neurons, expressing ion channels for signal transduction, have three main driving ions determining the membrane potential. In a typical mammalian neuron K^+, Na^+ and Cl^- are responsible for a resting potential of approximately -70 mV.[21–23] The relative permeability in rest for K^+ : Na^+ : Cl^- is approximately 1 : 0.05 : 0.45 as K^+ features the highest contribution, the resting potential is close to the equilibrium potential of K^+. During the peaks of an action potential, this permeability shifts to 1 :

12 : 0.045, due to the opening of sodium channels, resulting in a membrane potential closer to the equilibrium potential of Na^+ ions.[21,23,24]

2.2.1 Ion channel subtypes

Ion channels can be subdivided based on their gating mechanism. Non-gating ion channels are consecutively open, facilitating an unimpeded ion flux. In 1996 Lesage et al. identified the TWIK-1 as a leak channel responsible for maintaining the resting potential by background, inward rectifying K^+ currents. Today, several more are known.[25,26]

The other groups are gated ion channels subdivided into three gating mechanisms. (Figure 5) The family of mechanosensitive ion channels is responsible for sensing different mechanical stimuli, like heat, pressure and motion.[25] The transient receptor potential (TRP) is a prominent family among the sensory channels, identified by Cosens and Manning in 1969.[27] The vanilloid family (TRPV) serves different functions and trigger dependent on the organism they are expressed in. In mammals, they act as sensors for chemical, thermal and osmotic stress, whereas in insects, they were identified as a mechanical sensor by Walker et al.[28–30] Its essential role in the insects' physiology led to the development of two different insecticidal, chemical classes. The IRAC classified pymetrozine and afidopyropen as TRPV modulators acting at the chordotonal organ.[31]

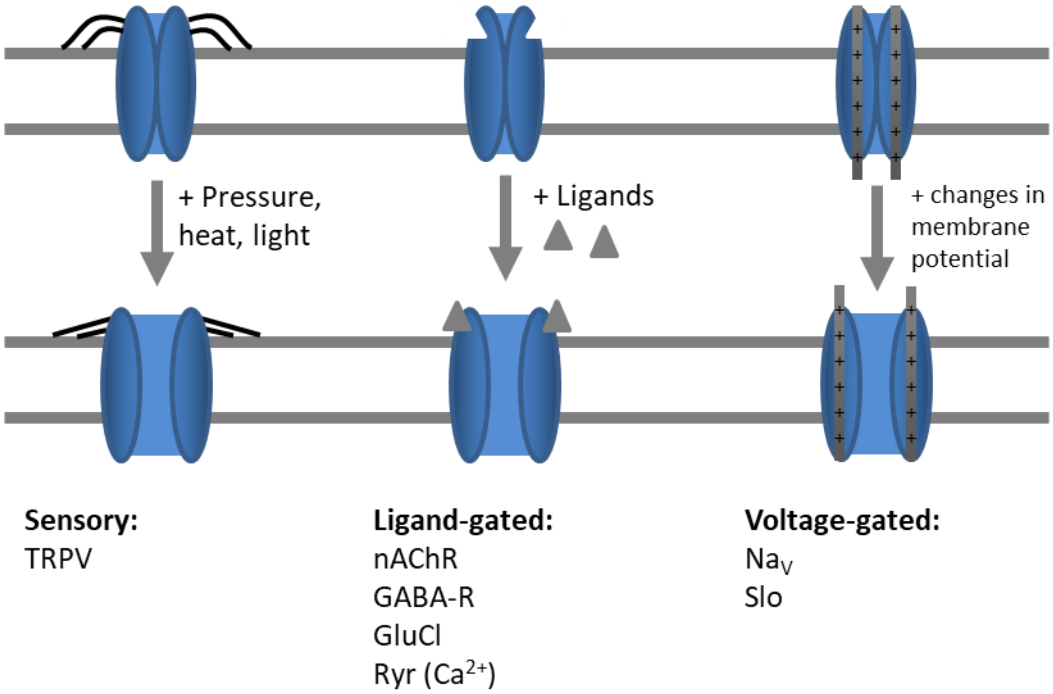

Figure 5 - Gating mechanisms for ion channels
Gating mechanisms assigned with exemplary ion channels showing insecticidal potential. Modified after Hadiatullah et al.[31]

The second subgroup of gated ion channels is the ligand-gated channel, playing an essential role in olfactory sensing and postsynaptic signal transduction.[32,33] Binding of ligands to the channel triggers conformational changes, which facilitates ion flux, either hyperpolarizing or depolarizing the cell.[32] An example of endogenous ligands are neurotransmitters, opening ion channels at the post-synapse after being released into the synaptic cleft.[34] The GABA Cl^- channel is one of the best-characterized inhibitory ion channels. Antagonists, like fipronil, lead to over-excitation of the pest organism.[35] Other ligand binding channels important for pest control are the nicotinic acetylcholine receptor and glutamate-gated chloride channel targeted by neonicotinoids and avermectines.[36–38]

The last gating mechanism is the voltage-gating ion channel essential for transducing signals among nerve fibers.[39,40] Voltage-gated channels are sensitive to changes in the membrane potential, sensed by voltage-sensing domains consisting of charged amino acids.[39] These channels are described in more detailed in the next chapter. (2.2.2 Voltage-sensitive sodium channel)

2.2.2 Voltage-sensitive sodium channel

Voltage-sensitive sodium channels are ubiquitously expressed in all neurons of the central nervous system (CNS) and peripheral nervous system (PNS).[39] Their crucial role is the depolarization during electrical signal conduction of senses, pain, reflexes and motions among all higher animals.[41] Their ability to quickly activate and inactivate allows fast and repetitive signal transductions by so-called action potentials (Figure 6).[42] These signals are generated due to the excitation of a neuron and range between the equilibrium potentials of potassium and sodium. At rest, neurons have a potential of approximately -70 mV.[43] Minor excitation leads to the opening of a small population of VSSCs, insufficient to generate a full action potential (Figure 6 – dotted line).[44]

Sodium channels are heterologous protein complexes consisting of a big α-chain (260 kDa) and a small β-chain (30-40 kDa).[45] The first evaluation of a VSSC structure was made in 1984 by Noda et al. on the first primary sequence isolated form an eel.[46] The first 3D-structure was gained by the crystal structure of the related bacterial homolog and the cryo-EM structure of american cockroach VSSC by Shen et al. in 2017.[47,48] The bacterial VSSC is a complex of four homolog α-units contrary to the mammalian VSSC.[48] In insect and mammalian VSSCs, the α-chain consists of 4 homolog segments (I - IV) with six transmembrane domains each.[45] The 4th transmembrane domain in each subunit is highly conserved with positively charged arginines and lysins and acts as a voltage-sensor.[49] The pore is formed by the four pore domains, S5 and S6, including their linker in each segment.[45] Within the linker, a conserved pore-loop (P-loop) is located, all four P-loops form the selective Na^+-selective filter containing four amino acids, DEKA or EEDD). The intracellular loop, linking segments three and four, acts as an inactivation gate. It features a crucial IFM motif, mediating the inactivation.[41,50] Although α-subunits are functional alone, they are complexing with β-subunits modeling the channel

kinetics, voltage dependence and trafficking. (Figure 7)[51–55]

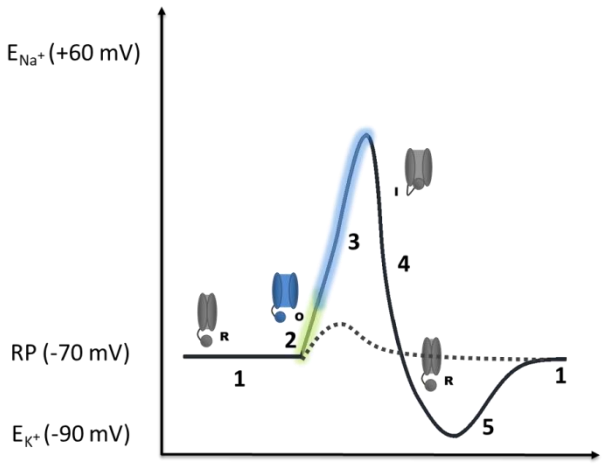

Figure 6 – Sodium channel states during action potential
Different steps of signal transduction (above threshold: action potential, below threshold: dotted line) and the assigned channel states. **1** Resting potential with closed sodium channel **2 & 3** Depolarization with open sodium channel (green: depolarization till threshold, blue: self-enforcing depolarization) **4** Repolarization with inactivated sodium channel **5** Hyperpolarization with closed sodium channel

At a certain threshold, the whole population of sodium channels opens (self-enforcing).[22,23,44] The voltage sensors are shifted up and the opening pore facilitates a sodium influx and drives the signal toward the equilibrium potential of sodium (depolarization). Within a few milliseconds, the inactivation gate closes the pore from the intracellular site and prevents further currents. Whereas the sodium channel cannot be activated again during this time, voltage-gated potassium channels open, facilitating potassium outflux. The signal is driving back to the equilibrium potential of potassium (repolarization). A long potassium outflux facilitates overshooting of the resting-potential (hyperpolarization).[22,23] At this stadium of the action potential, the sodium channels can be activated again as the pore is closed, the voltage sensing domains are down and the inactivation gate is open.[41] (Figure 6 & Figure 7) Inactivation and hyperpolarization are essential for signal transduction, as they prevent signals from being bidirectional.[50]

Due to its physiological importance, the VSSC was an interesting target before the development of insecticides and pharmaceuticals. The evolutionary pressure on predators, prey and plants leads to the design of highly potent modulators targeting the VSSC.[57,58] Activators can be found among all kingdoms in algae, anemones, bacteria, fish, plants, scorpions, snakes, snails, spiders and wasps.[50] Even though these toxins are not necessarily selective, some have evolved to target the insect VSSC specifically. Venoms of scorpions and spiders, for example, were developed to hunt insects as prey.[59,60] Some plants, on the other hand, have evolved pyrethrums to protect against insects.[61] So

far, Catteral, Lombet et al. and Soderlund et al. have identified nine binding sites at sodium channels targeted by these toxins. [62–64] (Table 2)

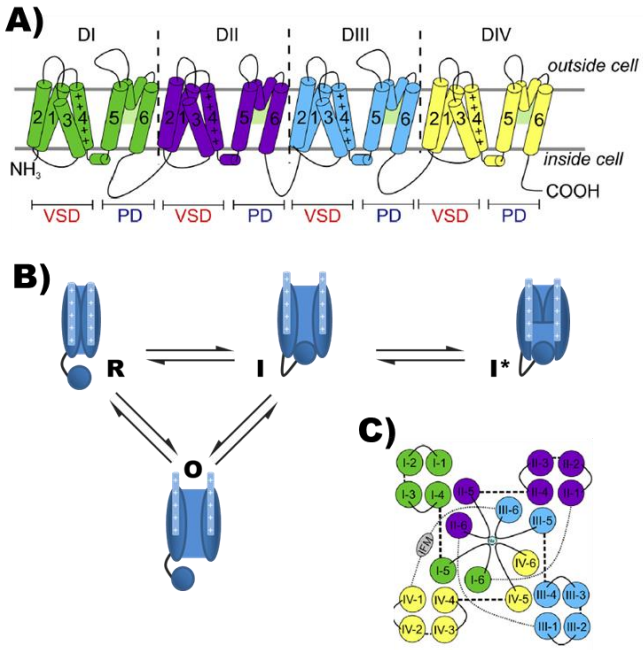

Figure 7 – Sodium channel constitution and different sodium channel states
A) snake plot of the overall sodium channel structure with the pore-domain (PD) and voltage sensing domain (VSD)[50] B) Different sodium channel states with the critical structures and channel conformations (R: resting state, O: open state, I: fast inactive state and I*: slowly inactivated state) modified after Zybura et al.[56] C) Plot of the open channel conformation of VSSC from the extracellular view.[50]

Table 2 - Classification of VSSC binding sites after Catterall, Lombat et al. and Soderlund[62–64]

Site	Modulator	Physiological main effect	Allosteric coupling
1	Tetrodotoxin Saxitoxin	Channel inhibition	None
2	Veratridine Batracotoxin	Persistent opening	3, 5, 6, 9
3	α-Scorpion toxin Sea anemone toxin	Prolonged inactivation	2, 6, 8
4	β-Scorpion toxin	Shift of activation	8
5	Brevetoxin Ciguatoxin	Shift of activation	2, 5, 6, 8
6	Pyrethroids DDT and analogous	Prolonged activation	2, 3, 5
7	Gonioporatoxin	Prolonged activation	None
8	Pumiliotoxin-B	Persistent activation	3, 4, 5
9	Local anesthetics Anticonvulsants Dihydropyrazoles	Channel inhibition	2

2.2.2.1 Insect Na channel

In insects, the α-VSSC subunit is encoded by a single para gene with more than 60 splicing variants as published by Loughney et al. in 1989.[65] Thackeray and Ganetzky identified the splice variants to be important in the different developmental stages of an insect, with different electrophysiological properties in 1994.[66] Ganetzky furthermore identified four different auxiliary subunits to interact with the α-subunit.[67] Homologue to the human β-subunits, TipE can enhance the amplitudes of the sodium current.[68] The pharmacology might vary between the different splicing variants of insect VSSC and could show an altered insecticide sensitivity as Tan et al. show for deltamethrin on two functional variants.[59]

According to expert market research, pyrethroids belong to the most important insecticides and vector control agents with a global value of 3.3 billion USD in 2020.[71] Pyrethroids are synthetic homologs of the pyrethrum, synthesized by different Tanacetum-members.[58] Since the beginning of the 19th century, the insecticidal effect of its extracts has been known. In 1924 Ruzicka and Staudinger identified the active metabolite pyrethrin and synthesized the first synthetic derivatives.[72] The effect of pyrethroids on channel physiology is diverse. Different substitution patterns mediate effects on the inactivated state or facilitate an activation shift.[73,74] All pyrethroids, however, have a prolonged opening time after channel inactivation in common.[73] Type I pyrethroids like permethrin were shown to have a faster dissociation constant than type II pyrethroids like β-cyfluthrin.[73,75] The effect of both subtypes is use-dependent, meaning that the effect becomes stronger every time the channel is activated.[73] The overexcitation, resulting from the prolonged opening times, leads to a breakdown of the nervous system resulting in paralysis of the pest organism.[76]

The intensive use of pyrethroids over the last decades led to the development of resistance in field-relevant pests.[77,78] The most prominent type of mutation for the VSSC is the knockdown resistance (kdr), mediating resistance by altering point mutations.[79] It was first reported in 1956 by Milani, who observed reduced sensitivity towards pyrethroids in house flies.[80] Nowadays, such mutations are found in almost all relevant pests and disease vectors.[81–83] Soderlund and Bloomquist showed cross-resistances of the kdr mutations between pyrethroids and DDT and its analogs.[84] Davies et al. identified 2007 the L1014F mutation as the most prominent in arthropod pests.[74] The exchange of leucine to phenylalanine takes place in the S6 segment of the second domain and results in a 10-20 fold loss of sensitivity towards pyrethroids.[85] Further types of mutations were comprehended by Dong et al. in 2014: V410 (M/A/G/L), M918 (T/L/V), T929 (I/C/N/V), I1011 (M/V) and V1016 (G/I). The different mutations and substitutions varied in their effect on pyrethroid resistance and showed significant differences in resistance towards pyrethroids and DDT.[85] While an M918T mutation, located in the linker of S4 and S5 in domain II, for example, comes along with high resistance towards pyrethroids, like permethrin and deltamethrin, it is not protecting pests towards DDT.[86,87] Hu et al.

identified the F1534 C mutation to discriminate type II pyrethroids by mediating resistance just towards type I pyrethroids.[75]

A combination of two or more mutations was shown to affect the resistance synergistically. Lee et al. and Vais et al. identified in 1999 and 2000 almost simultaneously the combination of L1014F and M918T exhibited almost 1000-fold loss of sensitivity, while single point mutations would have a ten-fold shift.[87,88] The double mutation was almost decreasing the activity of deltamethrin to *Drosophila melanogaster* entirely.[87]

A far smaller market share of insecticides is covered by indoxacarb. It came into focus due to its new mode of action and low mammalian toxicity.[89,90] Indoxacarb is a prodrug absorbed by the pest and metabolized to the more potent drug DCJW by N-de-carboxymethylation.[91] In contrast to pyrethroids, DCJW exhibits an antagonistic effect on VSSCs. In experiments on cockroach VSSCs, Song et al. have identified the mode of action for DCJW. It inhibits the recovery of the slow inactivated state, VSSCs tend to enter after a prolonged depolarization.[92] The effect was not shown to be use-dependent like described for pyrethroids. The new binding site, compared to pyrethroids, made it a promising candidate to counteract pyrethroid-resistant pests.[63] However, shortly after its admission, Shono et al. identified 2004 first cases of resistance for *Musca domestica,* and Wang et al. identified further resistance in Plutella in 2016.[93,94] While Shono et al. characterized a metabolic resistance, Wang et al. identified two target site mutations. The mutations F1845Y and V1848I were found in different strains collected in China and mediated up to 870-fold resistance *in vivo* experiments. [93,94]

2.2.2.2 Human Na channels

Humans have nine VSSCs, sharing the exact functional domains and 50 – 90 % of the identical primary amino acid sequence. The $Na_V1.1$ – $Na_V1.9$ differ in tissue distribution, voltage sensitivity and pharmacology.[95–97] $Na_V1.1$, 1.2, 1.3, 1.6 and 1.8 (SCN1A, 2A, 3A, 8A and 10A) are expressed in the central nervous system (CNS), while $Na_V1.1$ & NaV1.6 are also expressed in the peripheral nervous system (PNS) together with $Na_V1.7$ (SCN9A) and 1.9 (SCN11A). $Na_V1.4$ (SCN4A) is expressed in skeletal muscles and $Na_V1.5$ (SCN5A) in the heart.[95] Pharmacological highest relevance have $Na_V1.5$ and 1.7 due to their pharmacological role in the heart and the importance in pain sensation.[98,99]

Drug discovery extended the panel of potent drugs shown in Table 2 by synthetic modulators targeting the ninth binding site. The ninth binding site is the only one targeted by pharmaceuticals, targeted by local anesthetics, like lidocaine, and anticonvulsants, like carbamazepine.[63] The analgesic effect of lidocaine is thereby mediated by the inhibition of NaV1.7 in the peripheral nervous system.[100] Application is indicated in treating acute pain, in combination with opioids in chronic pain, and for surgeries to numb the operation area.[101–103] Carbamazepine's main indication as anticonvulsive is the treatment of epilepsy but is indicated for pain as well.[104]

The mammalian sodium channels, with a particular focus on the human VSSCs, are highly important for developing sustainable and safe VSSC-targeting insecticides. The self-enforcing nature of the VSSC, making it an excellent insecticidal target, makes it an important selectivity target.[105,106] While the insect expresses just one VSSC, in mammalian, several subtypes must be considered.[95] High importance for low mammalian toxicity of pyrethroids is the high target selectivity between mammals and insects at the sodium channel.[107] Smith et al. and Soderlund and Lee described the rat $Na_V1.2$ as pyrethroid insensitive, while the rat isoforms $Na_V1.3$, 1.6 and 1.8 showed minor pyrethroid responses.[108,109] In a rat model, Vais et al. showed that selectivity is reached by exchanging just a few amino acids. They showed that occurring field resistances (M918) in *Drosophila melanogaster* mimic the mammalian VSSC. By exchanging the isoleucine in position 874 of the rat IIA Na channel, analog to the M918 position in flys, by a methionine, the channel became 100x more sensitive towards deltamethrin.[110]

Discrimination of indoxacarb between different mammalian VSSCs was shown by the investigation of rat dorsal root ganglia, expressing two different groups of sodium channels, the TTX resistant channel $Na_V1.8$ and the TTX sensitive channels, $Na_V1.2$, 1.3, 1.6 and 1.7. The sensitive VSSCs were also shown to be more sensitive towards Indoxacarb and the metabolized drug DCJW. Besides NaV1.8, the heart-relevant, TTX-resistant NaV1.5 was shown to have a reduced DCJW and indoxacarb sensitivity. The overall DCJW sensitivity, however, is also reduced for mammalian channels.[110]

3. Methodology

3.1. Ion channel measuring techniques

3.1.1 Electrophysiological measurements

Since Hodgkin and Huxley developed the electrophysiological recording in the early 50s and Neher and Sakmann developed it further to the patch clamp technique.[111–114] Today, it is the method of choice for ion channel characterization.[115] They were able to implement cells into the electric circuit, as seen in Figure 10. Outer disturbances were eliminated by a high impedance connection between electrode and cell, with a resistance of at least 1 GΩ. The connection is therefore called gigaseal.[116] The most common types of measurement are voltage- and current clamps, entitled by the respective altered unit.[117,118]

To establish electric circuits like Hodgkin and Huxley described and to perform pharmacological experiments, various compartments have to be combined (Figure 8).[119,120] The minimal requirements for these experiments are a patch pipette comprising an AgCl wire in a glass capillary with internal solution (4), a cover slide with cells in external solution (3) and a bath electrode to close the electric circuit (8). The cell health is improved when the coverslip is located in a perfusion chamber, facilitating a frequent exchange of external solution (2, 5 & 6). The outflow must be higher than the cover slide to enable permanent perfusion without aspirating the external solution. Furthermore, the diameter of the tube for aspiration should be slightly higher to aspirate additional solutions applied during the experiment, preventing spilling. The perfusion has the advantage that compounds or solutions of different compositions used over a long time (7) are washed out of the chamber. In this setup, the U-tube reversed flow technique described by Fenwick et al. in 1982 was used to apply modulators.[121] It has the advantage that compound solution permanently flows through the tube system without reaching the cells. As soon as a valve downstream the tube is shut, the solution covers the area of interest within a few seconds leaf-shaped. When the valve is opened again, the negative pressure sucks the compound solution entirely away. Just applications over a long time have to be rinsed by the perfusion bath.[120,122]

The measurement chamber is embedded into a bigger patch-setup. The chamber is installed within an upright microscope to facilitate the visualization. Additional implementation with filter systems and external light sources enables the measurement of fluorescently labeled cells and optogenetic tools.

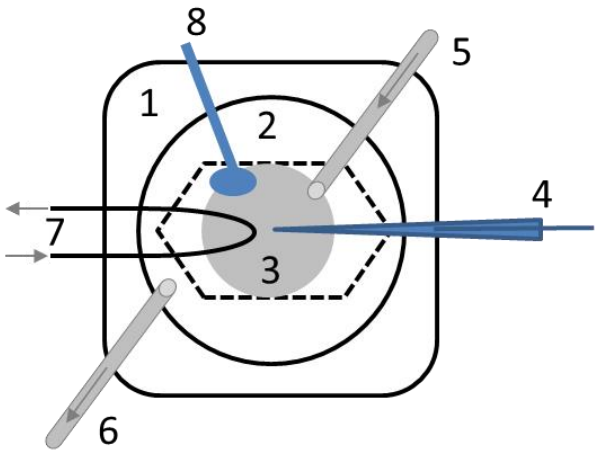

1 microscope table
2 petridish with deepened cellchamber (dashed line)
3 cell coated coverslide
4 patch pipette (filled with internal buffer)
5 inflow external buffer
6 outflow
7 U-tube compound application
8 bath electrode (AgCl)

1 upright microscope
2 faraday cage
3 amplifier (HEKA EPC10)
4 preamplifier
5 Micromanipulator (MP-285)
6 control-unit micromanipulator
7 vibration-damped table
8 stands
9 tank external solution
10 compound solution
11 U-tube application system
12 valve
13 pump
14 liquidwaste
15 light source (CoolLED pE4000)

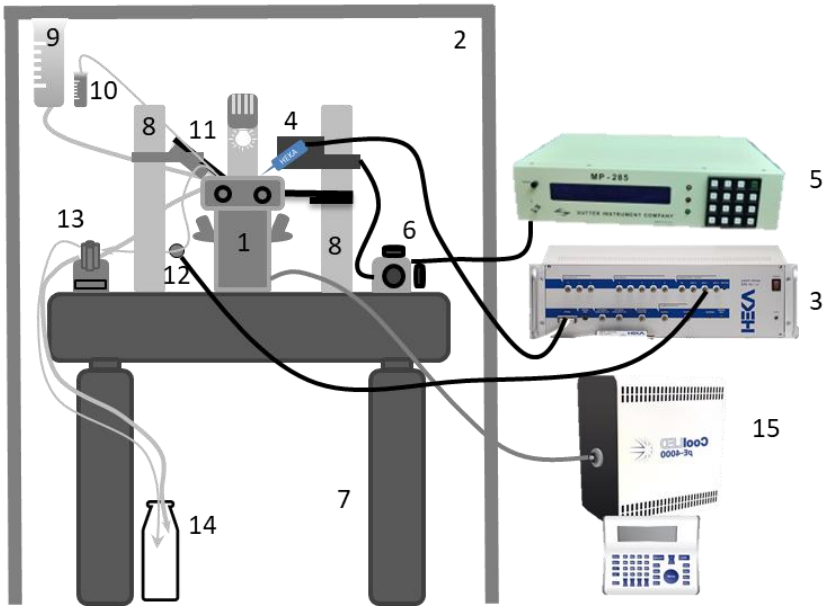

Figure 8 - Measurement chamber and assembly of a patch-setup
Chamber and assembly comprise the components required for electrophysiological experiments as performed in this thesis. A connected computer processed the data gained by the preamplifier.

All components reaching into the measurement chamber are fixed at two vertical stands. The gravity flow of a higher-located tank supplies the u-tube. Downstream the valve is located, triggered either by the patch clamp amplifier or manually by the experimenter. Furthermore, a pre-amplifier is attached to the amplifier and the stand. It is controlled via a micromanipulator, facilitating movements on a nanometer scale. When not powered by gravity, the tubing is driven by a pump, with all wastes channeled to a waste bottle. All devices are located on a vibration-damped table within a Faraday cage to exclude external disturbance factors. Vibrations would comprise the integrity of the seal and the cage prevents disturbing currents increasing the signal-to-noise ratio.[120,122]

In current clamp measurements, membrane potential changes are measured, facilitating the

detection of action potentials.[123,124] This thesis used it to ensure VSSC activation by blue light application. Nowadays, channel measurements are mainly based on voltage-clamp measurements.[118] The current changes in the voltage clamp are measured indirectly by a feedback mechanism. Thus, the measured current is injected into the cell to maintain the defined membrane potential. Different current kinetics allow conclusions to the ion channel composition in the present sample, as each ion channel family and subtype has some unique responses and features.[125]

The potential of these techniques was recognized early and further developed. Different conformations allow optimal adaptations to the experiment. At the beginning of every experiment, a cell-attached configuration is reached.[125] The pipette tip is placed on the cell surface to obtain a giga seal. The cell remains intact during this step, and intracellular signaling processes and ion distribution are not disturbed. Whole-cell configuration can be reached by rupture of the membrane patch inside the tip, either by an electrical pulse or slight suction through the pipette. The internal solution mixes with the intracellular lumen through the opening. The large opening furthermore provides better electric access. The circuit facilitates recording all populations of channels embedded into the membrane. The measured currents exhibit a linear correlation to the ion channel expression on the cell surface. However, there are limitations due to the substantial dilution of physiological cell mechanisms, like metabolism, enzyme activity and G-protein coupling not occurring. Nowadays tendency for automatization led to a high throughput enabled by planar patch systems underlying the same advantages and disadvantages of conventional whole-cell voltage clamps. This aspect can be circumvented by a perforated patch clamp, where antibiotics (for example, amphotericin-B and gramicidin) form pores into the membrane patch inside the tip. The pores facilitate an exchange of liquids between tip and cell, but proteins remain inside. This method allows recordings of channels requiring intact downstream signaling cascades.[123,125,126] (Figure 9)

Besides recordings from whole cells, also single channels can be measured. From the cell-attached configuration, one can come to the inside-out configuration. It is named after the orientation of the embedded channel. The intracellular part of the channel points towards the external solution, whereas the inner part remains in the tip. One can reach this configuration by lifting the pipette during whole-cell configuration to loosen a membrane patch off the cell. This configuration might be required for the pharmacological analysis of compounds binding from the intracellular site. The last conformation is the outside-out conformation, in which the intracellular part of the channel is located inside the tip. The advantages and disadvantages are similar to those from the inside-out patch. It is formed by withdrawing the patch pipette from the cell during the whole cell configuration. The loose patch surrendering the pipette is then reforming an intact membrane comparable to a vesicle. Both single-channel recordings allow the experimenter to characterize isolated ion channels precisely.[127,128]

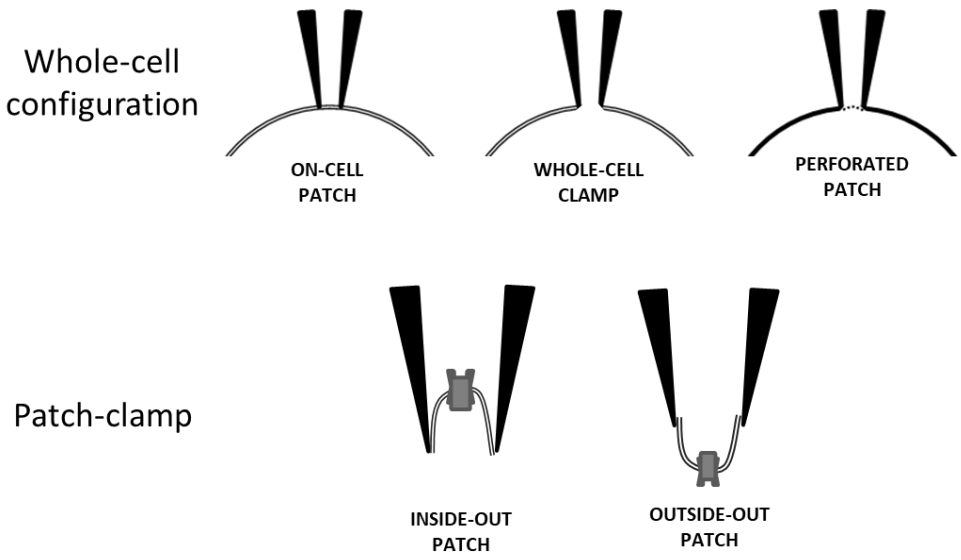

Figure 9 - Configurations possible in electrophysiological experiments[125]

All different configurations are not measuring the currents mediated by channel opening. But the compensation currents, required to adjust the set holding potential at every moment, are measured. [120,126,129] The simplified circuit in Figure 10 facilitates the current injection and measurement with just one electrode. Crucial for this circuit are the operation amplifier (OPA) and the feedback resistor (R_t). Both voltages, U_{pip} (-) and U_{soll} (+), are entering the OPA, and differences between both voltages lead to an output voltage at the end of the OPA, proportional to the difference. As a result, different voltages are present at the two knots originating from the feedback resistor. Based on Ohm's law, this leads to currents proportional to the voltage difference at Rt. The resistor prevents the current from going in another direction than into the pipette. The injected currents alter voltages as long as U_{pip} and U_{soll} differ. As soon as U_{soll} is equal to U_{pip}, the current injection stops. This harmonization is very fast and even minor variations are aligned.

In amplifiers, additional circuits are implemented to compensate for the delays resulting from recharging the capacitator. (Sigworth 1995), one of these capacitors is the feedback resistor. Additional capacitors are present at the tip of the patch pipette, resulting from the narrow hole at the tip and the different solutions facing each other. The last capacitator is the biomembrane of the cell. The lipids separating the various ions and charges from each other must be reversed and recharged. The bigger the cell is, the more significant the membrane surface and the capacitative artifacts. Therefore the capacitive artifacts can also be used to determine the cell surface by measuring the capacity.

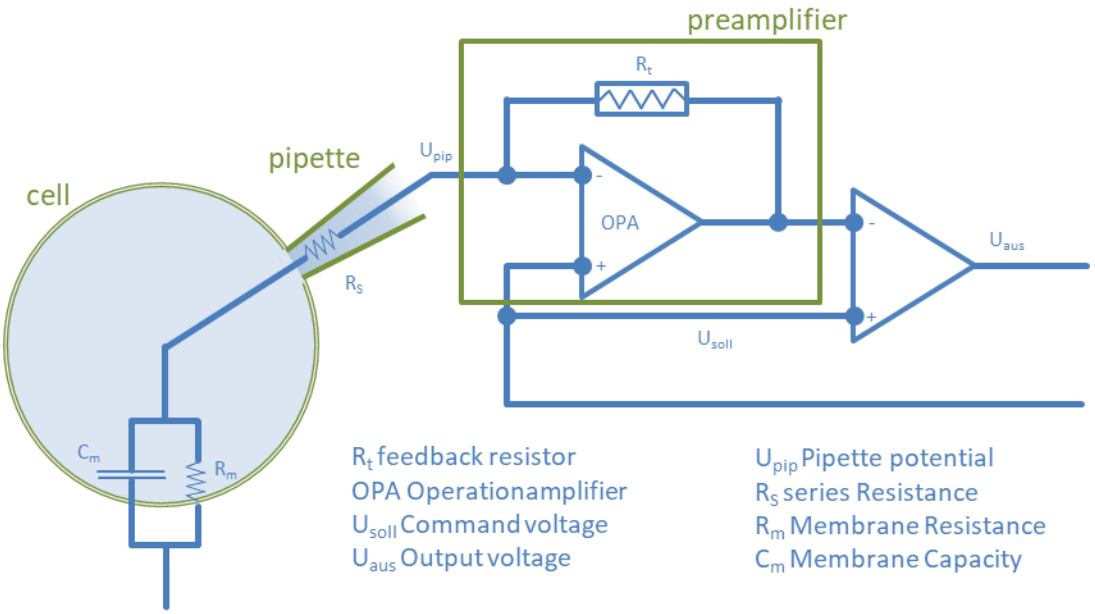

Figure 10 - simplified electric circuit during patch-clamp experiments[111,130]
Shown is the electric circuit as described by (Neher and Sakmann) during a whole-cell voltage clamp experiment in blue. The different sections required for this experiment are shown in green.

For larger cells, the one electrode measuring and injecting is not sufficient anymore. Xenopus oocytes, for example, have a diameter of 1 mm and a high cell surface compared to mammalian cells. These cells are measured by the two-electrode voltage clamp (TEVC) described by Guan et al.[131] In contrast to the common patch clamp techniques, two sharp electrodes are stuck into the cell but not attached to it. One of the electrodes injects the current required to maintain the holding potential and the other measures the needed current.[131]

3.1.2 Fluorescence Measurements

Fluorescence is a widely used tool in biochemistry and drug research. Jablonski described the physics behind fluorescence in 1933. The excitation of a probe with a distinct wavelength (λ_{exc}), elevating the molecule to an energetic higher level (S1'), is called absorption. This state is meta-stable and energy is rapidly transitioned to surrounding molecules (vibronic relaxation) or internal vibrancies (internal conversion), leading to a lower energetic level (S1). The fluorescence is the measurable wavelength (λ_{em}) resulting from the energetic drop from the S1 excited state to the ground state. The loss in energy results in a longer wavelength than the excitation and is, therefore, redshifted.[131] (Figure 11 A)

The classic fluorescence measurement consists of four different compartments. Depending on the application of specialized compartments, this may be reduced. In each experiment, a light source is required to generate the light to stimulate the probe. The light source can be restricted to a particular wavelength, as done in some fluorescent readers, using LEDs emitting the required

wavelength. Or the light source emits white light, consisting of all wavelengths of the visible spectrum. In the case of a white light source, an excitation filter is required to facilitate the transition of the excitation wavelength (λ_{exc}). The excitation filter builds the first part of the second complex required, a setup of two different filters and a dichroic mirror. The mirror reflects the light for excitation on to the probe (compartment 3). The probe is channeling through the other energetic states, as described in the Jablonski diagram and emits then the light of a defined wavelength. The emitted light passes the dichroic mirror permeable for wavelengths higher than the excitation wavelength and is further filtered by the emission filter. Afterward, the emitted light (fluorescence) hits on the detector. In fluorescence microscopy, this detector is the eye or a camera setup, while in most fluorescent readers, a camera is installed, quantifying the measured fluorescence.[132,133]

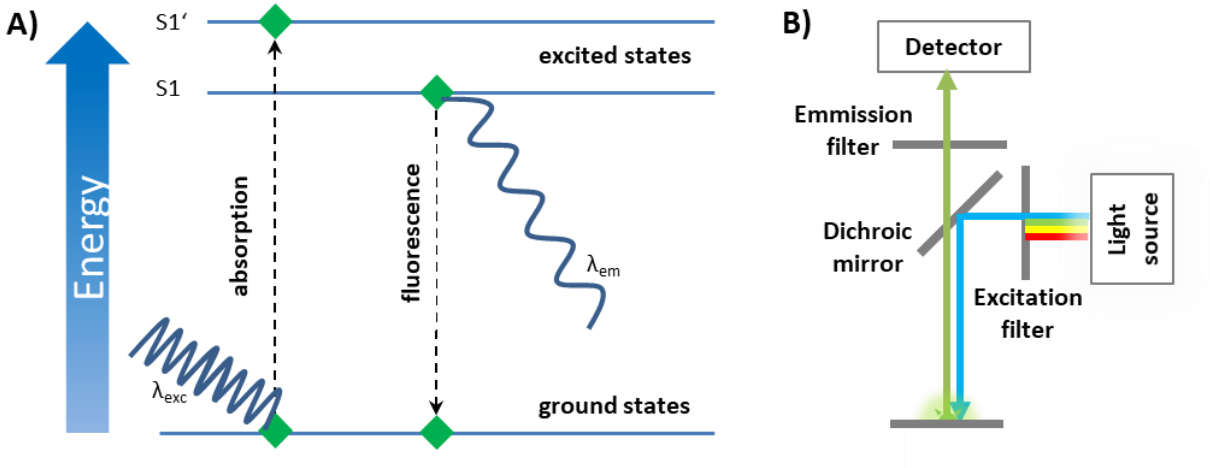

Figure 11 - Explanation of fluorescence in biochemical measurements
A) Jablonski diagram, showing the different energy states a molecule is transitioning through excitation and emission of light.[131] B) shows the simplified design of every fluorescence measurement device, from microscope to complex plate readers[132]

The number of biochemical areas fluorescence is applied, is increasing and the generation of new tools accelerates this development. Standard techniques with fluorescence are the localization of different structures, structures in the cell, cells in the body or tissues in the body.[134] Due to genetically encoded fluorophores, this can be either done by genetic modulation or externally supplied probes attached to antibodies or other anchors.[135,136] Methods like FACS (fluorescence-activated cell sorting) facilitate the characterization of cell populations based on fluorescently labeled target structures.[137] And even dimerization can be detected by different fluorescent-based methods, like proximity ligation assays or FRET (fluorescence resonance energy transfer).[138,139] On the nucleic level, fluorescent probes are used for quantitative real-time PCR, like recently performed in a highly frequent manner for Covid-19 testing.[140] This thesis focuses on a fluorescent method facilitating the screening of large compound libraries. In such assay systems, fluorescence can detect different changes, like in ion concentration, protein conformation or membrane potential.[141–143]

Even though electrophysiological measurements have the highest sensitivity, applying fluorescent dyes in high-content screening significantly reduces measurement time, costs, and technical know-how.[144] Therefore, different dyes are commercially available for high-content screenings on sodium channels featuring advantages and disadvantages. (Figure 12) Some dyes sense the internal sodium concentration directly.[145,146] An acetomethyl ester conjugate facilitates membrane permeability and cleaves intracellularly, trapping the cell's dyes. These dyes require washing out the remaining dyes in the external solution or quenching of extracellular dyes, as the extracellular sodium concentration is otherwise activating the dye.[147] Commercially available assay kits are CoroNa Green (Thermofischer Scientific) Asante NaTRIUM Green-2 (TEFLabs) and SBFI – Sodium-binding benzofuran isophthalate (Thermofischer Scientific). Even though sodium is measured, these dyes measure the VSSC effects indirectly, as currents are not detected, but changes in the ion concentration are.[147,148,149] (Figure 12)

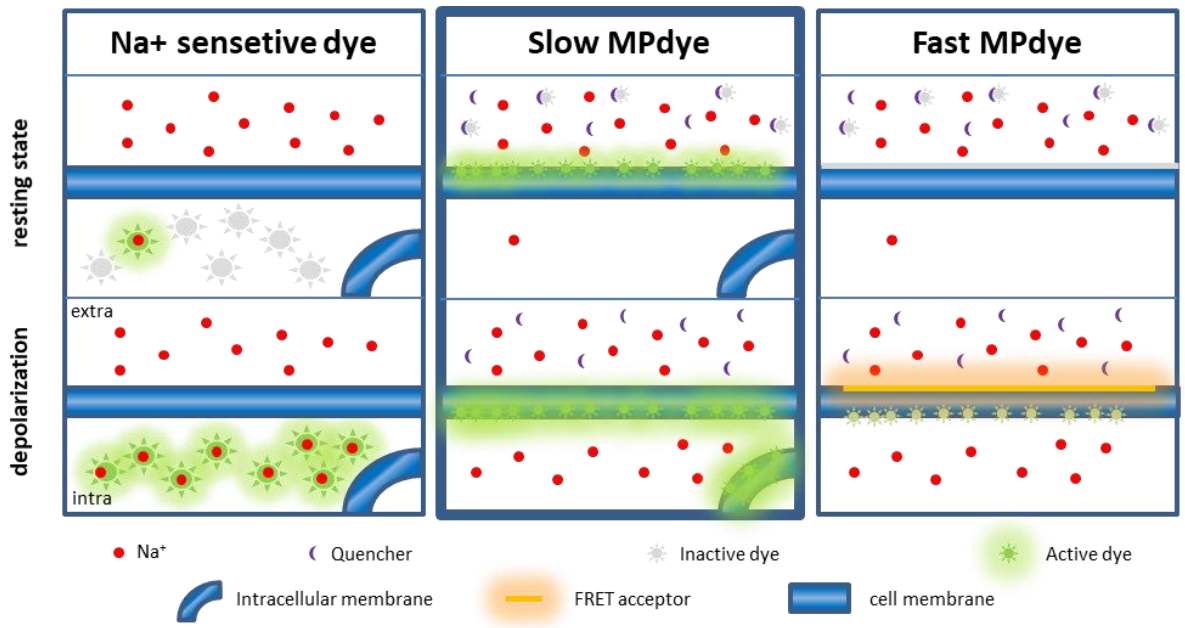

Figure 12 - Principal of different dyes which can be used in sodium channel HTS

Another form of measurement is the detection of changes in the membrane potential. Also, for this approach, commercially available systems, like FLIPR membrane potential dye (Molecular Devices) and DiBAC4 (Molecular Probes). Both dyes belong to the slow-responding membrane potential sensitive dyes.[150,151] The hydrophobic substances feature low fluorescence in the aqueous phase, quenched by other dyes, but gain higher quantum yields when incorporated into the membrane. After depolarization, the negatively charged dye enters the cell and binds to intracellular membranes to enhance the fluorescence.[149,152] Fast dyes exhibit a slightly faster response time due to FRET systems. Wolff et al. showed in 2003 that these dyes, however, have the disadvantage of a strongly reduced measurement window.[148] Whittaker at al. published in 2001 an advantage over the FLIPR MPdye with response times of 10 s over DiBAC4.[152] Due to these results, we decided to use the

membrane potential dye of Molecular Devices, with high measurement windows and relatively fast response times. The indirect measurement of the membrane potential instead of currents results in a comparably high number of false positives and potentially also to a low number of false negatives.[153] Implementing such technologies, therefore, requires suitable controls and precise validation.

3.2 Optogenetics

The development of optogenetics in the early 2000s gave a powerful tool to the hands of neuroscientists worldwide.[154] The potential of light-induced effector proteins was quickly recognized and adopted by other fields, like biotechnologists and genetic engineers.[155, 156] However, optogenetics is not the first approach for light-induced experiments in neuronal systems. In 1989 Kaplan and Somlyo developed caged compounds released by photolysis, later enhanced by Ellis-Davies (2007). [157,158] Disadvantages of this technique compared to optogenetics are limitations due to suitable light-inducible compounds and the cell-type unspecific effect.[157]

The initial purpose of optogenetics was the characterization of different neuron subtypes, which is essential for a comprehensive understanding of the operating principle of the human brain. Although the exact number of neuronal subtypes remains unclear, over 1000 different cell types are thought to be found in the human cortex.[159, 160, 161] Their differences in physiology, location, morphology and gene-expression impede the necessary separation of subtypes. Optogenetics steps into the breach, facilitating the excitation or silencing of genetically modified tissues and cells by light stimulation, apart from electrophysiology.[155] The controlled activation or inactivation of specific neuronal subtypes without modification of other cell-types allows their characterization (e.g. physiological function, interacting cell-types).[162] Light as inducer has advantages in the control of neuronal excitability. Light pulses can be induced with response times and precision comparable to those of ion channels with a narrow spatial resolution.[163] Targeted genetic expression is another advantage, leading to specific expression in the target cell or tissue. Successful implementations of optogenetics in experiments, however, require some considerations in advance.[164,165]

The decision for a suitable photo-receptor is the most essential one. Microbial photo-receptors, called rhodopsins, facilitate encroachments into the membrane potential of mammalians. To do so, applications are required to enable ion fluxes.[166] They can be differentiated into two different classes: On the one hand, ion channels (Figure 13 A) allowing specific ions to overcome the bio membrane along the electrochemical gradient. On the other hand, ion pumps transporting ions against the electrochemical gradient by ATP-hydrolysis.[167] Due to genetic engineering, significant variability of tools are available in these classes. They show differences in kinetics, sensitivity and selectivity towards ions and excitation wavelengths. These aspects have to be considered in the decision for the optimal tool.[168,169]

Typical optogenetic experiments require cell-type specific expression, which can be achieved by controlling the tools though cell-type specific promoters and enhancers. [170] However, this approach is unsuitable for most cell-types, as the specificity is usually not determined by a single regulatory element.[159, 171] A combination of different proteins and several promotors provides distinct discrimination between cell types. Another challenge is the sufficient expression of the optogenetic

tool required for either silencing or activating the cell.[172] These aspects can be circumvented by a combination of recombinase and viral transfection or laborious clone selection.[173, 174]

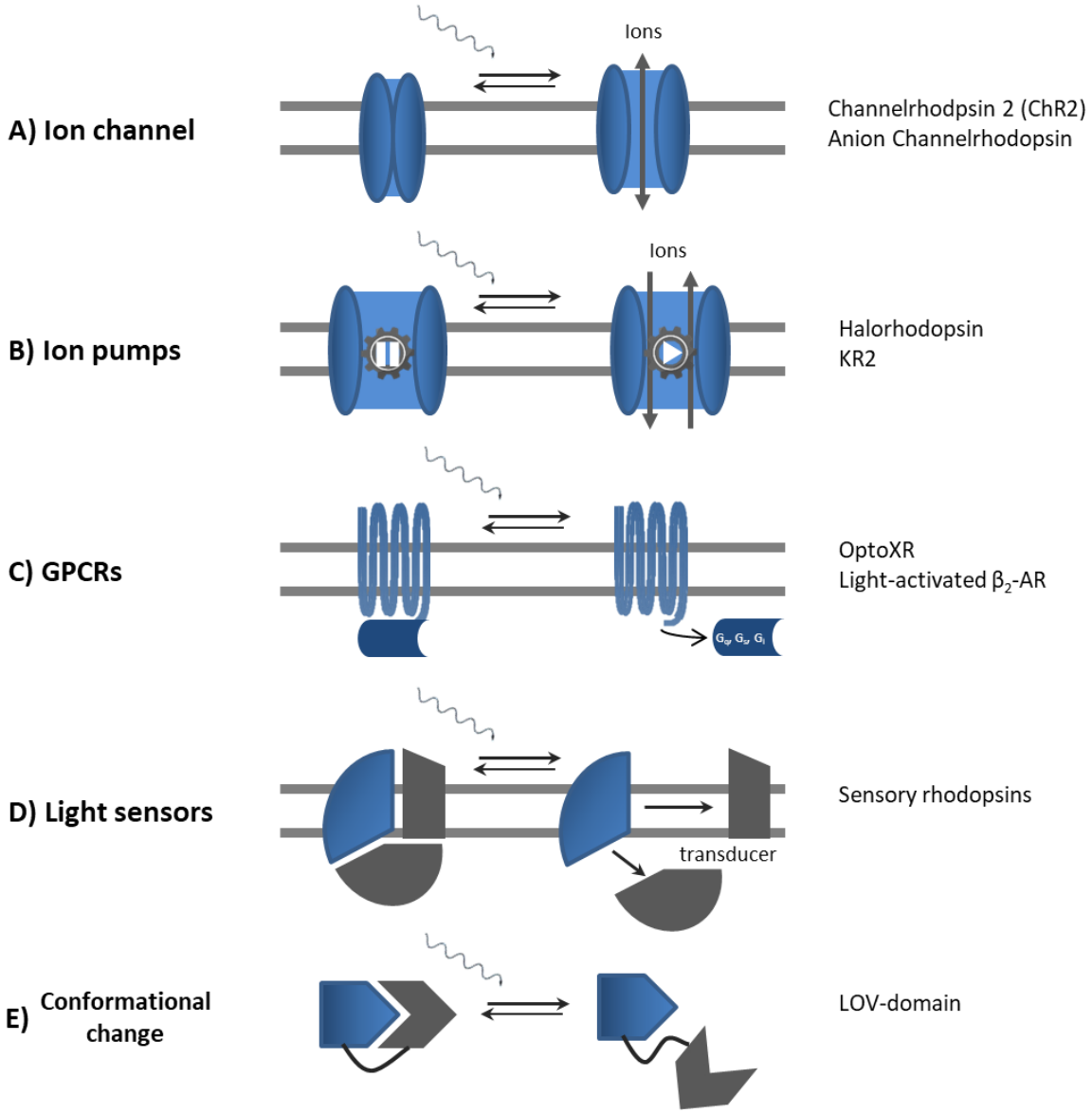

Figure 13 – Different applications of photoreceptors in research[175]
On the left, the mechanism is named with a depiction in the middle and examples for each mode on the right. The inactivated state is on the left side, while the excited state is on the right. (modified after Cho and Li)[175]

Another mode of action is G-protein coupled receptors (GPCR). They constitute the most common drug target due to their high variability and acceptance of different ligands. All GPCRs constitute of seven transmembrane domains and act as second messengers via G-proteins.[175] Type II rhodopsins, light-activated GPCRs, include the most prominent family of GPCRs with over 700 members.[175] Light-sensitive type II rhodopsins can act as a basis for generating chimeric GPCRs, like the light-activated β2-adrenergic receptor. These chimeras can investigate the different downstream signals mediated by different G-proteins coupled.[176]

Besides, also sensory photo-receptors are of higher interest for electrophysiologists, as they can act as a marker for various ions. Unfortunately, the signal transducers are not compatible with mammalian cell systems.[176]

Higher relevance have optogenetic tools inducing conformational changes. These proteins are found in plants, fungi and bacteria and can be implemented in mammalian cells. The LOV domain (light oxygen voltage domain) is the most prominent one undergoing conformational changes upon light induction. The primary use is the fusion of the LOV domain to effector proteins by allosteric coupling or steric inhibition.[177,178] The sterical change can activate kinases, GTPases and proteases, as described by Moglich et al. Wu et al. and Strickland et al. in 2009 and 2012.[179,180]

Channelrhodopsin 2 (ChR2) is a member of the family of microbial rhodopsins and was the first successfully expressed light-activated ion channel in neurons.[181] It is the best-studied and most prominent optogenetic switch. ChR2 has a retinal as chromophore covalently attached to a lysine residue. (Figure 14) The ion-conducting pore is formed by seven transmembrane helices capable of closing the pore at three different positions.[182]

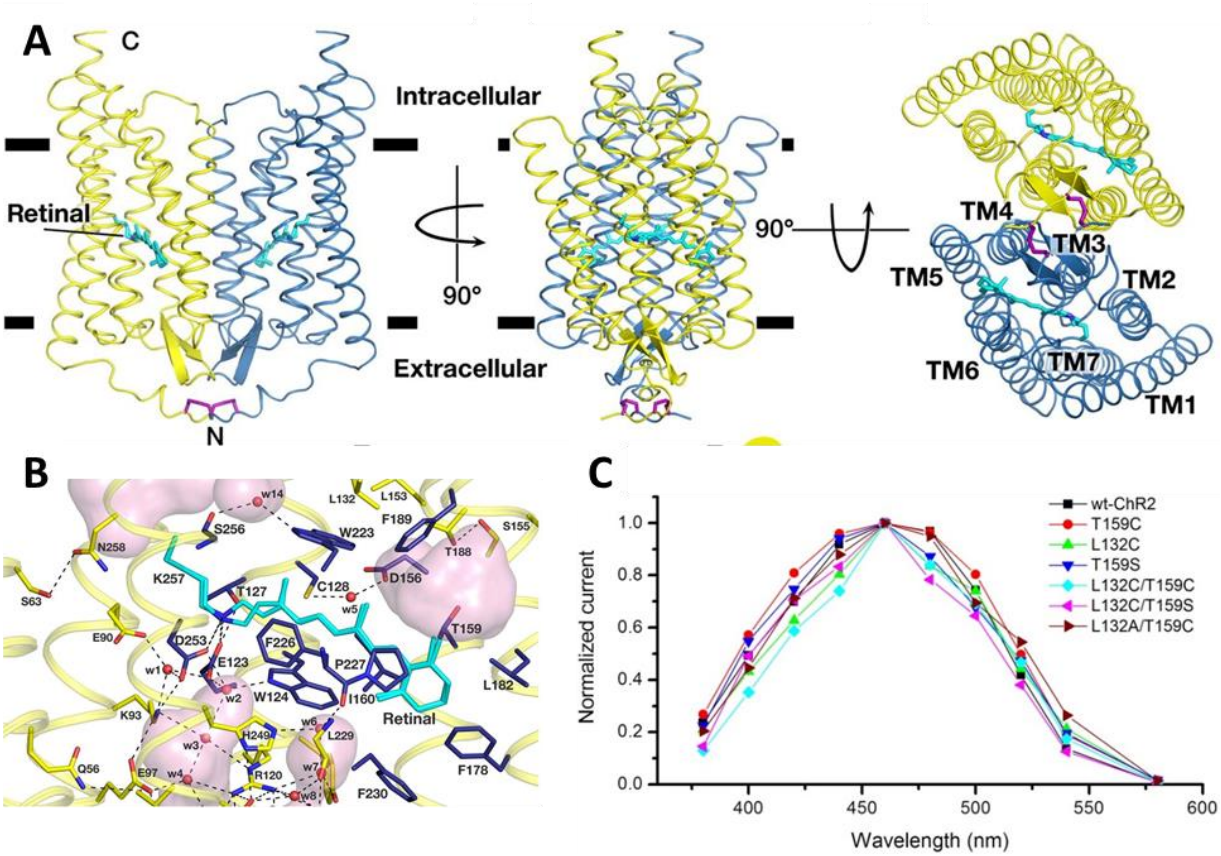

Figure 14 - Channelrhodopsin 2 (ChR2)
A structure of channelrhodopsin from different angles (cysteine bridges: purple)[183] **B** Retinal cavity (light blue: retinal, dark blue: interaction partners)[183] **C** excitation spectra of different ChR2 mutants[184]

The channel opens between 380 and 540 nm wavelengths with a maximum current at 480 nm. (Figure 14 C) Exposed to these wavelengths, the gates open and the channel becomes permeable to cations, leading to cell depolarization.[183] Single-point mutations in the retinal cavity are known to lead to altered channel kinetics. The T159C mutation used in this thesis has higher sensitivity and currents than the WT-ChR2, whereas the response time is unaffected.[184] Mutation L132C exhibits even higher currents, however, the decay time and the kinetic are impaired. WT-ChR2 and ChR2 T159C have a fast and adaptive signal initially, decreasing to the steady state level after repetitive activation.[184]

3.3 High throughput screening (HTS) strategy

As Fraietta and Gasparri described in 2016, introducing high throughput screenings has given a powerful tool for drug discovery.[185] In this thesis, an HTS campaign was established to test 1 200 000 compounds of the Bayer compound library on their agonistic effect on the insect VSSC. The HTS cell line was expressing the VSSC of *Musca domestica*. It was co-expressed with channelrhodopsin 2 T159C (ChR2) implemented in the screen as a light-sensitive channel to activate the sodium channel. The frequent light application (pacing) facilitate the numerous and synchronized transition through the VSSC states (Figure 15).[41,186,187]

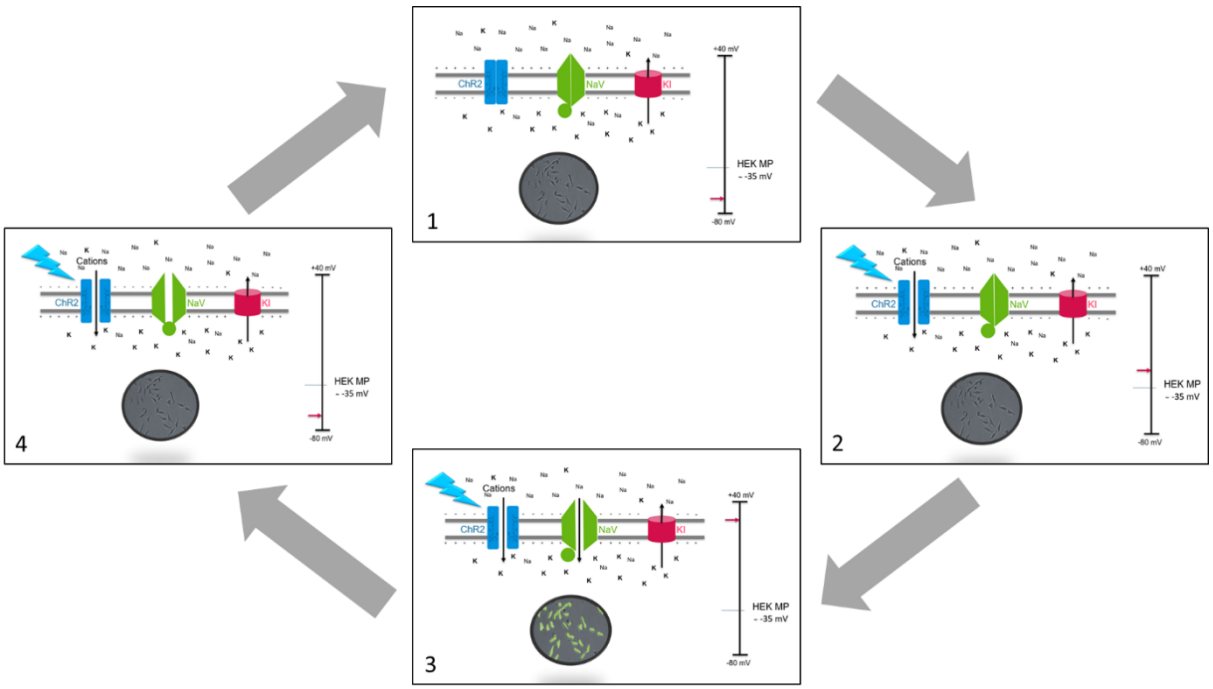

Figure 15 - depiction of the channel activations during light pacing.
Lightning: blue light pulse, blue channel: ChR2, green channel: sodium channel, red: potassium pore, scale: membrane potential

The demands on buffers in high throughput systems must fulfill high standards regarding buffer stability, expenses and device compatibility.[188] The FLIPR Tetra is a fluorescence imager produced and marketed by Molecular Devices. Even though the device can measure up to 4 different wavelengths, the flexibility regarding time and intensity is limited. The capabilities, however, were sufficient to optimize several aspects and give a proof of concept. The decision on the membrane potential sensitive dye was explained in chapter 3.1.2 Fluorescence Measurements.

The fast kinetics featured by ChR2 and the VSSC reported by Hodgkin & Huxley and others for the sodium channel and Pan et al. for ChR2 T159C do not match the kinetics of the voltage-sensitive dye. Whiteaker measured in 2001 a slow response of the dye towards depolarization.[41,186,187] Although the kinetics are too slow to display the fast switching of the VSSC, the channel is transitioning through the channel states.[152]

The structure of the HTS campaign features strong similarities to the cascade published by Yu et al.[153] The HTS cascades constitute different steps, with higher tier studies at each step. In Figure 16, the HTS strategy for the campaign is depicted to gain more confidence with each step. The chance to detect false positives is higher with each step, so the amount of compounds tested constantly decreases.

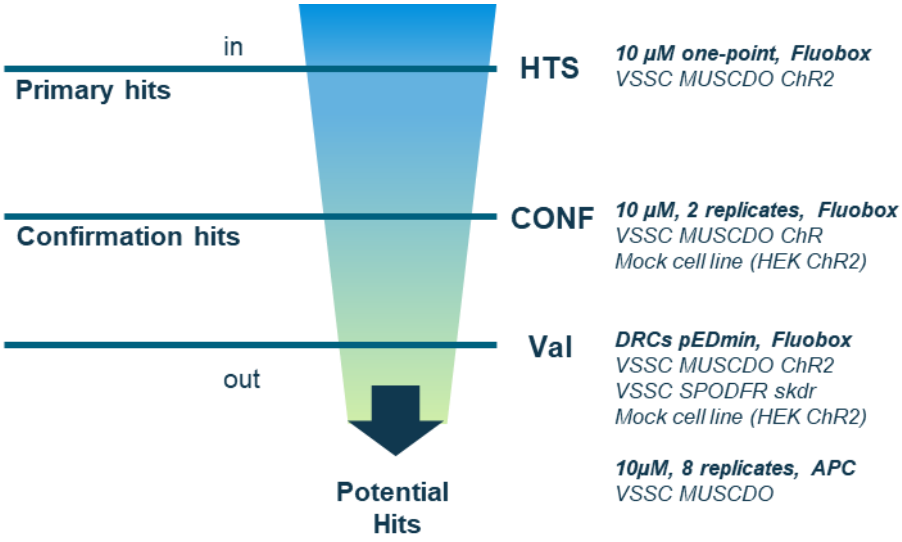

Figure 16 - Screening cascade including primary HTS, confirmation and validation
Besides the different screening steps, the applied test parameters, relevant values and used cell lines are listed.

As an orthogonal assay, the high throughput electrophysiology platform SyncroPatch384 is chosen for a second assay during validation, discriminating between false- and true positives. Automated Patch Clamp (APC) measures the Na^+ currents with a very high signal-to-noise ratio and is, therefore, less susceptible to false positives and more sensitive to weak modulators as shown by Bruegemann et al. in 2004.[195] Thus, it is a complementation to a fluorescence-based HTS assay, measuring indirect effects via the membrane potential.[153] The APC measurement not just facilitates the electrophysiological control over the VSSC but gains insight into the effect of the modulators and provides another high throughput readout method. [153,196] The advantages like direct readout, MoA classification, and sensitivity of the electrophysiological measurement over the fluorescence are comparably expensive to fluorescent readouts and therefore implemented late in the cascade. More decisive for the nomination of compounds for biochemical validation is the performance in the orthologue APC assay.

After identifying primary hits, the chemical cluster is determined in a hit expansion. Therefore the chemical surrounding is investigated to synthesize close chemical analogs or search for available libraries. The identified cluster members are then checked in the same tests to prove the consistency among the whole clusters.

The last step of verifying ion channel modulators is the evaluation in manual patch clamp as the highest tier study and nerve recordings to complete the characterization and validation. Modulators also performing in this step will show a certain level of selectivity towards the human VSSC, have a known effect and exhibit resistance-breaking potential. Those candidates are promoted to the hit exploration to synthesize further compounds with similar chemical structures to enlarge the knowledge about structure-activity relationships.

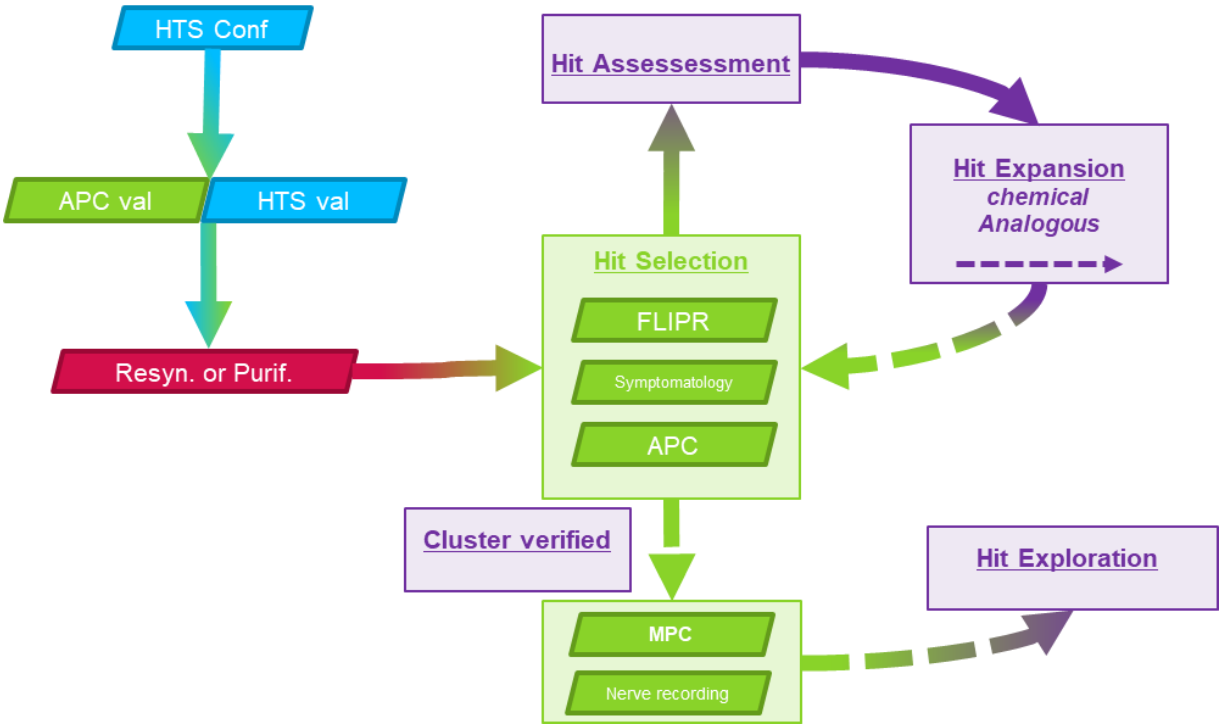

Figure 17 - Biochemical cascade for the verification of HTS-derived hits
Shown is the testing cascade containing HTS (High throughput screening, optogenetic-based fluorescence readout), APC (automated patch clamp), purification FLIPR measurements (fluorescence readout), symptomatology (injections in Spodoptera larvae), MPC (manual patch clamp) and nerve recordings, (in situ recordings at isolated nerves).

3.4 Mutagenesis

Mutagenesis is the targeted exchange of nucleotides in protein-coding regions (mutations). After transcription and translation, these altered genomic sequences are transferred into proteins. Mutations can have different effects on the product. They can either be silent, non-sense or missense mutations. Silent mutations are of little interest as they mostly do not affect the product. They can occur as several nucleotide triplets may code for the same amino acid.[198,199] In non-sense mutations, an amino acid coding triplet is now coding for a stop codon.[200–202] This kind of mutation is just required for deletion mutants and the investigation of single protein domains. Mis-sense mutations result in an exchange of one amino acid with another, for example, in identifying binding sites and post-translational modifications.[203]

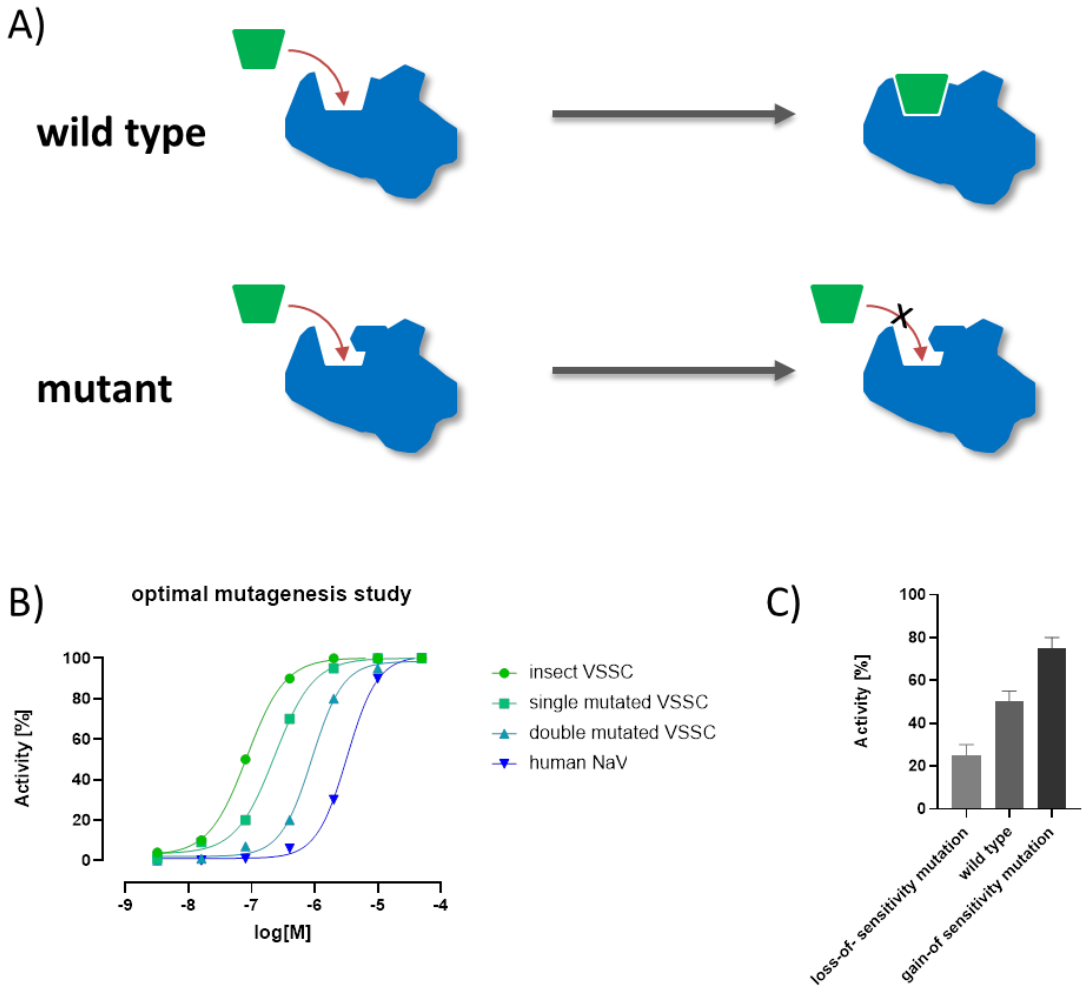

Figure 18 - Mutagenesis studies as planned in this thesis
A) Illustration of mutagenesis studies as performed to generate loss-of-sensitivity mutation for binding site detection. B) Illustration of a concentration-response measurement for insect selective compounds at wild-type and mutated channels. Shown are fictive results for generating loss-of-sensitivity mutations by taking advantage of insect selectivity. C) Bar chart for exemplary results for a loss-of-sensitivity and gain-of-sensitivity mutant.

The investigation of these mutated proteins can have different advantages in research. It can be used to investigate the role of a protein in diseases and animal models by silencing or enhancing protein functionality.[203] Furthermore, it can be used to examine the role of post-translational modifications on the protein function and the importance of single amino acids on the catalytic, steric and localization features.[204] In this study, mutagenesis was used for the identification of the binding site of newly found VSSC modulators as Cane did in 1995.[205]

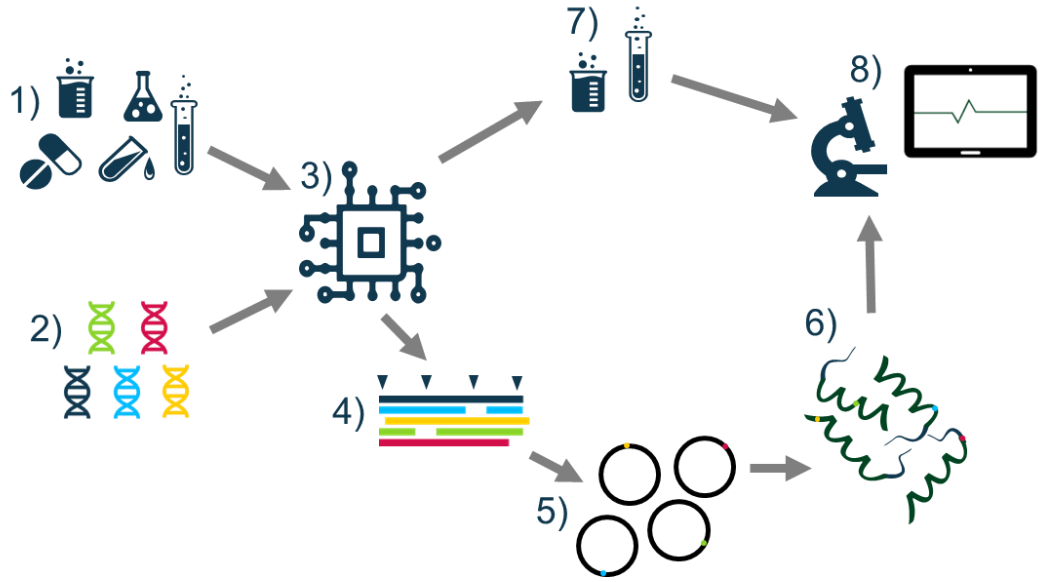

Figure 19 - Depiction of workflow for mutagenesis studies
1) Compounds with selectivity information, 2) protein sequences, 3) bioinformatic analysis, 4) alignment of protein sequences, 5) plasmid ordering, 6) protein expression, 7) tool compound selection, 8) mutagenesis experiment

Identifying binding sites with mutagenesis can be approached in two ways: generating either a gain-of-sensitivity or loss-of-sensitivity towards the substance of interest.[206,207] Typically, amino acids are exchanged with close homologs for this purpose, differing in one structural feature, a functional group, lipophilic side chain, etc. Typical partners for exchange in both directions are: Ser vs. Ala or Tyr vs. Phe (OH-elimination), Phe vs. Ala (benzol-elimination) and Gln vs. Asn (chain-reduction).[208] Knowledge of the region where the modulator binds is advantageous, as it drastically reduces the possible mutations. Functional studies, literature known homologs and protein structures can make conclusions about the regions. In the case of the investigated VSSC modulator, taking advantage of the target-selectivity between insect and human channels was possible. The strategy was to humanize the insect channel to create a loss of sensitivity mutation. (Figure 18) Alignments of insect VSSCs and human NaVs determined the insertion of a surrogate amino acid. Inserting a human surrogate amino acid enhanced the chances of maintaining functionality.[209,210] Functional expression was essential for the investigation, as activities were quantified by electrophysiology. (Figure 19 8))

Suppose the first mutation shows a significant decline in sensitivity. In that case, a second mutation is implemented to strengthen this tendency, homolog to the natural occurrence of the kdr (single point mutation) and skdr (double point mutation).[214]

3.5 Cryo-EM as uprising technology for structure elucidation

Cryogenic electron microscopy (cryo-EM) is a method developed and improved by Henderson, Frank and Dubochet. In 2015 cryo-EM was voted the method of the year by nature and in 2017, it was awarded the Nobel Price.[208] Cryo-EM is a powerful method for structure determination, a powerful tool for the structure elucidation of membrane-embedded proteins, which are hard to crystalize.[215]

The availability of electron detectors and the enhancement of algorithms used for image processing supported this technique's rapid gain of importance. Besides others, two main approaches exist for the generation of 3D models via cryo-EM. SPA (single particle analysis) cryo-EM studies analyze isolated macromolecules and protein complexes *in vitro*. Cryo-EM via ET (electron tomography) is mainly used to analyze cellular structures. Methods like micro-electron diffraction and cryo-scanning transmission electron microscopy (cryo-STEM) are not as relevant today.[216]

In cryo-EM, SPA 2-4 Å resolution 3D atomic models are generated by aligning several thousand images using state-of-the-art processing algorithms. The rapid freezing of samples ensures the maintenance of the natural state of the investigated protein. The low effort regarding sample size and purification makes it an exciting method for generating multiple atomic maps.[216] Critical for a good SPA sample is the density of investigated complexes embedded in a thin layer of ice. Sample preparation was shown to be the bottle neck for cryo-EM. Several scouting trials need to be performed to identify the optimal parameters, like changes in concentration, detergent or addition of support films. The sections chosen for analysis are selected carefully. Nowadays, live image processing is supporting the decision for valid sections. Better user-interfaces facilitate a simplified introduction to the topic and further boost the area of research.[215,216]

Cryo-EM was used to study channel-ligand complexes to understand the mode of action better and binding modalities. The resolved structures can be used to deduce the chemical surrounding of potential ligands.[216]

4. Aim of the thesis

The aim of the thesis was the electrophysiological characterization of a voltage-sensitive sodium channel, including the investigation and identification of state-dependent compounds. Furthermore, an optogenetic pacing protocol shall be developed which is suitable for high throughput screening. For this implementation we need to investigate the interaction between light-induced ChR2 activation, voltage-sensitive sodium channel response and fluorescent readout (voltage-sensitive dye).

The overall goal of this thesis is the implementation of a VSSC screening campaign at Bayer Crop Science, including the first optogenetic high throughput screening, to find new lead structures. This part also comprises the HTS validation by electrophysiological and symptomatological investigations and selectivity studies on the human VSSC.

To overcome the problem of cross-resistances, an additional project focused on mutagenesis studies to identify and investigate different binding sites and binding modes of compounds at channel proteins.

5. Results & Discussion

5.1 Introduction of pEC_{10} as decisive value for VSSC modulators

The EC_{50} or IC_{50} are the most common values, calculated based on dose- or concentration-response curves, to compare compound efficacy. They describe the dose or concentration mediating 50 % of the effect in the used test system, either the effector (EC) or inhibition (IC). The half effect can be calculated and represents the inflection point of the sigmoidal curve when concentrations are plotted logarithmically.

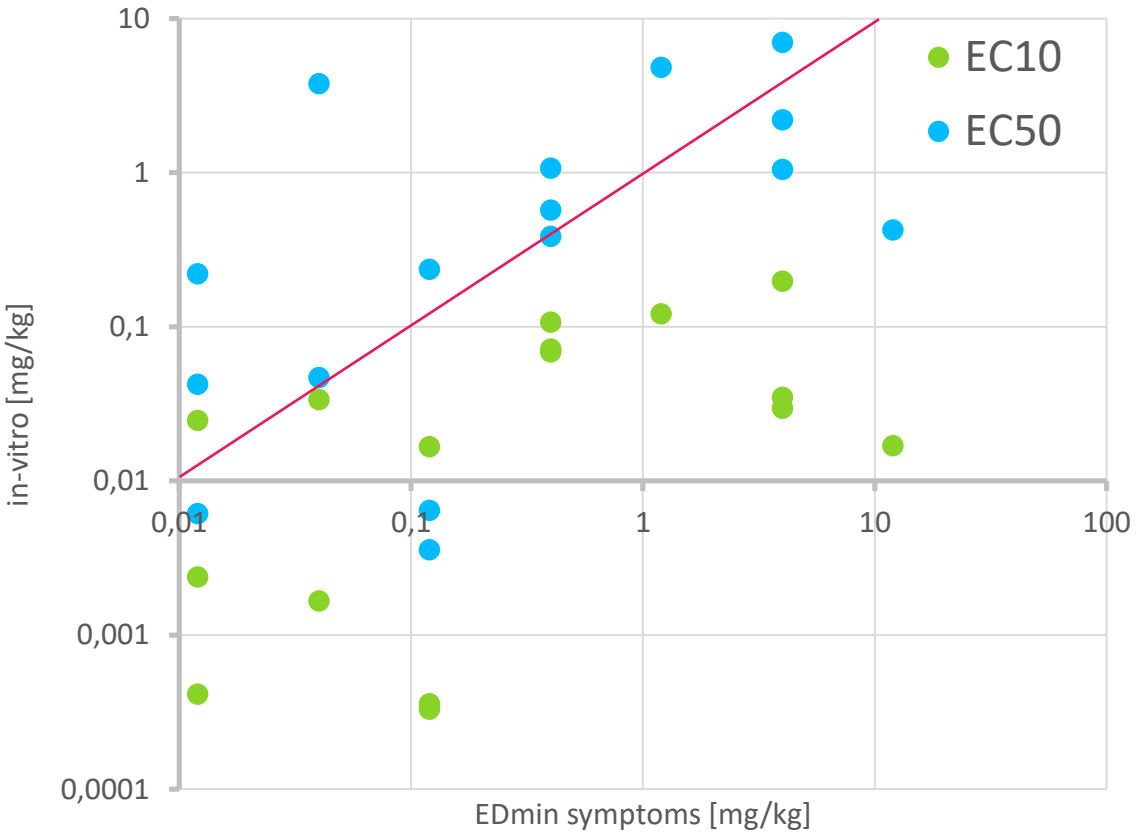

Figure 20 - Correlation of *in vivo* vs. *in vitro* data of pyrethroids
In-vitro activity (EC-values, gained on Na channel in FLIPR assay - fluorescent readout) plotted towards the in-vivo activity (minimal effective dose to induce symptoms acquired by injection in *Spodoptera frugiperda* larvae). In-vitro data were transferred into doses instead of concentration to prevent data aggregation and have them comparable. Straight line indicates bisectors of an angle with a slope of 1 (line).

In Figure 20, the measured *in vitro* values, calculated based on concentration-response curves, are plotted against the doses required to induce symptoms in injection tests. Each compound is represented by two points, one in green showing activity of 10 % (EC_{10}) in the fluorescence assay and

one in blue representing the point of half activation (EC_{50}). Almost 70% of the EC_{50} values and one EC_{10} are above the straight line, pointing out the stronger in-vivo activity of most compounds than the in-vitro activity indicates. Most compounds showed an approximately 2-20-fold stronger and one compound a 100-fold stronger in-vivo activity compared to the in-vitro efficacy by using EC_{50}. This effect becomes even stronger when considering metabolization and excretion. The enhanced correlation of EC_{10} compared to EC_{50} could be explained by the self-enforcing nature of the sodium channel, as described by Gilly and Armstrong, lowering the *in vitro* activity necessary to see in-vivo effects.[197] As soon as the membrane potential reaches the threshold potential, all available sodium channels open and affect the nervous system. Electrophysiological measurements show that 1 % of modified sodium channels already have a physiological function on relevant pest organisms like *S. frugiperda*. (personal communication with Ebbinghaus-Kintscher) In fluorescent assay systems, 10% activity represents the threshold for reliable discrimination between signal and noise, as shown by Whiteaker and is, therefore, the lowest activity to be reliably determined.[152] Besides the higher target effectivity, the distribution above the lines could be explained by compound accumulation at the target side or a side target for the pyrethroid, which could be targeted by compartment purification and quantitative spectrometry.

These results describe the pEC_{10} as an adequate value to determine predictive values for in vivo activities.

5.2 Validation of HTS cell lines (VSSC ChR2 and skdr VSSC)

The optogenetic VSSC cell line was developed at AXXAM, and the tool compounds required for the internal verification of proper channel expression at AXXAM were provided by colleagues from Bayer AG. The validation of the cell lines is crucial for the different experiments planned. The cells were validated based on their activity and pharmacological profile. After arrival, the cell lines were tested in-house to prove sufficient expression and assay compatibility. The first cell line tested was the optogenetic cell line stably expressing channelrhodopsin 2 T159C from *C. reinhardtii* and the α and β-chain of the VSSC of *M. domestica* HEK293 cells. The functional expression of both channels was proven in manual patch clamp experiments. The expressed channel responded with a short, activated state and a subsequent inactivation during elongated depolarization. (Figure 21 A) After repolarization, the channel can be activated again, as reported by Hille in 1984 and Stühmer et al. in 1989.[217,218] The VSSC exhibited robust currents of 5 – 10 nA in response to a depolarization from -100 mV to -10 mV. The presence of ChR2 was proven by applying blue light with the wavelength of λ 480 nm (Figure 21 B). The fast primary response at the beginning of a peak was adaptive. After repetitive activation, it was reduced to the permanent current. This behavior is characteristic of the ChR2 response as published by Nagel et al. in 2003.[181] The high and robust currents published by Berndt et al. in 2011 and Pan et al. in 2014 for the T159C mutant were also visible in the expressed channel.[184,219]

Besides the electrophysiological measurement of the VSSC, a second requirement on the cell was the measurement in the fluorescent-based assay with a membrane potential sensitive dye. The response in the second system was part of the characterization due to its importance for the later performed HTS. With rudimentary pacing capabilities, the kinetic baseline (till second 200) was elevated for both conditions (in the presence and absence of TTX). After applying the reference compound, the insect-selective VSSC modulator leads to a substantial signal increase. TTX application did not lead to increased signals, and the kinetic remained at the elevated baseline level. The baseline elevation indicated a reliable measurement of ChR2 (by blue light). Discrimination between the endogenous expression of human VSSC in HEK (human embryonic kidney) cells, as described by Zhu et al. in 1998, and the insect VSSC was done pharmacologically by applying the insect-selective reference compound Bayer Cpd 8. (Figure 21 C))[220]

The ChR2 was implemented into the cell to gain control of the membrane depolarization and activate the VSSC. The interaction of both channels was investigated in current clamp measurements. This interaction was investigated in current-clamp experiments on the cell line (Figure 21 D) as described by Agus.[221] At holding potentials of -120 mV, blue light application (480 nm, 50 ms) activated the ChR2 and increased the membrane potential to -60 mV. The increase was insufficient to reach the threshold, activating the whole VSSC population and generating action potentials as shown by Olson

et al.[69] A slightly elevated holding potential to approximately -100 mV facilitated the ChR2 response to overcome the threshold and led to the activation of the whole sodium channel population. In response to a light application, the threshold potential is reached by ChR2 opening and all sodium channels open, resulting in a fast peak signal comparable to action potentials described by Hodgkin and Huxley, reaching potentials of 30 mV.[112] The repetitive light application leads to action potential-analog signals close to sodium's equilibrium potential, indicating the sodium channel's frequent transition through the different states, as shown by Zhang.[222] This frequent activation lays the ground for the concept of the enhanced HTS assay and might support the identification of state-dependent modulators.

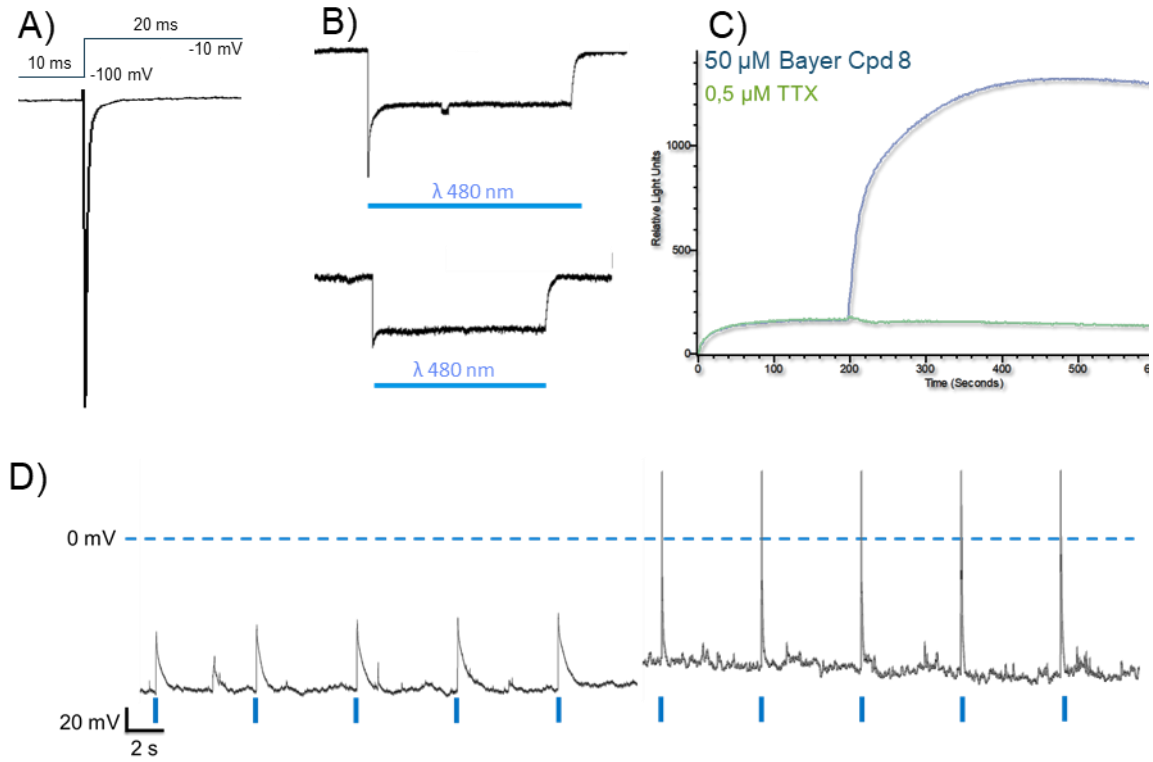

Figure 21 - Characterization of the optogenetic VSSC cell line
A) Identification of the *M. domestica* VSSC based on the electrophysiologic and pharmacologic behavior B) Proof of functional channelrhodopsin 2 expression after multiple excitations after blue light pulses (λ 480 nM, blue bar) C) proving the ChR2 VSSC cell line measurement conditions in the fluorescent assay at the FLIPR Tetra D) Current clamp measurements at the optogenetic VSSC cell line at two different membrane potentials to validate the postulated channelrhodopsin – VSSC interaction.

Another essential cell line ordered at AXXAM is the skdr cell line, expressing a pyrethroid insensitive mutant (T929I & L1014F) of the VSSC heterodimer of *S. frugiperda,* as described by Sawicki in 1978.[214,223,224] The cell line was ordered to give an early prediction on the resistance breaking potential of compounds during validation steps, enclosed to the hit validation for the HTS campaign.

Analog to the *M. domestica* channel, the cell line was validated pharmacologically in electrophysiology and the cellular fluorescent assay. (Table 3)

Table 3 - The activity of compounds selected for electrophysiological characterization at WT and resistant VSSC

Figure 23.	Bayer Cpd	MUSCDO WT	SPODFR resist
A)	Bayer Cpd 1	4.3	<4.3
B)	Bayer Cpd 2	5.6	<4.3
C)	Bayer Cpd 3	5	<4.3
D)	Bayer Cpd 4	7.1	<4.3
E)	Bayer Cpd 5	7.4	<4.3
F)	Bayer Cpd 6	5.3	5.7
	Bayer Cpd 7	5.9	6.5

Bayer Cpd 7 belongs to the same class as cpd 6 and features structural similarities

The switching behavior of the channel as a response to a depolarizing pulse is a homolog to the behavior of the *M. domestica* VSSC. After a short channel opening, it transitions into the inactivated state, which is not closing completely compared to the WT *M. domestica* channel. The result is a slowly decreasing current from 20 % directly after depolarization compared to 10 % current after 700 ms, mutations can cause such altered channel physiology as Li already described.[225] The response after pyrethroid (β-cyfluthrin) application was similar to the control trace (Figure 22), indicating the expected loss of sensitivity towards pyrethroids as described by Martinez-Torres et al.[214] The tool compound with another mode of action and resistance-breaking potential shows equal activity in the inactivated state at the skdr mutant compared to the WT.

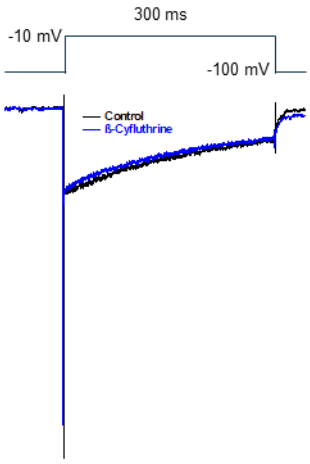

Figure 22 - Characterization of the s-kdr VSSC cell line
Superimposed current responses of the double point mutated *S. frugiperda* VSSC (skdr) after voltage pulse application before (black trace) and during application of 10 µM β-cyfluthrin (blue trace). The cell was clamped to holding potential -100 mV, pulse consisted of 300 ms depolarization to -10 mV

5.3 Electrophysiological characterization of VSSC modulators

The HTS assay aims to identify all kinds of VSSC agonistic modulators. An assembly of all known VSSC effects is listed to point the focus on the requirements and features of the developed assay. Modulators binding to one of the four channel states (see Figure 7) can have one or more effects. Figure 23 shows which effects could be measured by targeting the channel states electrophysiologically. Automated patch clamp experiments gained the data on stable cell lines expressing the VSSC of *Musca domestica*.

Various effects are altering the inactivation of sodium channels. Different neurotoxic peptides (α-scorpion toxin and δ-conotoxin), isolated from scorpions and marine snails, facilitate conductance during fast inactivation as described by Kirsch et al., Benoit and others.[226–230] The application of Bayer Cpd 1 inhibits the same state and shows a sustained opening during the fast inactivation (Figure 23 A). After repolarization, the channel is transferred into a closed resting state, preventing ion flux The comparably low pEC_{10} measured in the fluorescent screen might be traced back to a degradation of the compound. Another effect, mediated by Bayer Cpd 4 is delayed inactivation, resulting in broadened sodium peak during activation. Within a few milliseconds, however, the inactivation is complete, and sodium flux is no longer impeded. Both kinetics convey a binding during the open state. The effect of 10 µM Bayer Cpd 3 is contrary to the delayed inactivation. However, it also modifies the fast inactivated state. The sodium channel peak remains unaffected and almost recovering to the level of the control trace in contrast to Figure 23 A and B. During fast inactivation, the channel opens again, with currents getting stronger over time (Figure 23 C). After repolarization, currents decline with far lower kinetics than observed for A). This kinetic conveys modulator binding during the fast inactivated state with slow dissociation after repolarization.

Bayer Cpd 4 affects fast inactivation as well as repolarization. The VSSC does not convert to the closed state following the inactivated state but remains open. This pattern is typical for pyrethroids and was first described by Narahashi.[73] It requires prior channel activation, which indicates binding during the open state.[73,231] Within the pyrethroids class, the effect level on the inactivated state varies from significant effects on the state to effects restricted to the subsequent effect (tail-current).[232] The tail current is always higher than the current on the inactivation. The electrochemical driving force for sodium influx is significantly higher at more negative membrane potentials, as the Goldman-Hodgkin-Katz equation describes.[19,20] Another aspect typical for pyrethroids is the use-dependency as first described by Vijverberg.[233,234] Therefore, I measured the pulses in Figure 23 E at a frequency of 50 Hz, with an increase of the pyrethroid-mediated effect of 50% between pulses one and two and a 25% increase between pulses two and three. This indicates an increase of pyrethroids binding to parts of the VSSC population upon each activation and more VSSC stay in the open state as Zhorov and Dong were showing recently with an AI-guided AlphaFold2 model.[74,234,235]

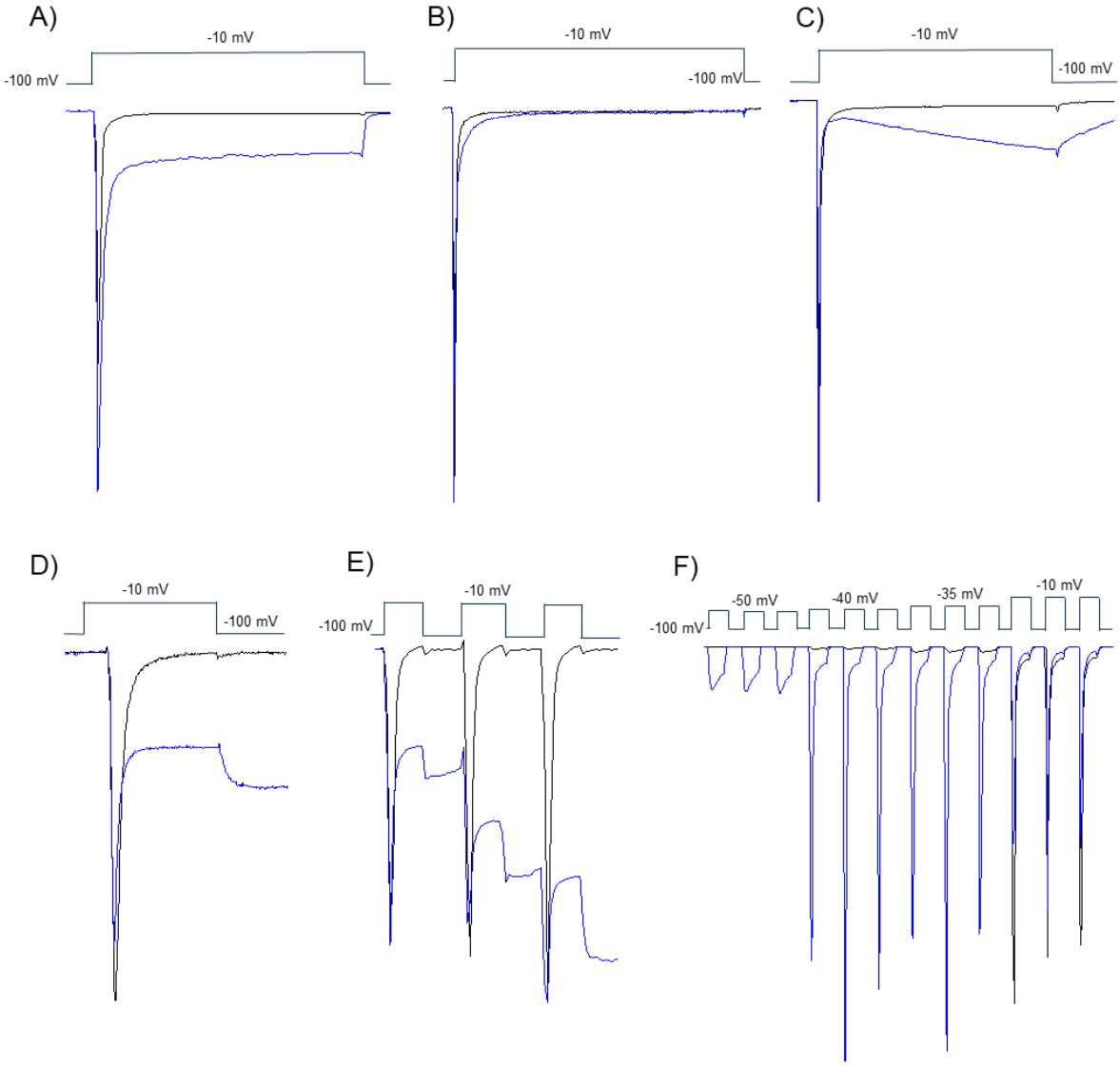

Figure 23 - Different modes of action at the sodium channel
Shown are different modes of action at the sodium channel in the presence (blue) and absence (black) of different tool compounds. The effect is dependent on the pulse protocol used to mediate particular channel states: A) Inhibition of fast inactivation mediated by 10 µM Bayer Cpd 1 B) Slowing of inactivation mediated by 10 µM Bayer Cpd 2 C) activation during inactivation mediated by 10 µM Bayer Cpd 3 D) tail current mediated by 10 µM Bayer Cpd 4 E) use-dependency mediated by 10 µM Bayer Cpd 5 F) voltage shift mediated by 10 µM Bayer Cpd 6.

The effects observed (Figure 23 A-E) were mediated by modulators sharing the same binding site, as indicated by a lack of activity at the skdr mutant (see Table 3 in 5.2 Validation of HTS cell lines). All of the used modulators are presumably binding to the pyrethroid binding site (site six characterized by Lombat et al.)[64] and are therefore considered pyrethroid-like. The sodium channels of Musca domestica (MUSCDO) and Spodoptera frugiperda (SPODFR) were used in the test. Nevertheless, the data are conclusive, as pyrethroids are active in both species, as shown by Casida et al. and Smith et al.[236,237] The voltage shifter exhibits an enhanced activity at the pyrethroid-resistant mutant,

favorable for the development of new insecticides.

Contrary to the suggestion of Catteral, Lombet et al. and Slotkin et al. trying to assign VSSC binding sites to different VSSC effects, the data show that the identification of binding sites only based on the modulatory effects is not possible.[62–64] If modulators with new effects are found on the VSSC, this aspect may hint at new binding sites at the VSSC and resistance-breaking potential. The classification of binding sites based on the effects of all these tool compounds facilitates just assumptions. For clarification, mutagenesis or radioligand binding studies with docking experiments can gain more confidence, as done by Morandi and others.[238–241] Those techniques may also be affected by allosteric effects, so only structural clarification via crystallization and cryo-EM can precisely define a binding site.

The voltage shift of the activation to more negative potentials is another agonistic MoA known on the VSSC (Figure 23 E) and described for β-scorpion toxin and brevetoxin by Campos et al. and Catteral et al.[242,243] Compound binding mediates an early opening at potentials below the threshold. It has the same kinetics under control conditions, with a fast inactivation and a lacking tail current. The effect leads to the assumption that such shifters are binding at the resting state and open the channel at more negative potentials.

These data showed the relevance of optogenetics to facilitate transitioning between different channel states to expose binding sites during HTS and establish an optimal pacing protocol.

5.4 High throughput screening optimization

5.4.1 Buffer-conditions

Implementing optogenetics in this assay required adding extra agents into the buffers. The first tests to ensure these aspects were conducted at the FLIPR Tetra to optimize buffer and culture conditions. The assay window or response over baseline (RoB) was one quality parameter. A high RoB is important for the discrimination between weak modulators and false positives, it grants low thresholds for later hit picking and is therefore desirable. [244]

The first adjuvant required is retinal from an external source. It is the light-sensitive co-factor for channelrhodopsin 2. Our studies on the effect of retinal on the HTS cell line showed increased signals with substitution of 5 nM retinal in advance to the measurement of 38 %, coherent with the *in vivo* results of Srinivasan.[245] The retinal was applied 60 min before the experiment started. The increase remained unaffected after applying 0.5 µM tetrodotoxin, a well-known sodium channel blocker (Figure 24). Besides cost reduction, a reduction or even elimination of retinal in the buffer would have resulted in higher stability of the buffer. Granit et al. and Nakanishi reported in 1939 and 1991 the conformational change of the retinal in response to light stimulus, making it unusable for ChR2.[246,247] To circumvent any issues with the retinal, all experiments were performed in the dark or, if not possible, under yellow light to prevent unbound retinal or channelrhodopsin activation

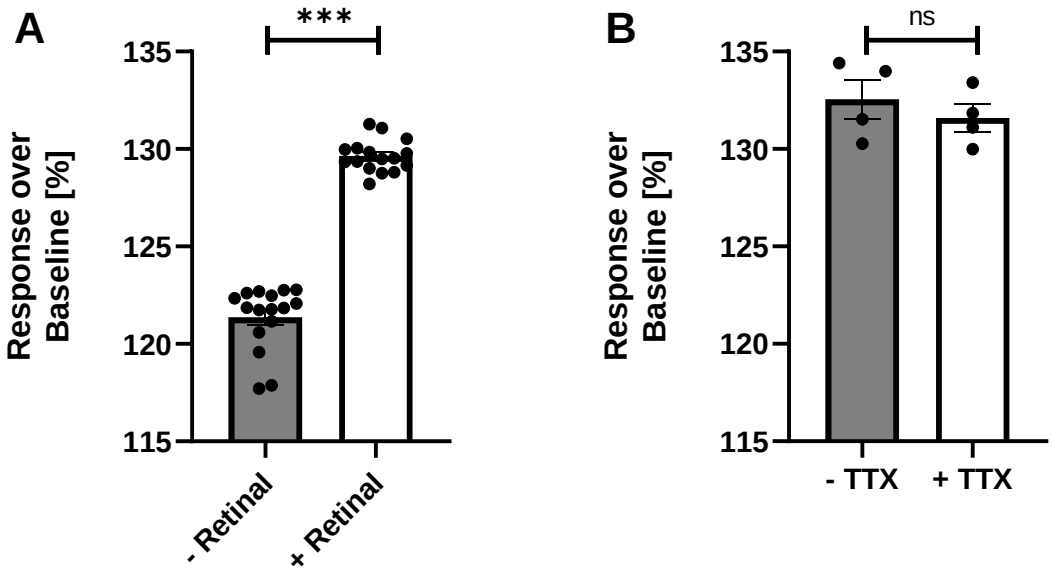

Figure 24 - Importance of retinal for the optogenetic VSSC assay
Shown is the importance of retinal for the channelrhodopsin response. **A** shows the effect of retinal on the target cell line. The addition of retinal in the buffer led with high significance to a 38 % stronger signal (p = <0.0001). B The addition of 0.5 µM TTX did not affect the response.

All following improvements required the application of VSSC modulators to detect signal changes. As a tool, the reference compound was chosen to identify changes in the RoB, as a potent VSSC

modulator, the same reference implemented as standard in the later HTS campaign. For the characterization of the reference compound, a concentration-response curve was measured. (Figure 25) By norming all values to deltamethrin like Tay et al. did in 2019, a concentration of 10 µM reference compound reached 100 % VSSC activity. As 10 µM mediates a 100% effect and is not impaired by precipitation, this concentration was applied in the follow-up studies. Besides the EC_{max}, the pEC_{50} and pEC_{10} were measured and all values exhibited low standard deviations, making reference compound a suitable standard, based on the demands proclaimed by An and Tolliday.[248]

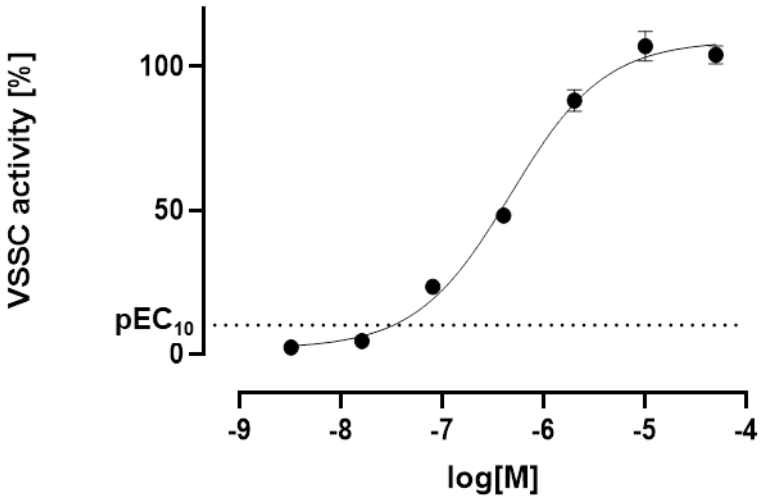

Figure 25 - Concentration-response-curve (CRC) of reference compound on *Musca domestica* VSSC
CRC was measured on stable and functionally expressed house fly voltage-sensitive sodium channels (VSSC) using a fluorescence-based membrane potential sensitivity assay. All values are normed to 1 µM deltamethrin resulting in a pEC_{50} of 6.33 ± 0.059 and a pED_{10} of 7.35 ± 0.136 with a maximal intrinsic activity of 100 %.

The optimal cell incubation was the next aspect under investigation. Incubation conditions and times are of tremendous importance for cells expressing insect proteins. Besides the maximal RoB, these experiments also calculated the slope as the second success factor. The hill slope is highly important in the later HTS, as the optogenetic approach and the fast channel physiology of the VSSC require quick response times and kinetics of the dye. The data shown in Figure 26 were gained with loading buffers containing 5 nM retinal and 0.75 mg/mL voltage-sensitive dye (VSD), half of the manufacturer's recommendation. However, this concentration was sufficient to feature advantageously in reproducibility and sensitivity.[149]

With 24 h incubation at 26°C directly after cell seeding, RoBs of approximately 275 % (SEM ± 13 %) were observed. A preincubation for 24 h at 37°C before the 26°C incubation was significantly advantageous with an RoB of 372 % (SEM ± 12 %). The same is true for the slope, where an increase of 40 % from 0.32 (SEM ± 0.02) to 0.53 (SEM ± 0.02) was shown for the preincubation at 37°C. The

RoB reduction might result from reduced cell health and a reduced number of attached cells, as seen in other assay systems.[249–251] After showing the advantage of a 37°C preincubation, the impact of two different incubation periods at colder temperatures was investigated. Prolonged incubation of 24 h at 26°C was significantly advantageous in both factors over shorter incubation at colder temperatures. The RoB is about 20 % higher (301 % ± 7 % vs. 372 % ± 12 %) when 24 h incubation at 26°C and a slope increase of 15 % (0.46 ± 0.1 vs. 0.53 ± 0.02). The discrepancy between 24 h at 26°C and 6 h at 20°C shows that a proper VSSC expression requires time and 26°C

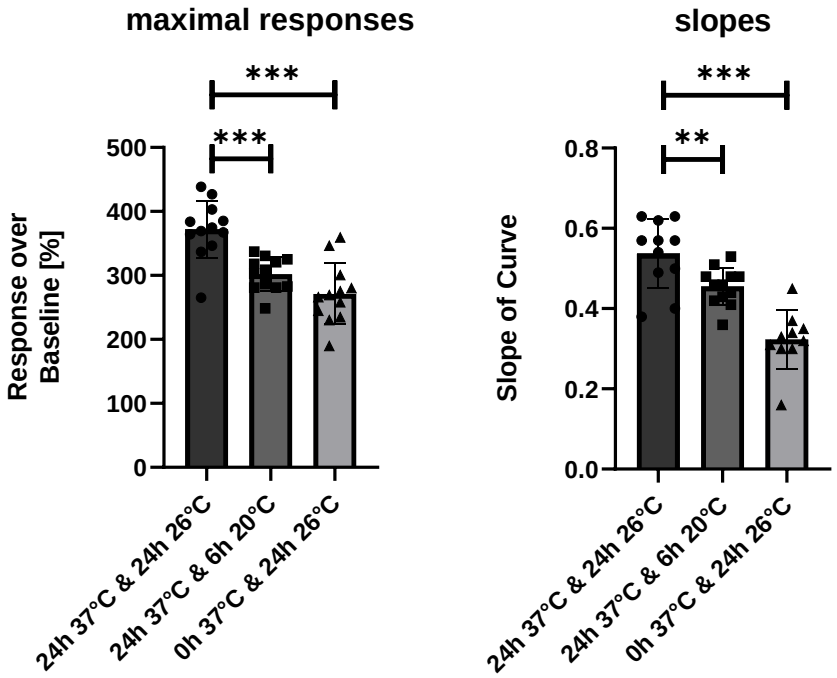

Figure 26 - Effect of different incubation parameters on the kinetics of the sodium assay
The effect of different incubation times on the window size (Response over Baseline) and the slope is shown. The factors were measured after applying 10 µM reference compound and the slope was calculated from the moment of application to the point of the kinetics' maximum.

The next step was proving the importance of the potassium ionophore (KI: Bayer Cpd 9) by showing significantly increased measurement windows from 300 to 400 in rudimentary experiments on the FLIPR Tetra (Figure 27). The ionophore comes along with two advantages to enhance the measurements. The potassium efflux mediated by the KI leads to reduced membrane potential on an excitable level, similar to potassium leak channels, as published by Miller and Wiedmann et al.[252,253] The voltage-sensitive dye used (VSD) for measurement is responding to a decline in membrane potential with a decreased baseline fluorescence. As the measurement window is calculated as a response over baseline, the low fluorescence measured as a baseline with an unimpaired maximum resulted in an enlarged measurement window. Furthermore, the KI is required for acquiring optogenetic control over the sodium channel. Jiang et al. have proven a resting potential for HEK

cells of -35 mV, leading to the transition into the slowly inactivated state of the sodium channel, as shown by Adelman & Palti in 1969 and Chandler & Meves in 1970.[253–255] They were also able to show that a transition from slow inactivated state to the open state is not possible and would therefore stand in conflict to the aim of the optogenetic implementation. The enhanced availability of VSSCs might have furthermore improved the RoB. After activating the sodium channel, the ionophore supports the repolarization of the cell. It shifts the sodium channel back from a fast inactivated to a closed state, similar to voltage-gated potassium channels in neurons. This aspect facilitates a frequent and simultaneous activation of the whole sodium channel population, as shown by Berndt et al., leading to an increased signal.[219] The optimal concentration of ionophore was determined by considering different pulse protocols (see 5.4.2 Development of light pacing protocol).

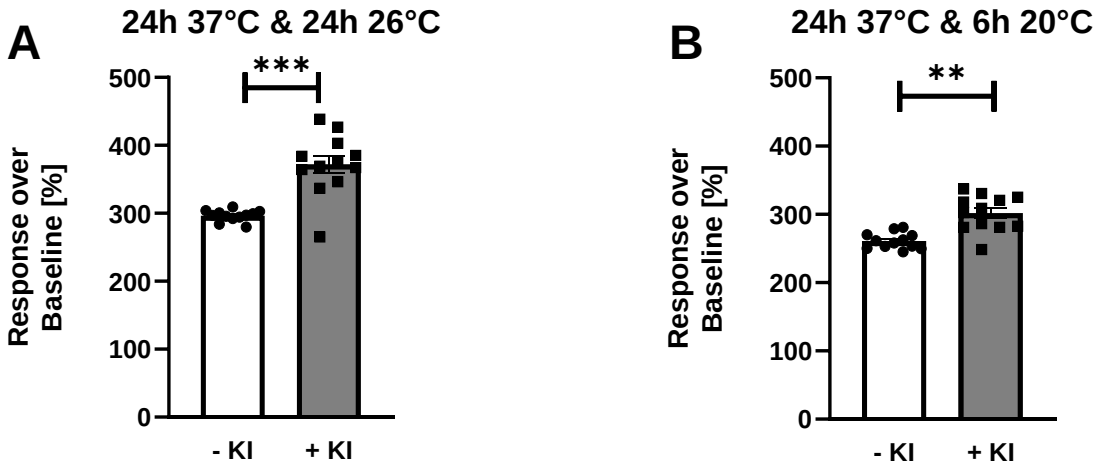

Figure 27 - Effect of the potassium ionophore (KI) on the window of the VSSC assay
A & B Show the influence of the KI (Bayer Cpd 9) on the window of the optogenetic VSSC assay under two different culture conditions. The white column with the dots represents the data gained in the absence of the KI, whereas the grey columns with the squares represent the data points in the presence of 20 µM KI.

To prevent detection by mistake of auto-fluorescent compounds, a quencher can be implemented in the loading dye as published by Marmor et al.[256] Wolff et al. and Jager et al. published the capability of ink quenching fluorescence in the liquid phase, while the fluorescent measurements on the z-axis of the cell layer remain unaffected.[148,257,258] The addition of 0.01 % brilliant black showed no significant change in the signal (Figure 28). Due to the missing disadvantages, it was added to the buffer.

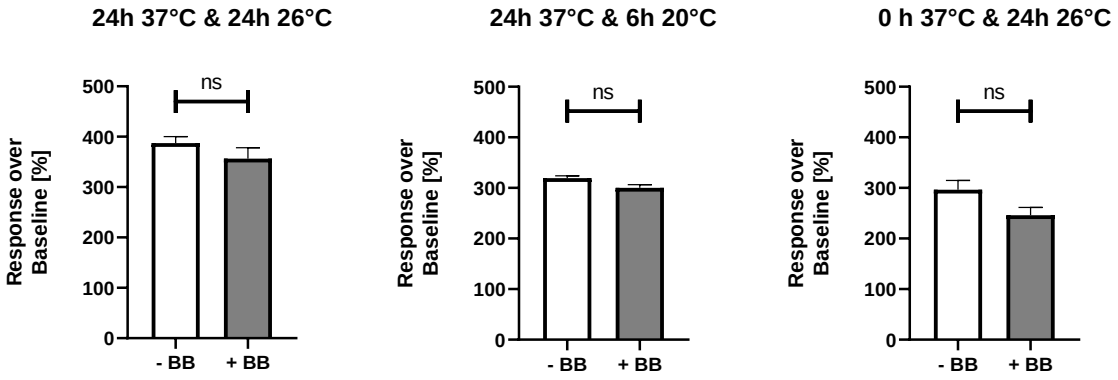

Figure 28 - Effect of brilliant black on the optogenetic VSSC assay
Shown is the effect of brilliant black (f.c. 0.01 %) on the window size of the VSSC assay after different culture conditions

This work has provided a suitable assay buffer for a medium-throughput assay. For a proof of concept on the advantage of the optogenetic screening approach, different tool compounds were tested on the regular VSSC cell line versus the optogenetic VSSC ChR2 T159C cell line. Both cell lines were measured under the same conditions regarding culturing (24 h 37°C & 24 h 26°C) and buffer composition (5 nM retinal, 20 µM potassium-ionophore, 0.75 mg/ml VSD, 0.01 % brilliant black). Adjustments on excitation intensity, frequency and measurement intervals were later performed at the Assay Imager.

Table 4 - Tool compounds used for assay optimization

Compound class	Bayer Cpd	Effects (see Figure 23)
Pyrethroids and pyrethroid-like	Bayer Cpd 10 Bayer Cpd 11 Bayer Cpd 2 Bayer Cpd 12	Tail current (open block)[233] Inhibition of inactivation[233] voltage shift[233]
DDT-Likes	Bayer Cpd 13 Bayer Cpd 14 Bayer Cpd 15	Tail current (open block)
BCS-Class	Bayer Cpd 16 Bayer Cpd 17	Inhibition of inactivation
ß-Scorpiontoxin-like	Bayer Cpd 18 Bayer Cpd 19	Voltage shift of activation

A comparison between the old assay and the new assay was not performed, as the concentration of the VSD was set 5-fold higher in the new assay setup. This change would have resulted in a far higher signal of the optogenetic cell line under all circumstances independent of the optogenetic pacing.
One significant advantage of the new assay was detected even without compound application. The

baseline values measured for calculation in the old assay system were randomly oscillating (data not shown). This made proper RoB calculations difficult and raised the baseline values, calculated over AUC. The new assay does not feature these oscillations. Oscillations were most likely spontaneous activations of VSSC, as also seen by Grimm et al. in iPSCs, as the membrane potential of the HEK cell fluctuated close to the threshold potentials.[220,259,260] Implementing the potassium ionophore and the ChR2 circumvented this effect and guaranteed more stability and control over the membrane potential.

Most window sizes were comparable between VSSC and VSSC ChR2 (Figure 29). Just minor variances were observed, with mostly higher values in the optogenetic cell line. However, these variances were within the tolerance of cellular assays. Pyrethroids, pyrethroid-like modulators, and DDT-likes are chemically optimized to reach market maturity and show high efficacies in in-vitro assays.[261–263] The high RoBs run towards saturation and efficacies point towards the activation of the whole VSSC population, explaining why signals cannot be further enhanced. Just for three compounds, more substantial deviations were observed (Figure 29). Both voltage shifters significantly increase 3 – 4-fold due to optogenetics. The difference between both signals is the discrepancy between detection and missing the MoA in a screen. Another increase was observed for Bayer Cpd 21, with a 2-fold increase for the inhibitor for inactivation. The other inhibitor for inactivation exhibits just a minor increase.

This increase can be explained by the voltage-shifting effect mediated by this compound class analog to the β-scorpion toxins as described by Wheeler et al. and others.[264,265] Opening of VSSC under HEKs physiological conditions is from the present state, as described earlier. The potassium-ionophore applied to the buffer in the new assay set-up reduces the membrane potential to achieve a neuron-like membrane potential.[266,267] At this membrane potential, the *M. domestica* VSSC is in the resting state, facilitating channel opening as a response to membrane potential increases. Blue light-induced ChR2 opening leads to an unselective cation influx pushing the membrane potential to a more positive potential as described by Bamann et al. in 2008.[268] This elevation is strengthened by the shift of activation due to modulator binding the VSSC.[269]

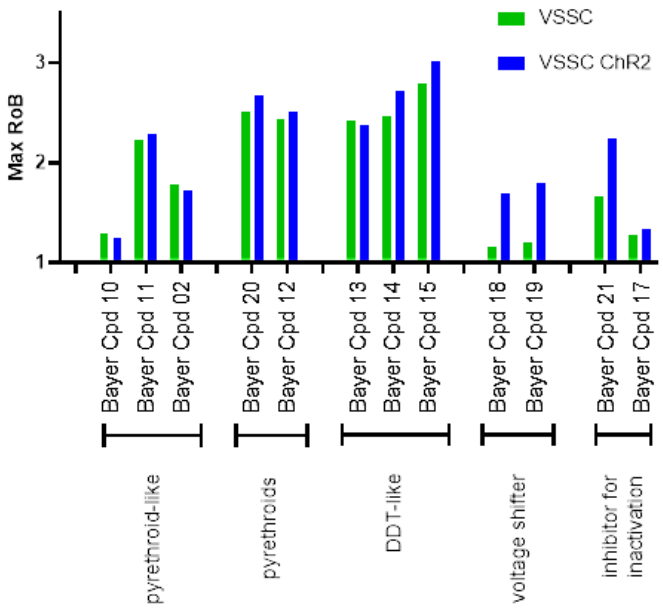

Figure 29 - Proof of concept for the benefit of optogenetics in the VSSC assay at FLIPR Tetra
Shown is the RoB for different tool compounds with different MoAs assigned.

In cell-based high throughput screening systems, frozen cells are favored over permanently cultured cells. Frozen cells have the advantage of consistent quality, as the cells in all measured plates exhibit a low and identical passaging count. To circumvent biological variance, the assay was tested on the compatibility with frozen cells as performed for other high throughput campaigns by Seitz et al., Rotordam et al. and Smilkstein.[270–272] Results in cultured cells might differ due to the varying cell cycle times and minor inconsistencies in culture conditions. Throughout the campaign, aging effects like poor channel expression or reduced cell growth, as described by Kaur et al., can be circumvented.[273] Cryo vials were ordered at Accelerate with a declared cell concentration of 10^7 cells with a passaging number of seven.

Tests for the proof of concept and approval of the Accelerate cells were performed on the FLIPR Tetra with a rudimentary but comparable pacing system to the later Assay Imager, developed by Bayer AG for flexible and high throughput pacing. The RoB is similar among all MoAs and compounds when cultured and frozen cells are compared. The voltage shifter and the inhibitor for inactivation, exhibiting a significant difference in the former comparison, are also detectable in the frozen cells (Figure 30). In most cases, the cultured cells showed a minor advantage over frozen cells, which is negligible regarding the benefits of the frozen cell approach.

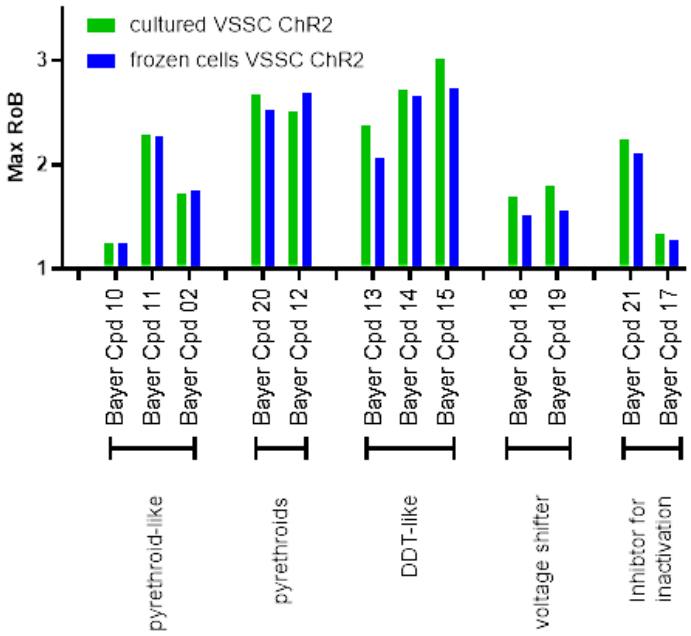

Figure 30 - Investigation of assay tolerance towards frozen cell approach at the example of different tool compounds

5.4.2 Development of light pacing protocol

The transfer from rudimentary optogenetic measurements performed on the FLIPR Tetra (Figure 29) to actual light-induced pacing in a suitable device requires adaption. It facilitates enhanced control over the light application and the application of different pacing protocols (excitation intensity 1-100 %, excitation time and simultaneous application of various wavelengths). Due to the issues regarding the light application, the actual screen was performed on the Assay Imager, designed and built by Bayer AG (Bayer Business Services, former Bayer central research).

The conditions were tested one after another with the more advantageous condition compared to before. The amplitude height was evaluated as a response to excitation with 30 ms blue light pulses (475 nm – 485 nm) with a frequency of 0.1 Hz. Channel amplitude was defined as the difference between the signals measured in the presence and absence of 0.5 µM tetrodotoxin (TTX). TTX was applied as a control, it is described as an open sodium channel blocker by Yasumura[274], maintaining the channelrhodopsin activity intact. High sodium channel amplitudes were considered an advantage, representing higher populations of VSSC opened synchronically.

First, experiments were performed with different potassium concentrations as the driving force for repolarization. The first approach was strengthening the potassium gradient by loading the cells with potassium. Therefore, the cells were preincubated with K_{10}-buffer (10 mM potassium) for 120 min before loading dye application, leading to a significant 300 % increase in the VSSC amplitude. (Figure 31 A) The second approach to enhance the gradient is the reduction of external potassium from 5 mM to 0 mM during measurement. It led to a significant increase in the VSSC amplitude of

approximately 400 % (Figure 31 B). The most substantial effects were seen by implementing the potassium ionophore to take advantage of the increased gradient. Concentrations of 50 µM potassium ionophore were shown to be cytotoxic (data not shown); therefore, concentrations from 0 – 20 µM were tested. The highest amplitude was measured at potassium ionophore concentrations of 20 µM, with an amplitude height of 10 %. The reduction of the ionophore concentration (10 µM) comes with a signal reduction (5 %). The cell system's enhanced capability to repolarize and get closer to the neuronal resting potential facilitated the physiological VSSC function, as reported by Zhang et al. in similar setups.[275] Repolarization is essential, as otherwise, the high membrane potentials force the majority of VSSC into an unexcitable, slowly inactivated state. Repolarization is necessary, as otherwise, the high HEK membrane potentials force the majority of VSSC into an unexcitable, slowly inactivated state, as described by Pavlov et al.[276]

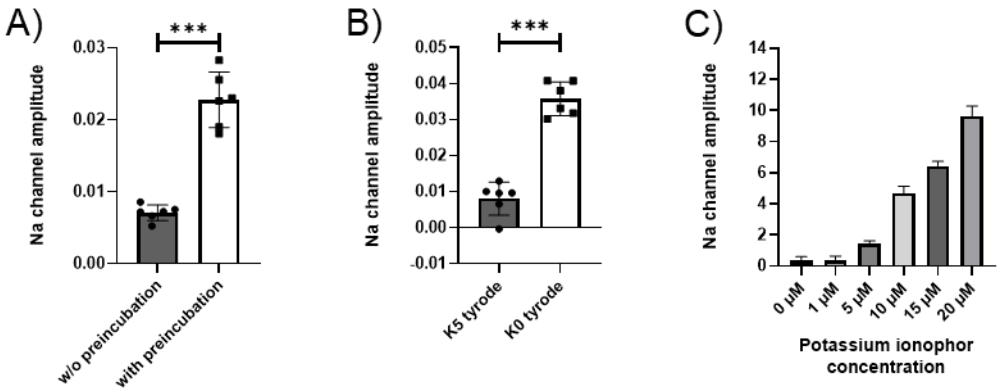

Figure 31 - Effect of potassium and ionophore concentrations on the VSSC amplitude after blue light application

Shown are the VSSC amplitudes in response to 30 ms blue light pulses (λ_{exc}: 465 – 485 nm) with a frequency of 0.1 Hz. For A) were the cells measured with and without 120 min preincubation of K_{10} buffer before the application with loading buffer. B) Shows the VSSC amplitudes with two external potassium concentrations after preincubation with K_{10} buffer. C) Na channel amplitudes at different KI concentrations, with preincubation of K_{10} buffer and K_0 tyrode

Further aspects investigated are cell number per well and incubation time with loading dye. (Figure 32) The amplitudes measured were decreased for long incubation times. The highest signals were observed for a cell concentration of 50 K cells, with a minor amplitude reduction for 25 K cells per well. The signal decrease of almost 50 % between 30 min and 60 min is the highest. After 60 min, minor declines over time were measured for both cell concentrations. An extended incubation was shown to be disadvantageous. A possible reason could be the equilibrating potassium gradient was equilibrating over time due to the ionophore. The shorter the incubation time was kept, the higher the gradient was during the actual measurement and facilitated the generation of robust sodium channel amplitudes. The signal for all incubation times was decreased for low cell concentrations.

The conditions for optogenetic pacing in advance of the actual measurement were completed. All

pacing experiments were conducted according to the results above. Different pulse protocols were tested with 120 min preincubation of K_{10}-buffer, loading buffer prepared with K_0-tyrode and a loading dye incubation of 30 min with 25 000 cells per well. For evaluation and identification of the actual VSSC signal kinetics, the presence and absence of 0.5 µM TTX were measured.

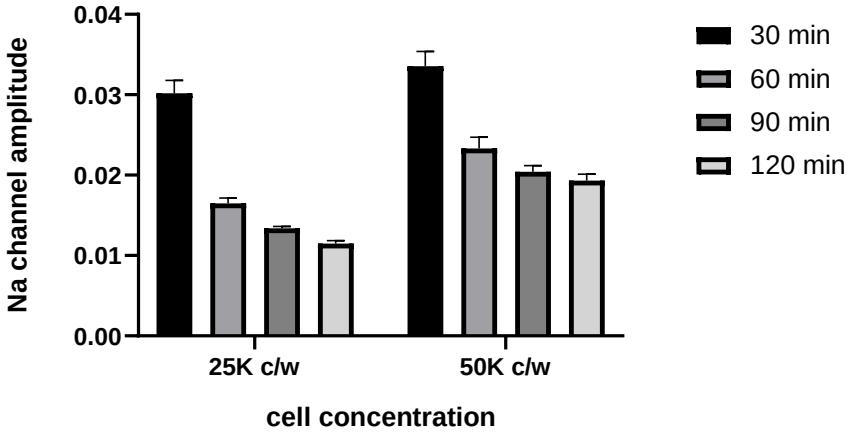

Figure 32 - Effect of cell density and incubation times on the amplitude level after blue light application
Shown are the Na channel amplitudes in response to 30 ms blue light pulses (λ_{exc}: 465 – 485 nm, 0.1 Hz). The amplitude level is shown for two different cell concentrations with regard to the incubation time with loading dye.

The protocols were tested on the optogenetic cell line to investigate the effect of different pulse types. Following Whiteaker et al. and Berndt et al., a combination of two different wavelengths is required for the assay, green light (λ: 515 – 535 nm) as excitation for the voltage-sensitive dye and blue light (λ: 465 – 485 nm) for the ChR2 activation.[152,219] Different settings were chosen, varying in frequency, pulse number, readout intensity and pulse length. The intensity for green light application was shown to be highly important for pacing results. Application of 10 % λ_{exc}: 525 nm – 545 nm (thick green bar) activates the implemented channelrhodopsin 2 mutant and raises the baseline fluorescence. The slope in the absence of TTX is higher. The maxima of the kinetics are not affected by TTX. Blue pulses do not affect the kinetics (data not shown). Reducing green light intensity to 1 % prevented unintended signal increase and facilitated responses to blue light pulses. These results explain what was earlier hypothesized for the effects of the FLIPR Tetra, the green light activates the ChR2 as well. The elevated baseline measured comes with an elevated membrane potential and a transition of VSSCs to the unexcitable slow inactivated state. (see 5.4.1 Buffer-conditions)
Based on these findings, different pacing strategies were developed. Different frequencies of pulses were shown to activate ChR2 and, thereby, VSSC. Applying blue light pulses with 0.1 Hz leads to minor activation of ChR2 with distinguishable but additive responses of VSSC, to an RoB of 1.09. Increasing the frequency to 1 Hz leads to a 5x fold increase of the ChR2 response to an RoB of 1.05.

Furthermore, it enhanced the VSSC activity to a maximal RoB of 1.12, the total VSSC amplitude was not altered.

In contrast to the elevation by 10 % green light, the elevation is caused by ChR2 and the VSSC. However, it did not increase as many times as the ChR2 signal. The signal kinetic equals the dye kinetic and the amplitudes are no longer distinguishable. The electrophysiological measurements showed that a frequency of 1 Hz is short enough to get repetitive pulses of the fast-switching VSSC (see 5.2 Validation of HTS cell lines). In the fluorescent readout, the single pulses cannot be resolved due to the inertia of the voltage-sensitive dye.[149] (Figure 33) The effect of pulses on a single signal required a reduced frequency of light pulses, facilitating discrimination between pulses however could also benefit the test system, as possible new lead compounds might affect the area under the curve and amplitude width. The frequency of 0.1 Hz was sufficient to discriminate between single events. Protocols were either implementing one or multiple highly frequent pulses within the frequency of 0.1 Hz. The amplitudes for the high-frequency pulses are sharper compared to the single pulse amplitudes, as the artifacts eliminated from the kinetic were extrapolated towards the first measurable points. The amplitude height of the high-frequency pulses was higher (1.13) due to stronger ChR2 activation (1.06). The additive effect seen for both pulses is based on the inertia of the dye. The amplitude for the single pulses is the lowest with 1.09, but the measurable effect is just based on the sodium flux as the blue light excites ChR2 just strong enough to induce sodium channel opening.

The decisive aspect of the decision on one of the pacing protocols was the performance with tool compounds of different strengths and modes of action. Some of these effects are known to be state-dependent, a feature this screen was designed to detect. Soderlund described the pyrethroids as a state-dependent example, requiring prior opening. Furthermore, other modulators were implemented, targeting the inactivated state (see 5.3 Electrophysiological characterization of VSSC).[233] This diverse selection was expected to give a clear picture during the development. To find the optimal protocol, each aspect was tested separately, the frequency with 30 ms pulses first. (Figure 34 A) Slightly advantageous was the lower frequency pacing among all classes. The minor effects detected, however, are primarily based on the calculations. Evaluated is the ratio between baseline measurement and the actual compound effect. This ratio becomes lower when the baseline is elevated due to higher blue light exposure. Besides this slightly elevated RoB, we have the advantage of individual responses to the blue light and therefore stuck to the low-frequency pacing.

The next step was the testing of the repetitive pulsing versus single pulses. Ten light pulses, meaning ten VSSC activations, are translated into one pulse. The expectation was a high frequent passing through all VSSC states and therefore, the opening of the different binding sites as seen *in vivo* by Kadala and Soderlund independently.[233,277]

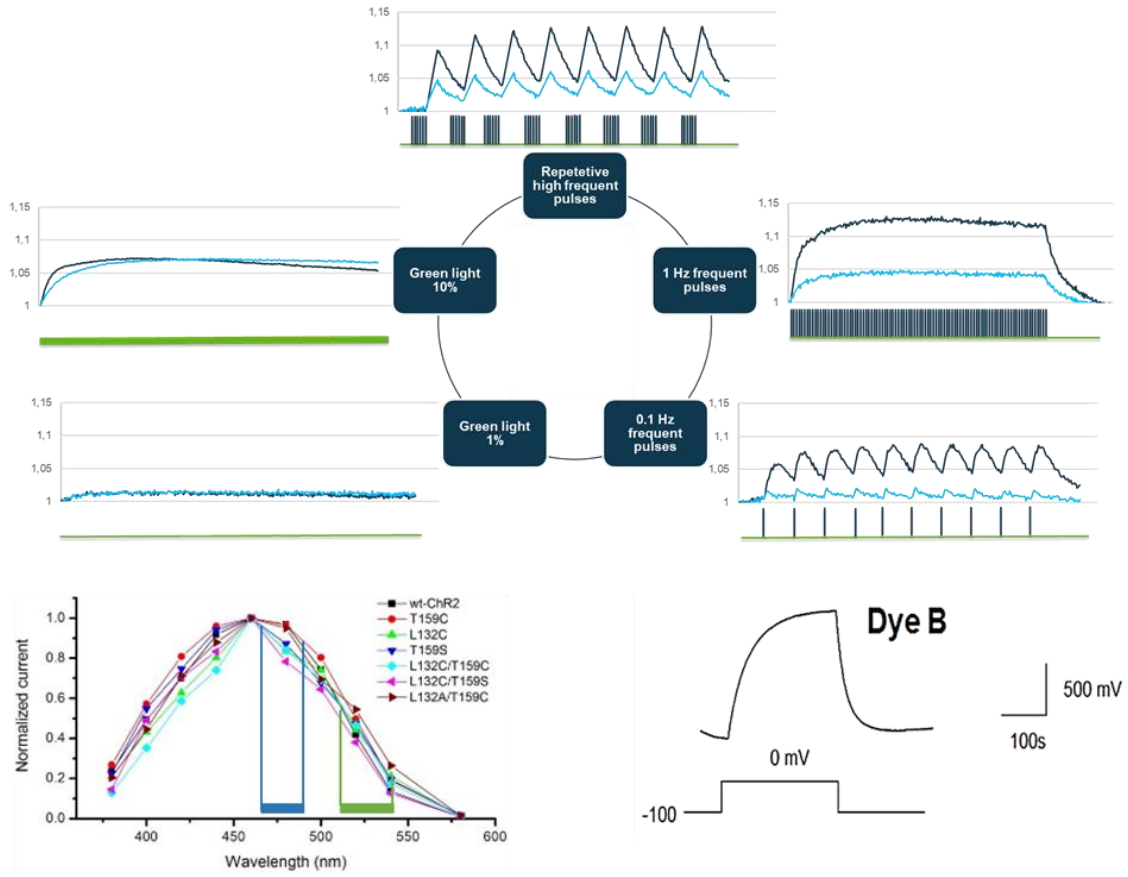

Figure 33 - Effect of pulse protocols on the VSSC kinetics.
A) kinetics of different pulse protocols over time in the presence (light blue) and absence (dark blue) of 0.5µM TTX, light application is indicated as bars and columns below the graphs. The inlet shows the Assay Imager, a tailor-made fluorescent and luminescent reader. Artifacts due to blue light application are removed from each kinetic. B) Excitation spectrum for different channelrhodopsin 2 (ChR2) mutants of Pan et al. extended on the inlet containing the excitation spectra used by Assay Imager LEDs[184] C) Emission kinetic of voltage-sensitive fluorescent dye after depolarization

Single pulses show slightly better results for the same reason as proclaimed for the 1 Hz pacing. The high blue light exposure elevates the baseline, just ChR2 mediated and VSSC independent. The next step was the length of the blue light application, varying between 30 and 90 ms. The results of almost all compounds and MoAs are slightly better for more prolonged exposure. For the pyrethroid and the DDT-like substances, the effect is stronger. Both classes exhibit comparable effects and bind the same binding site according to Davies et al., Ranson et al. and Chang and Plapp Jr.[74,79,278] The more prolonged exposure was therefore taken for further experiments.

Last but not least, the advantage of the optimized pacing protocol (1x, 90ms, 0.1 Hz) was proven over the old assay system without blue light application (just the green light). The slight enhancement of the effects of potent modulators was negligible. The most significant advantage is optogenetic pacing for voltage shifters, which are not detectable without pacing. The frequent application of blue light facilitates the detection of all three voltage shifters with RoBs of approximately 40. This assay was

designed to identify structures with weak effects and provide new starting points for chemical optimization, as Yu et al. showed for HTS.[279] Strong modulators would have attracted attention during an *in vivo* screening. These weak voltage shifters were just detectable after implementing ChR2 into the cell (Figure 34). With particular regard to the mode of action, this visibility can be explained by the effect, it is not persistent but can be measured frequently due to repetitive opening.[278,280] Furthermore, voltage shifters are just shifting the threshold potential for VSSC towards a more negative potential and might support the opening of VSSCs in response to optogenetic stimulation.[280,281]

The z'-factor for the assay as performed during the HTS was 0.81, which can be considered stable and suitable for the screening campaign as defined by Zhang et al.[244] Crucial for proceeding was the effect on the voltage shifter (Figure 34 D), which is a comparable weak modulator not yet optimized as a market product.[279] The pacing protocol with one pulse in a frequency of 0.1 Hz and a duration of 90 ms was chosen to perform the HTS measurements.

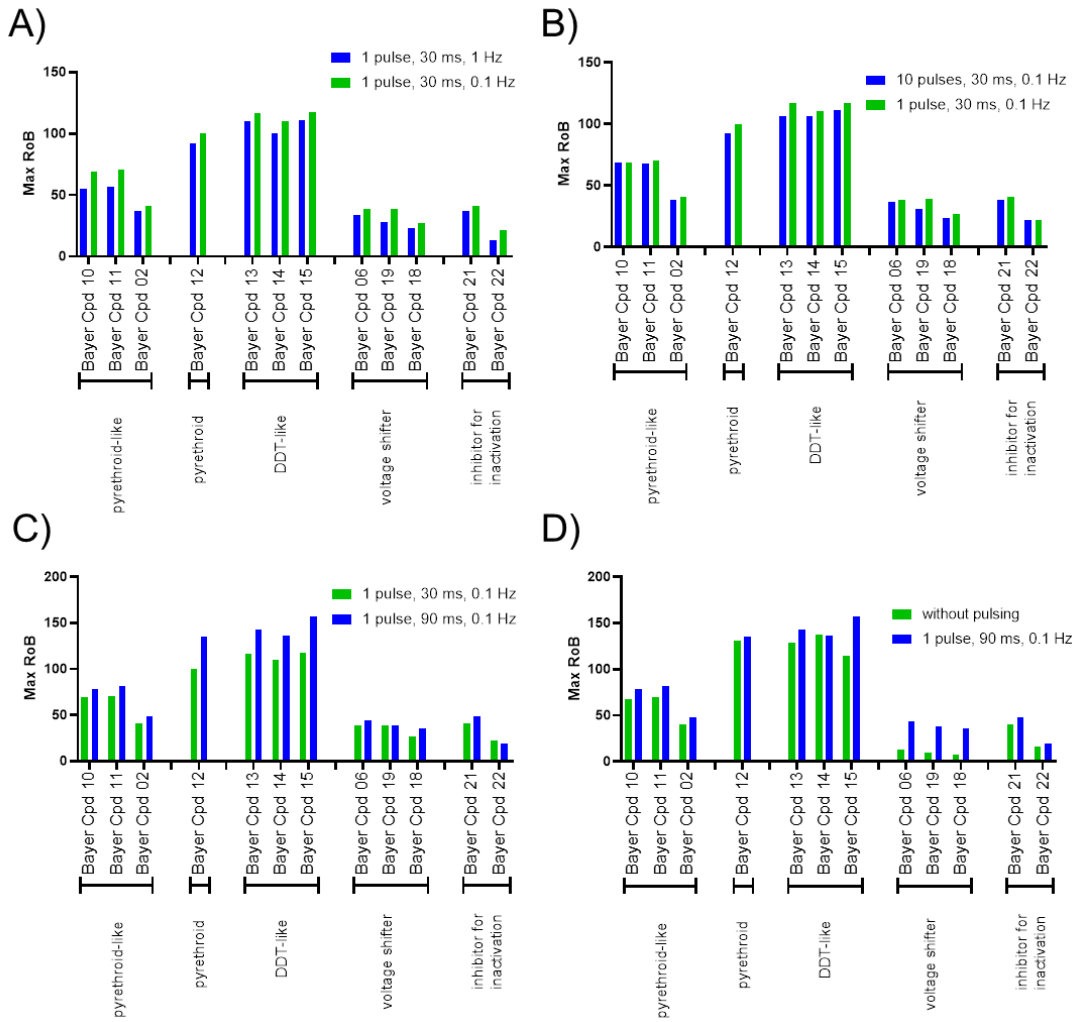

Figure 34 - Advantage of optogenetic pulsing by the example of different tool compounds
A-D) Plotted is the maximal response of representative tool compounds for different MoAs and classes measured with different pulse protocols

5.5 High throughput Screening Campaign

5.5.1. High Throughput Screening

All experiments were conducted according to the developed assay and the optimizations conducted in this study. For identifying VSSC agonists, approximately 1 200 000 test compounds were measured at a concentration of 10 µM in single point measurements. All areas under the curve (AUC) were normed to 50 µM reference compound (200 % activity) and DMSO (100 % activity), as also described by Riniker et al.[189] (Figure 35)

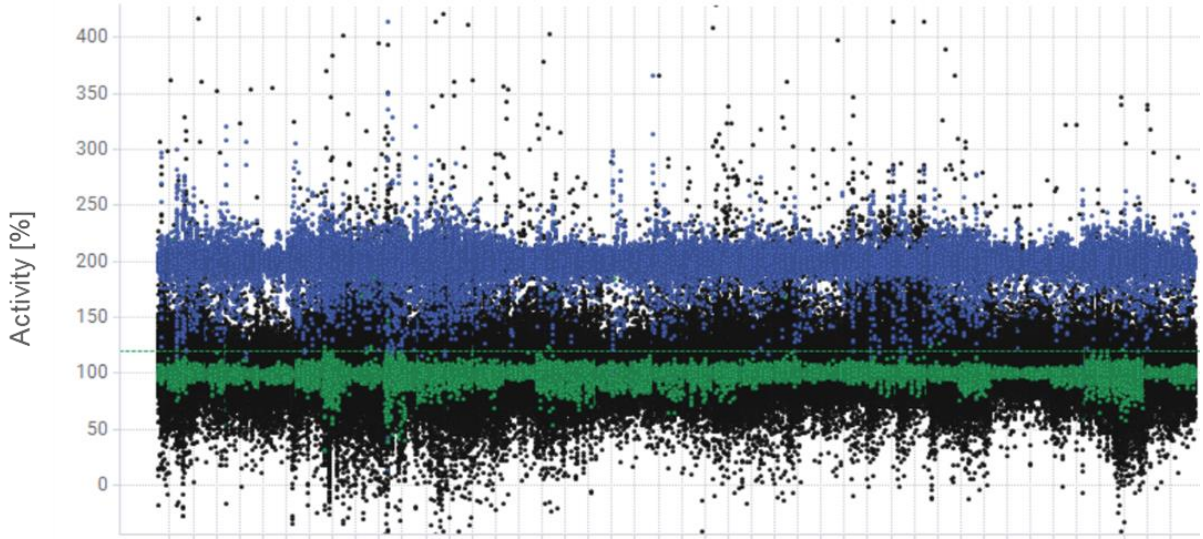

Figure 35 - Results of primary high throughput screening (HTS)
The hit rate of primary HTS with black dots representing compounds, green dots representing DMSO controls (normed to 100 %) and blue dots representing standard (reference compound, normed to 200 %). The activity threshold was set to 120 % (indicated by the green line).

Based on the experience of prior HTS screens at the VSSC without optogenetics and the low number of hits identified during those screens, the threshold activity was set to a low percentage. By doing so, the risk of a higher rate of false positives increased, but it also reduced the risk of false negatives (enhancing sensitivity) balanced on the criteria of Zhang et al.[190] This enhances the possibility of finding weak agonists, later filtered by higher tier experiments like electrophysiology and symptomatology. The automated patch clamp measurements in later steps can nowadays be implemented to filter true positives with an orthogonal high throughput assay. Higher thresholds were considered to enhance the confidentiality of true hits (Table 5) 120 % represented the scattered activity of the DMSO negative controls, usually exhibiting a stable distribution at the 100 % limit. The chance of finding potent modulators was considered low. Otherwise, they would have been discovered in a previous HTS assay or in-vivo assays. Almost 50 000 compounds reached the threshold of 120 %. Therefore, two filters were applied to further reduce the amounts of hits to 40 000 preliminary hits. A selection of putative hits with a given activity was made based on two criteria.

The compounds were chemically clustered, for each cluster, just up to 20 cluster members with the highest activity were chosen. Another filter was a chemical desirability score for agro-like compounds based on chemical properties, an adapted Lipinski rule of five for agrochemicals.[191,192] This way, the number of hits in the primary screen was reduced for the confirmation screen.

Besides an activity-guided analysis, a kinetic analysis was performed with artificial intelligence (AI) based autoencoder. As others performed this analysis and due to confidentiality reasons, the exact parameters of the analysis are not further detailed. The limit for the activity-guided analysis was set to 30 000, while the new AI-guided analysis had a threshold of additional 10 000 compounds. (Figure 36) Both analyses had an overlap of 15 000 hits. Frequent hitters were not nominated for further testing, as considered as either unselective or false positive, as described by Yang.[282]

Table 5 - hit rate for different activity thresholds

Threshold activity	Amount of hits	Hit rate*
120	49 243	5.2
125	33 228	3.5
130	23 746	2.5
140	13 697	1.4
150	8 622	0.9
200	1 532	0.2

*Hit rate was calculated based on 953.271 compounds screened in a first approach

All of the already known modulators included in the tested libraries were detected in the assay, showing the reliability of the assay. As a further quality control, a quality check plate was measured twice a day with tool compounds to evaluate the assay stability and comparability between the experimentation days.

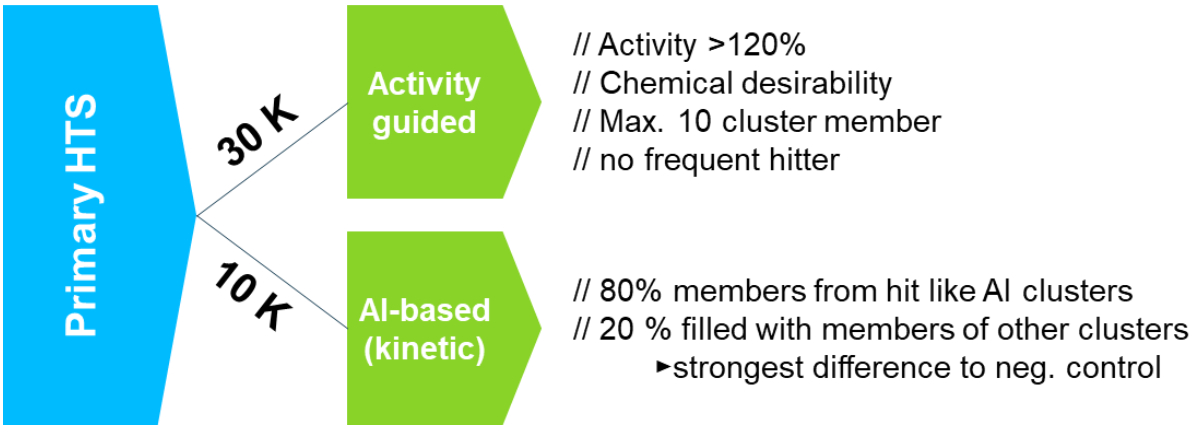

Figure 36 - Matrix for different approaches for hit-picking after primary HTS

All 40 000 primary hits were then tested in duplicates at 10 µM at the mock cell line (ChR2) and target cell line (VSSC ChR2), as similarly performed by YU.[153] The activities measured during the primary HTS were reproducible but slightly higher than those for confirmation. The activities reaching into the area with activities below 120 % were mainly chosen kinetic guided and cannot be expected to reach the formerly defined threshold. The reproducibility within the confirmation screen is shown in graph 2 of Figure 38. Both replicates are plotted against each other, with the standard enclosing the 200 % activity mark (red) and the DMSO negative control located at the 100 % activity mark (blue). The majority of compounds are close to the bisector of an angle with a gaussian normal distribution. Just a fraction of the compounds exhibiting a low activity have a shift towards replicate 1.

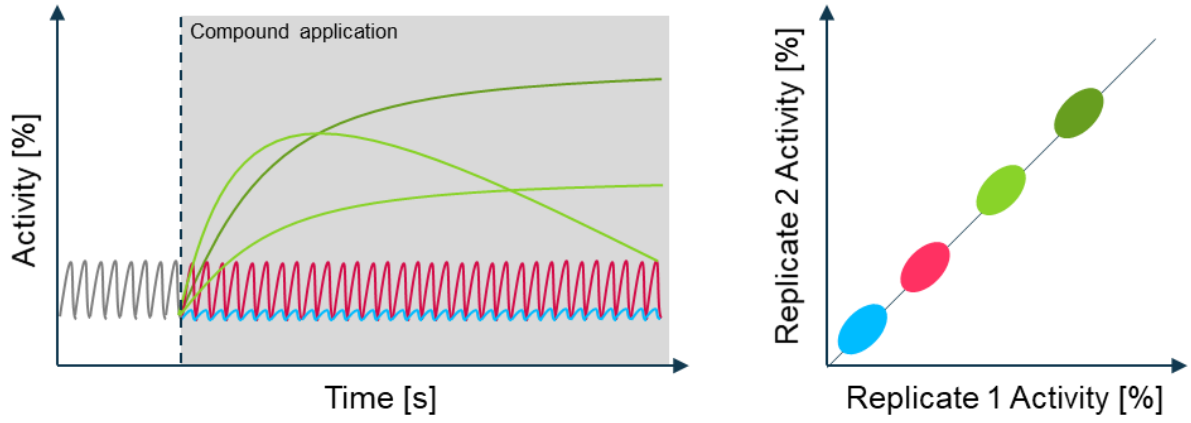

Figure 37 - Example kinetics for agonists and antagonists in the optogenetic screen
Shown is a depiction of the kinetics for different modes of action expected on the screen. After compound application the kinetic changes and the location in a plot of two replicates, based on the applied compound (green: two different agonistic effects, transient and weak effect in light green and permanent/strong effect in dark green; red: no effect and antagonism in blue)

Figure 37 shows example kinetics, measured on the screen, with their respective position within the comparison of replicates. The subset of negative modulators is most likely quenching the signal or acts as an antagonist, as indicated by Caroll et al.[283] This subset of compounds is mainly derived from the kinetic approach and had to be analyzed separately. The potent modulators are located in the upper right corner. Due to the evaluation by AUC, the values cannot discriminate between strong transient and weaker effects.[283]

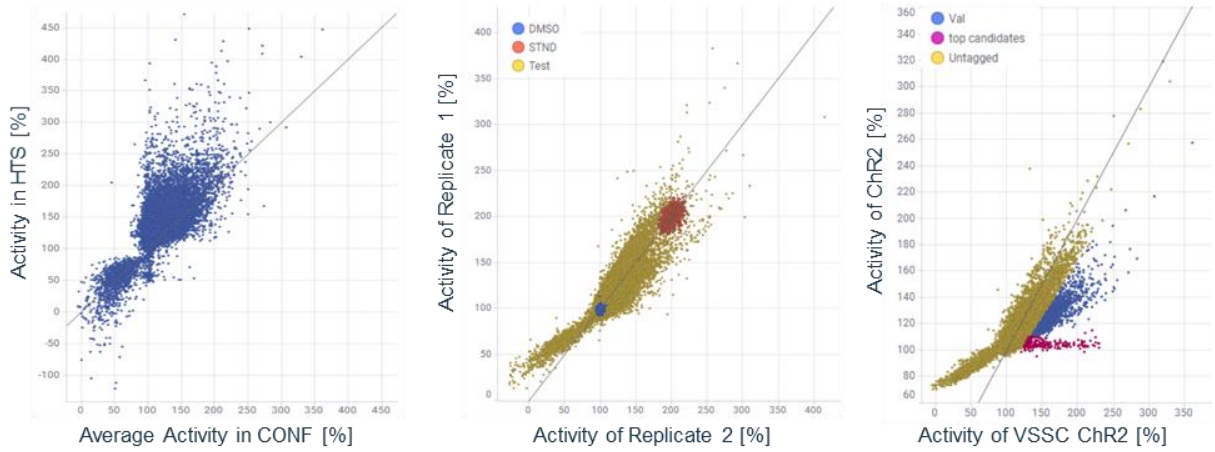

Figure 38 - Confirmation results after primary HTS
A) Reproducibility of activity in primary HTS versus activity of confirmation. **B)** reproducibility among the replicates. **C)** Specificity was shown by the activity ratio between mock- and target cell lines

The most crucial aspect tested in the confirmation screen is the specificity and reduction of false positives. To reduce it, the mock cell line expressing the channelrhodopsin 2 was measured similarly to the target cell line expressing both the VSSC as the target and the ChR2 as a tool. The comparison revealed that the validation screening candidates were divided into two groups. The violet-labeled compounds feature high selectivity between target- and mock cell line. Different tool compounds are located within this group, mainly strong pyrethroids. The other group of interest is the blue-labeled area with a target- to mock activity ratio of >1.2, consisting of weak potential hits.
Those compounds showing at least 20% higher activities at the target than the mock cell line were considered selective and nominated for next-step validation.

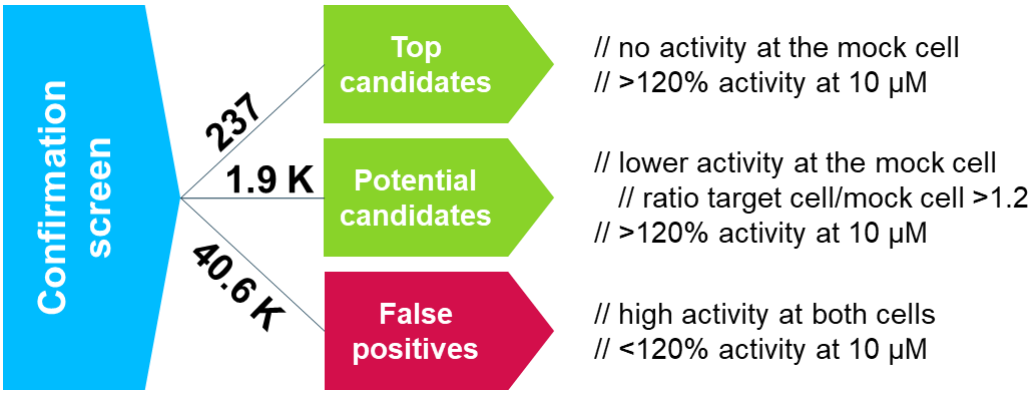

Figure 39 - Activity-based approach for Hit selection after the confirmation screen

Validation was performed with two different readout systems. In total, 2050 compounds were measured, including 129 known modulators, which were all identified. The reliable identification of known modulators indicates a good sensitivity of the established assay. The compounds shown in Figure 40 are selected and de-selected based on the criteria of Figure 39. The data were derived from

concentration-response curves (30 µM to 3 nM), as shown in the inlet. They were recorded in a fluorescent assay to identify pharmacologically relevant values, such as pEC_{10}, pEC_{50} and pEC_{max} and the activity max. The measured target cell values were compared to the ratio of both cells (VSSC & ChR2/ChR2) to identify modulators with discriminating and high activities at the target cell line. The known modulators set into this step of the testing cascade were mainly located on the bisector of an angle, as they showed high selectivity for the VSSC. Some minor selective VSSC modulators were located below the others but with an enhanced activity at the target cell line, compared to the mock cell. Some of the hit candidates were found in the respective area, too. While most were inactive or even unselective, a minority of compounds were plotted within the known VSSC modulators. The concentration-response curve in Figure 40 shows the selectivity of one promising candidate out of ten (Table 6). Bayer Cpd 23 has an intrinsic activity of 148% normed to reference compound (200 %) and a pED_{10} of 7.2 at the target cell line, while exhibiting no activity at the mock cell line. Selectivity towards the mock cell line is the key to identifying valid modulators, as described by Seethala et al.[284] Candidates nominated for further testing after validation had to feature mock-to-target cell pED_{10} ratios of >1.1. In the case of an 'inactive' label in electrophysiological experiments, this activity profile triggered a re-evaluation of the electrophysiological data.

This step consisted of two different test systems, which turned out to be advantageous in previous screens and is also independently recommended by Walters et al. and Yu et al.[153,193] One test was an analog to the former assays, comprising concentration-response curves from 30 µM to 3 nM, measured with the HTS cell line, the mock cell line and a pyrethroid insensitive mutant (skdr) described in chapter 2.2.2.1 Insect Na channel and by Soderlund.[194] The comparison of the HTS and mock cell line facilitated the consolidation of the selectivity of the compound. The values gained by the skdr cell line allowed an early estimation of the tested fraction's resistance-breaking potential or pyrethroid contamination.

The candidates were nominated for further testing based on the APC measurements. The orthogonal assay had the highest impact on the selection of hits for further characterization. It was performed with the same compounds as in fluorescence measurements, however, processed individually for the electrophysiological measurements. Only compounds with a firm activity profile in the fluorescence assay were nominated without activity in APC.

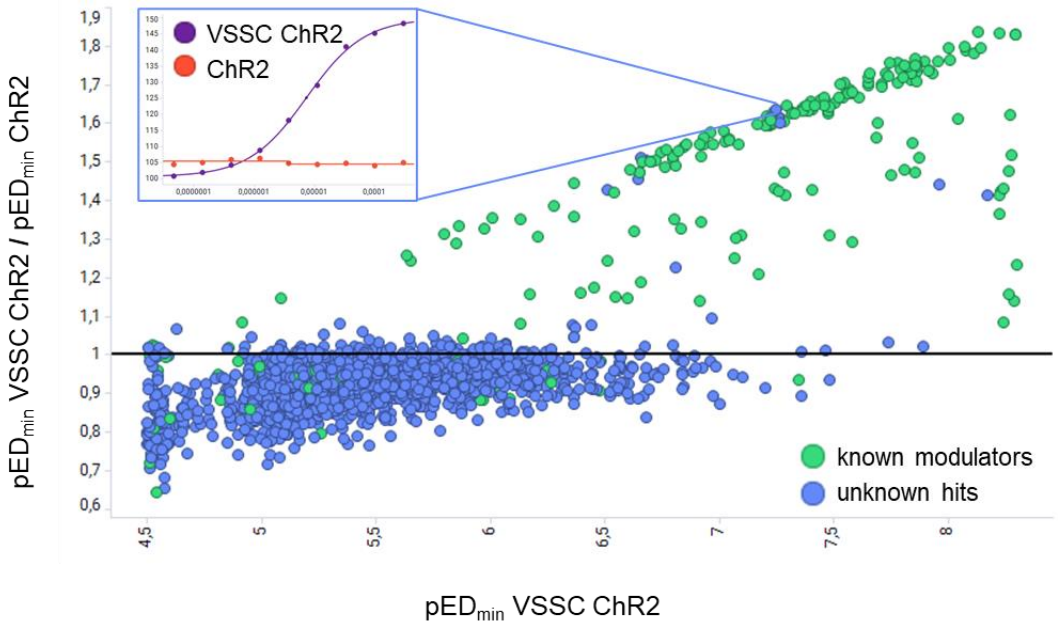

Figure 40 - Validation results
Plotted are the pED_{10} of the VSSC ChR2 cells versus the ratio of pED_{10} VSSC ChR2 and pED_{10} ChR2. The green dots represent the known VSSC modulators, while the unknown hits are labeled in blue. The inlet shows the measured concentration-response curves at the mock- and target cell line for Bayer Cpd 23.

Table 6 - Confirmation results of the ten most promising candidates based on the fluorescence readout

Compound	Activity Max [%] VSSC ChR2	pEC_{10} VSSC ChR2	pEC_{10} Mock ChR2
Bayer Cpd 24	40	6.80	5.6
Bayer Cpd 25	60	6.50	<4.5
Bayer Cpd 26	63	6.60	<4.5
Bayer Cpd 27	52	6.70	<4.5
Bayer Cpd 28	66	6.70	<4.5
Bayer Cpd 23	**48**	**7.20**	**<4.5**
Bayer Cpd 29	69	7.30	<4.5
Bayer Cpd 30	35	8.00	5.6
Bayer Cpd 31	33	8.20	5.7
Bayer Cpd 32	64	7.30	<4.5

*Values were gained based on concentration-response curves normed to reference compound, the bold compound of DRC inlet in Figure 40

5.5.2 Pulse protocol design SyncroPatch384FX

Measurement of the VSSC required the development of a pulse protocol capable of detecting different effects and addressing all channel states (5.3 Electrophysiological characterization of VSSC) as described by Goldman.[196] Compounds covering all known effects were chosen for evaluation.

As the measured values were gained by measuring the VSSC population of just one cell, the measured effects are underlying higher biological variance.[153] Different parameters were considered to circumvent artificial effects due to these single-cell measurements. All compounds were measured in at least three cells, with seal resistances after the patch of at least 200 MΩ and sodium currents of at least 200 pA. Currents below the threshold were not considered as they might result from endogenous expressed human VSSCs or did not exhibit an acceptable signal-to-noise ratio to identify actual modulators confidentially.[195,285] The data were evaluated with and without leak correction to discriminate between real effects and compensational artifacts as well as to identify compounds mediating leak-like effects. As a negative control, DMSO was applied, with minor results on some cursors, explainable by the small leak currents occurring over time, as also seen by Lei[286].

For evaluation, cursors were implemented into the pulse protocol picking out important and characteristic values. This way, an automated analysis could have been performed to differentiate the different effects by monitoring all cursors over time. All values were normed to the maximal current measured for the -10 mV amplitude. Values detecting a voltage shift are recorded at the third peak of each clamped membrane potential from the activation curve. Other cursors were placed during the inactivation of -10 mV pulses, the triple pulse, and the long 10 mV pulse. The long pulse cursor can detect effects requiring prolonged inactivation. The third pulse of the fast inactivation is to detect the use-dependent effects on the inactivation. The last cursor is set to detect potential tail currents after the inactivation of the third -10 mV pulse. Characteristic traces for the different MoAs and the cursor behavior over time can be seen in Figure 41.

The holding potential during APC experiments was set to -100 mV to have the whole VSSC population excitable. Furthermore, it facilitated a measurement over a long time with a stable giga seal. A rudimentary activation curve was implemented, enabling the detection of voltage shifters with 20 ms pulses to membrane potentials of -50 mV, -40 mV, -35 mV and -10 mV. The first three membrane potential changes were chosen to be below the threshold potential of VSSC from *Musca domestica*, while a depolarization to -10 mV guarantees activation. The voltage shifter tool compounds (exemplary 10 µM Bayer Cpd 6) were identified with strong signals at membrane potentials of -40 mV and some minor effects below the other peaks at -50 mV. The signal reaches just 500 pA, as -50 mV does not match the new threshold potential. So, just a subset of the VSSC population opens as also observed for other voltage shifter characterized by Buczek et al. and Zhang et al.[280,281] Other cursors were not affected by this compound class. (Figure 41)

The activation curve consisted of three pulses for each membrane potential to find use-dependent effects on the measured potentials. Use-dependent effects were shown to be measurable with prallethrin leading to currents after channel inactivation (tail-currents) as described by Amar et al. in 1992.[285] The visible tail current is additive after high frequent pulsing as proclaimed by Kadala et al.[277]

Besides the main effect on the tail current, this pyrethroid also led to use-dependent currents below the threshold potential.

A permanent open VSSC can be observed after applying 10 µM Bayer Cpd 15. The currents recorded equal those of a leak during the measurement. Discrimination between leak currents and actual effects required further analysis. This effect is critical to monitor, as it can be either a false-positive hit or a positive. Discrimination based on the cursor is not possible and requires further investigation, such as monitoring the early effects when the effect is established. For example, false positives inducing this effect might permeabilize the membrane, as described by Ishibashi et al. and Linely, leading to unselective and undirected ion fluxes across the patched cell.[287,288] If the sodium channel mediates the effects, the channel is open consecutively, leading to a permanent sodium current among the electrochemical gradient. Furthermore, the main sodium current, measured at -10 mV, weakened over time when the sodium channel is kept open, as the electrochemical gradient for sodium intra- and extracellular comes alike.

The last aspect considered in the design of the pulse protocol was a long pulse to identify modulators targeting the inactivated state. Therefore, the previous pulse is prolonged to identify all effects on this particular state, from a fast response like delayed inactivation to a delayed opening during the inactivated state, as described in 5.3 Electrophysiological characterization of VSSC modulators.

All compounds and effects were identified, and the effect was reliably assigned to the tool compound. The chosen cursor facilitated a clear identification of the effect. Smaller effects were difficult to detect via the cursor, as deviations in control traces might lead to misjudgments. Therefore, all traces during pulse protocol design and hit verification were inspected visually to detect weak effects, as expected for VSSC hits.

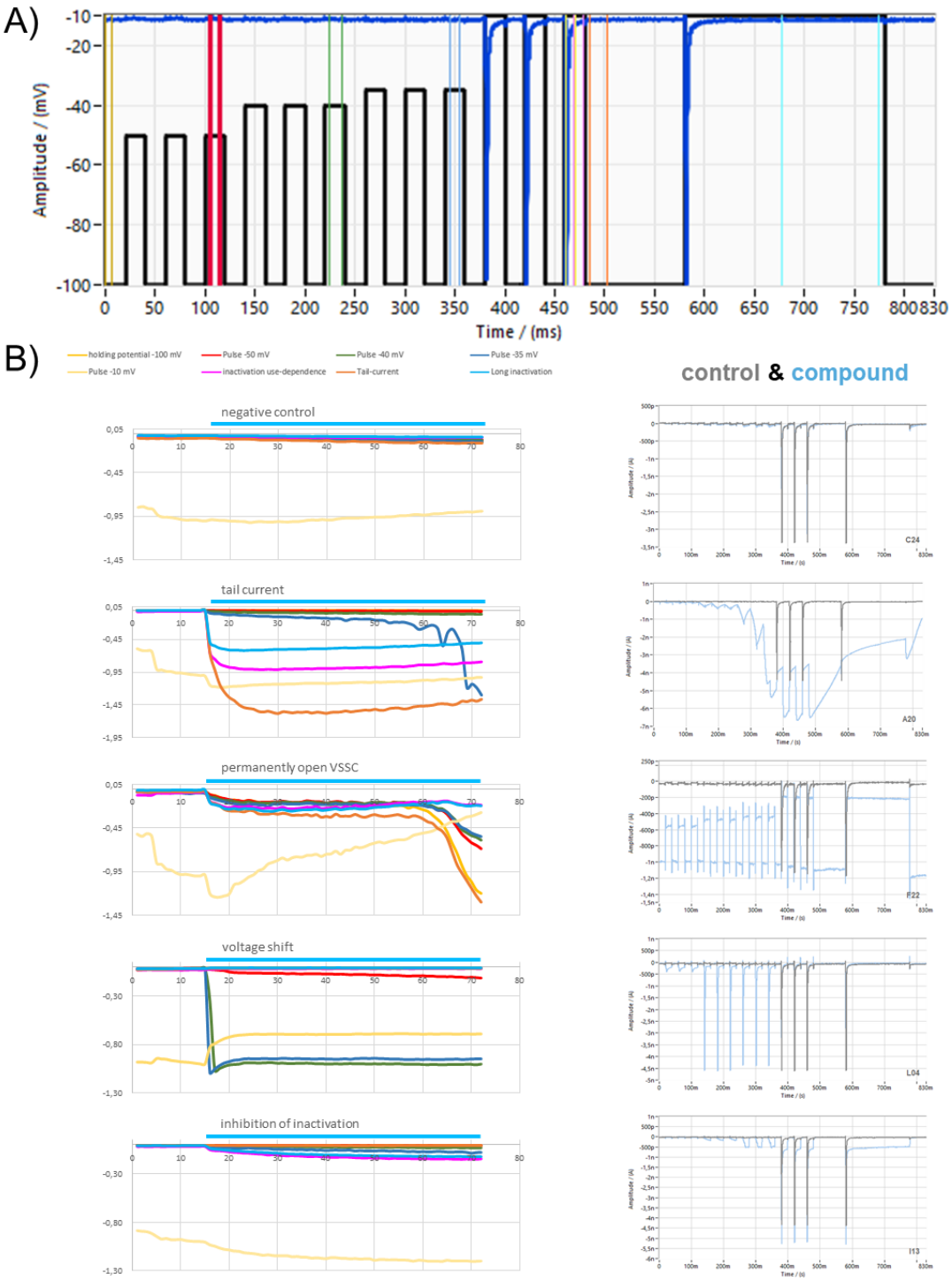

Figure 41 - Development of a pulse protocol for the validation of potential HTS-hits

A) Pulse protocol (black) developed for the identification of a board spectrum of VSSC mode of actions with a characteristic trace (blue). The protocol consists of a total of 13 pulses, nine subliminal pulses of 20 ms representing a rudimentary IV curve in triplicates (-50 mV, -40 mV, -35 mV), and four pulses at -10 mV overcoming the threshold potential of the sodium channel (3x 20 ms and 1x 200 ms), the protocol was repeated every 10 s for 72 sweeps. The colored areas indicate cursors used for evaluation. **B)** Collection of different modes of action, with characteristic behavior of the cursors over time on the left (blue bar: compound application) and characteristic APC traces recorded on the right. Compounds were applied after 17 sweeps, the final evaluation was done after sweep 70 (9 min of incubation).

5.5.3 Electrophysiological validation of HTS hits (orthogonal assay)

Tested were 2049 compounds at a concentration of 10 µM in automated patch clamp. In these experiments, the VSSC ChR2 cell line was exchanged by a just VSSC expressing cell line, as channel opening was controlled electrophysiological. I measured each compound eight times to ensure a dataset of at least a triplicate. Classification and hit picking required a minimum of two cells with the same effect or a minimum of 60 % success rate. Otherwise, they were considered inactive. The majority of compounds did not show any effect. For quality check and data confidence, known modulators among all MoAs were blinded and included in the test. All 129 compounds were identified and assigned to the correct MoA. In the end, 51 candidates with high overlap between both validation assays were identified as potential hits and selected for the tailor-made verification cascade. (Figure 42)

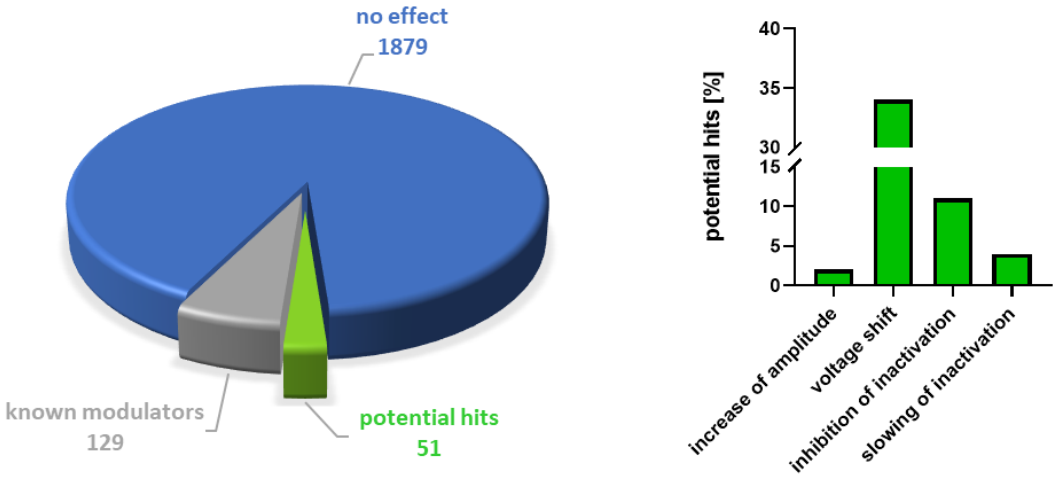

Figure 42 - APC results in Validation of 2049 compounds
left pie chart summarizing the validation results of the APC experiments, **right** potential hits, broken down to the respective mode of actions.

These candidates were assigned to different MoAs. Two compounds enhanced the current by at least 20 %. Eleven inhibited the fast activation with a similar electrophysiological profile as seen in Figure 23 C. The inactivation was sharp and the tail current remained unaffected. The inactivation was affected by four further compounds slowing down the inactivation. The majority of detected compounds induced voltage shifts of different strengths at the VSSC (n=34). This met the expectations, as the optogenetic implementation already revealed strengths in detecting these modulators during the pacing protocol design. (see 5.4 High throughput screening optimization) Although a bigger substitute of voltage shifters was expected due to the strengths of the assay, not all of them must necessarily be true positives. This MoA has the highest vulnerability of false positives within the electrophysiological measurement.

5.5.4 Hit selection and cluster optimization

In hit selection, the purified compounds are investigated in three test systems in parallel. Automated patch clamp experiments were performed at the Musca VSSC cell line to check the consistency of the previously seen effect and validate the FLIPR results. Those compounds exhibiting activity in the FLIPR assay, restricted to the HTS cell line but not the skdr cell line, were tested in APC at the skdr channel. As shown in chapter 5.4.2 Development of light pacing protocol cell lines not expressing the ChR2 cannot find all modulators in the FLIPR. In APC, the resistance-breaking potential could have been proven or disproven. Compounds performing in all tests were further nominated and chemical homologs were identified. The hit candidates resulting from the parallel approach in APC and the validation by the fluorescent assay at the Assay Imager were further verified. After HPLC purification or resynthesis, the candidates were biologically and biochemically characterized. Resynthesis was required as previous screens showed that even minor contaminations with VSSC modulators of the tested fraction could lead to false-positive results.[197] The new fractions were then measured in a tailor-made cascade of biochemical assays. The hit cluster selection was made based on the results of the 51 selected and purified compounds in three parallel assays. The APC results shown in Figure 43 validated the effects of 36 compounds with a consistent effect. Fifteen compounds, however, were no longer positive. Even weak effects were considered true to increase the sensitivity analog to the HTS strategy. Twenty-four of the candidates had a voltage shift as MoA, with just two candidates exhibiting a strong effect. Nine purified compounds inhibit the inactivation with just one strong effect. The last MoA detected was a weak slowing during the fast inhibition in 3 modulators.

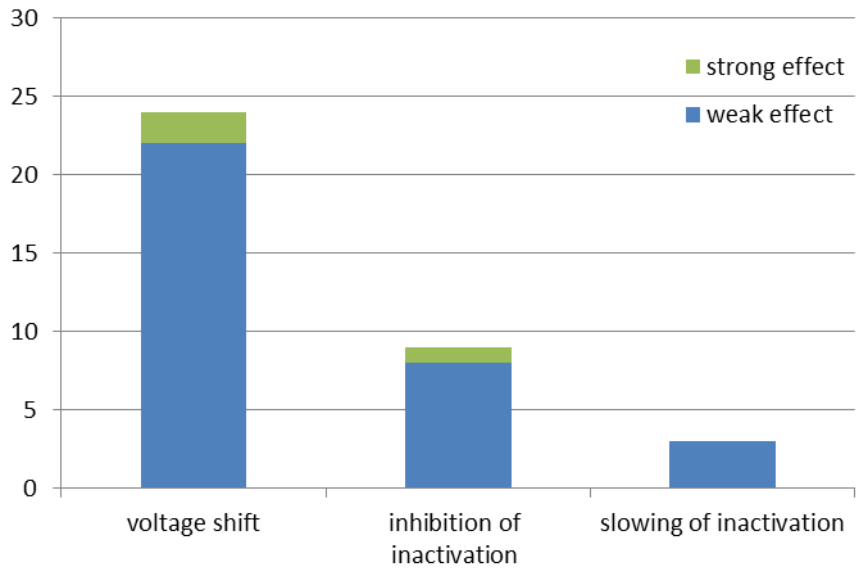

Figure 43 - Automated patch clamp experiments of purified fractions

Symptomatology was performed to test *in vivo* activity and to see whether the expected excitatory symptoms appeared upon injection. Four compounds were showing activity, differing in their symptoms. Two had inhibitory symptoms starting after 48 or 72 h, indicating actions aside from the VSSC or disadvantageous pharmacokinetic parameters. VSSC modulators, besides prodrugs, feature a fast and excitatory response *in vivo,* as proven for different compound classes at Bayer and pyrethroids by many.[76,212,289] The other two modulators featured excitatory symptoms from the beginning. One of those compounds was active for 4 h just at concentrations of 40 mg/g, while the other was significantly more potent with an *in vivo* activity until 2 mg/g. At high concentrations, this compound was lethal. The excitatory symptoms were switched to inhibitory at high concentrations or after a couple of hours. Even though the inhibitory symptom seems to contradict the excitatory MoA, these results are evident for an excitatory MoA. The excitatory symptoms result from the VSSC modulation in the first hours after the injection. The muscles contract with high frequency due to the modulation in the central and peripheral nervous systems. The inhibitory symptoms are a result of the larvae's exhaustion, as also reported for pyrethroids by Yamamoto.[72,197,221,295]

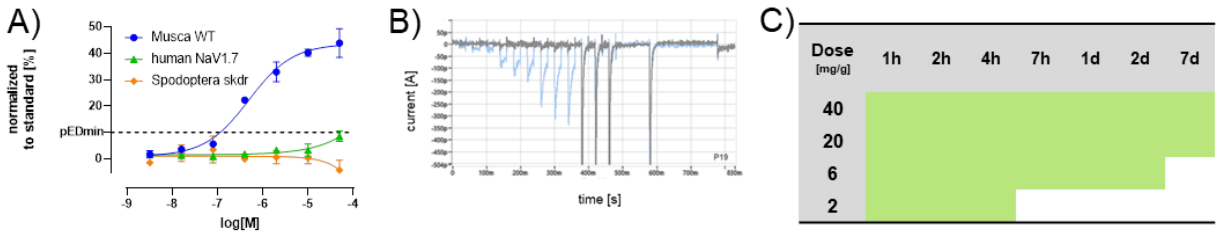

Figure 44 –Hit selection results of Bayer Cpd 23
A) DRC recorded in the FliprTetra at three different cell lines (WT and skdr normed to reference compound, human NaV1.7 normed to Bayer Cpd 33) **B)** APC trace recorded during validation at SyncroPatch384 in the presence (blue) and absence (grey) of 10µM compound. **C)** Injection experiments with *Spodoptera frugiperda* larvae L5 at different dosages, screened at different time points

The FLIPR assay measures analog to the HTS assay three different cell lines, HTS cell line, skdr cell line and human $Na_V1.7$. The last test during hit verification was the fluorescence measurement in the FLIPR Tetra at different cell lines (HTS cell line, skdr cell line and a cell line expressing human $Na_V1.7$). Some of the compounds were not exhibiting activity at either one of the cell lines. Other compounds exhibited more than 50 % stronger activities than the reference compound, which is why they were considered false positives. Yang et al. have shown that autofluorescent or reactive compounds (false positives) and promiscuous compounds with disadvantageous side targets might be the reason for these activity values.[282] The human $Na_V1.7$ was chosen because of its good characterization as a pain target in the pharmaceutical context and its sequence similarity of approximately 40%. Compounds were considered attractive, which exhibited activity in the insect cell lines, but lacking activity at the human cell line. Compounds acting at the human VSSC were discarded as they were missing

selectivity towards the insect. A strong activity among all three cell lines would hint to frequent hitting or unselective compounds. Activity at both insect cell lines was required as resistance-breaking potential is necessary to approve new insecticides.

Bayer Cpd 23 was the only compound leading to positive results in all three test systems, as seen in Figure 44. In APC, the voltage shift was validated, showing weak sodium channel peaks until membrane potentials of -50 mV. During the injection studies, it featured the strongest symptoms, persistent for seven days at high dosages, even leading to lethal effects. FLIPR Tetra measurements showed strong activity at the HTS cell line, with a pED_{10} of 7.0 and E_{max} of 45 % (5.1). No significant activity was measured in the skdr cell line and the human cell line. The lack of activity is unfavorable. However, as shown in 5.4.2 Development of light pacing protocol, detecting weak modulators requires optogenetic control, especially those with a voltage shift. This dependence was already described by Prigge et al. for the Ca^{2+} channel.[194] The resistance-breaking potential was therefore proven in electrophysiological experiments in MPC measurements (Figure 45).

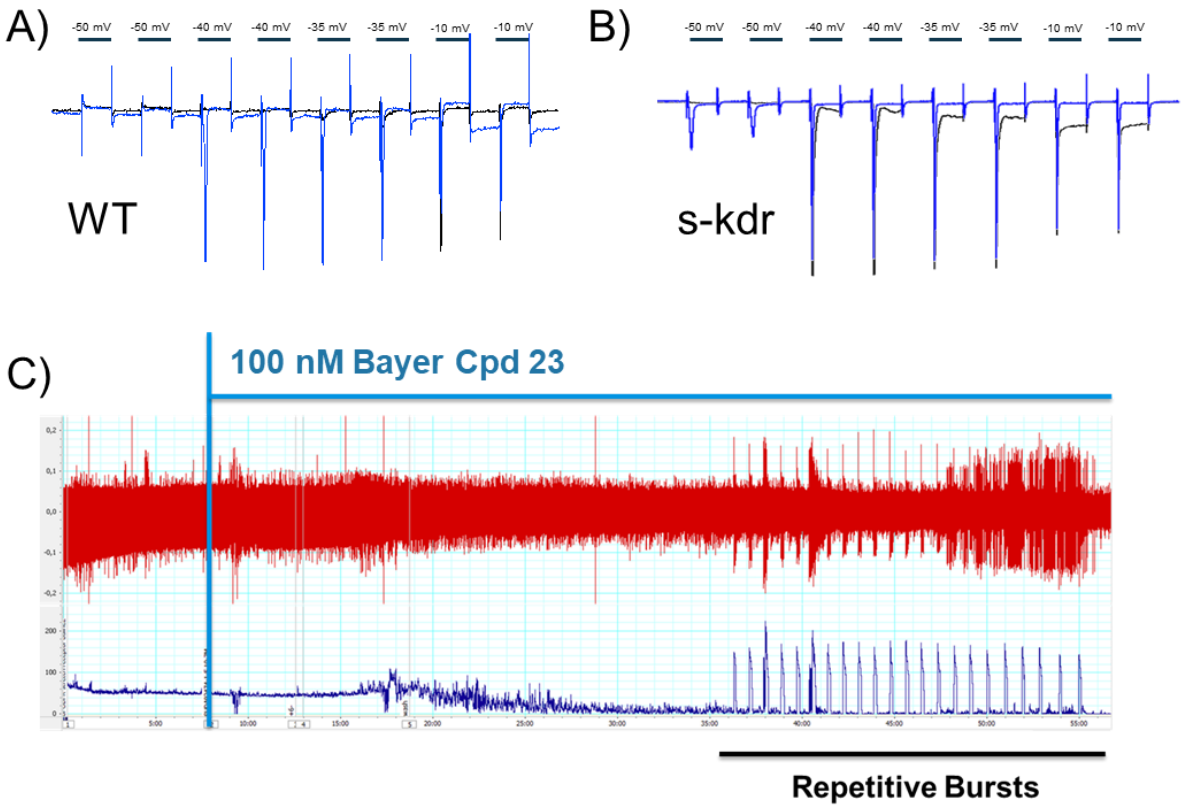

Figure 45 - further electrophysiological characterization of the hit class
C & D) MPC traces of WT *Musca domestica* VSSC and skdr *Spodoptera frugiperda* VSSC in the presence (blue) and absence (grey) of 30 µM compound. **E)** ex vivo nerve recording of 100 nM compound with the action potential amplitude (red) and frequency (blue).

The voltage shift was confirmed at the WT and the skdr cell line. These results indicated the resistance-breaking potential of Bayer Cpd 23 even though it was not measurable in the fluorescent

readout. Further tests on the non-optogenetic human cell line verified the selectivity towards the insect sodium channel.

The next step in verification was the in situ testing of Bayer Cpd 23 on the isolated efferent nerve cord of *Spodoptera frugiperda* (7.2.6.2 In situ nerve recordings). Electrical discharges after the application of 100 nM compound revealed repetitive burst activity. VSSC modulation periodically increased the action potential amplitudes. The periodic elevation of action potential frequencies correlates with the rhythmical contractions of the animals in the *in vivo* studies. This phenotype correlates with the excitatory effect of other voltage shifters, like beta scorpion toxin, as published in 1982 by Couraud and fits the rhythmic contractions seen in the injection studies.[291] The drop of action potential frequency between the bursts results in a shift of high portions of the VSSC population into the slow inactivated state due to the overexcitation of the cell and the persistently elevated membrane potential.[292]

All results confirmed Bayer Cpd 23 as a valid, potent and resistance-breaking VSSC modulator. In the hit expansion, chemical relatives of Bayer Cpd 23 reentered the testing cascade. The whole clusters were tested in all verification assays to give structure activity estimations, check for data consistency, and validate the hit cluster as true. The FLIPR results allowed a primary SAR showing chemical target points for at least three positions at the structure. Also, the results of the APC were consistent among the cluster, showing the voltage shift and the resistance breaking potential. In the injections, intrinsic activity for several members of the hit cluster was proven. The *in vivo* activity correlated strongly with the *in vitro* activity (pEC_{10} measured in FLIPR). (Figure 46)

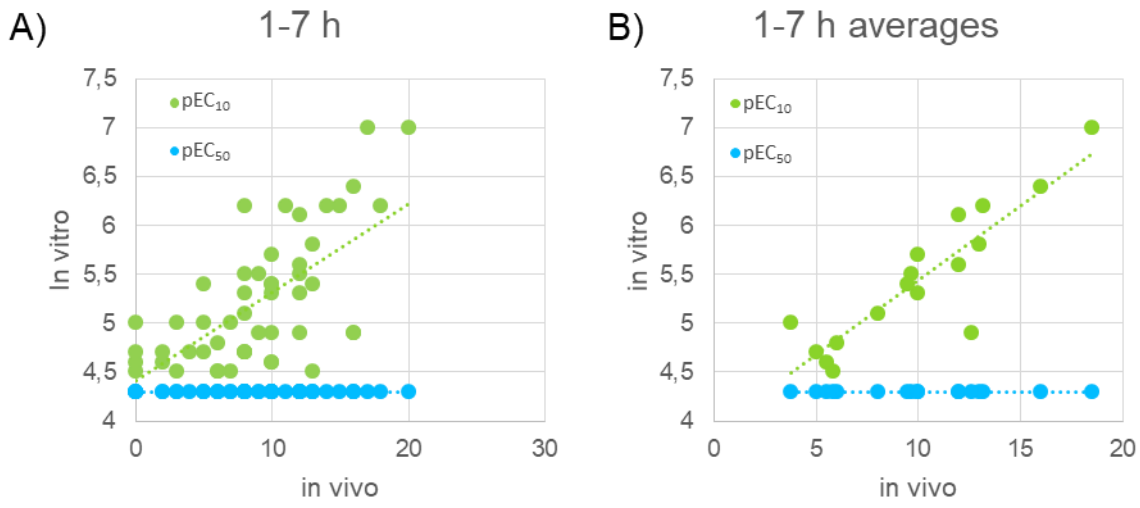

Figure 46 - In-vivo/in-vitro correlation of Bayer Cpd 23 cluster members
Correlation of in-vitro data (pEC_{10} and pEC_{50}) measured in FLIPR Tetra vs. in-vivo data (number of green boxes from 1 – 7 h among all measured dosages). Shown are values for all cluster members **(B)** and aggregated based on their pEC_{10} **(C)**.

A new approach to correlate the *in vitro* and *in vivo* data were investigated for this analysis. Different time points and systems were considered, like lethality and the number of symptoms after two hours, within two hours, seven hours or two days. It was shown that the number of symptoms within the first seven hours (at 1 h, 2 h, 4 h and 7 h) among all measured concentrations assists as predictive transfer value to the *in vitro* pEC_{10} data. The pEC_{50} data were not correlating as they were not measurable in this setup, pointing out the relevance of the pEC_{10} as a relevant value for the VSSC.
These data give a comprehensive overview of the features of the hit Bayer Cpd 23 and the whole chemical cluster. Electrophysiology proved resistance-breaking properties, and a good preliminary *in vivo* performance was verified.

5.6 Identification of Binding Site at the VSSC via Mutagenesis

For the identification of the binding site, mutagenesis studies were performed in different areas of the VSSC according to the strategy discussed in 3.4 Mutagenesis. The sequences were blasted on the internet based on the *Musca domestica* sequence. All ten human sodium channels were analyzed and compared to four insect channels of different species for alignment. Those were the sequences of *Musca domestica* & *Spodoptera frugiperda* as species with available VSSCs and *Anopheles funestus* and *Leptinotarsa decemlineata* to enlarge the aligned panel with two further insect classes and pest species.[211–213] Based on the primary sequences available on the internet, an alignment was made to identify the variable amino acids between insect and human VSSCs (see Figure 47). As decisive VSSCs, the human $Na_V1.7$ and the *Musca domestica* channel were chosen, as the selectivity profile was conducted based on these two channels. Based on these alignments, the amino acids and their surrogates were determined (amino acids highlighted with arrows in Figure 47) to humanize the fly channel and create a loss of sensitivity mutant.

The mutants were ordered at GeneArt and expressed transiently in a HEK293 cell, already stably expressing the β-subunit. In the next step, this mutant was treated with selective and unselective compounds from one cluster to see whether a decline in sensitivity was reached and a human Na_V-like pharmacological pattern was seen for the mutant. Besides the selectivity, two additional parameters were chosen to decide on areas to mutate. On the one hand, a binding site located in the upper funnel of the voltage sensor in domain three was identified by co-crystalization of a $Na_V1.7$ antagonist in the Na_V by Ahuja et al. making it an interesting area to investigate.[210] Furthermore, the effect on the VSSC was considered by making conclusions on the binding site based on the measured effect. Besides the humanization of whole areas, also point mutations were tested, covering another area than the voltage sensor of domain three. These minor interventions were not expected to lead to a complete loss of sensitivity.

The first area of interest was the voltage sensor of domain III, which came into focus as Ahuja et al. were publishing compound binding of a human $Na_V1.7$ inhibitor in the upper funnel.[210] Nineteen amino acids in the entire region were then humanized (see Figure 47), some with drastic changes like from glutamine to glutamic acid (polar to negatively charged) or from aspartic acid to tyrosine (negatively charged to hydrophobic). Others with minor modifications, from lysine to arginine or valine to isoleucine, where the chemical properties remained the same, but minor steric differences occurred.[293] The functional expression was successful, but the activity of the reference compound showed no significant decline in the humanized mutant compared to the WT *Musca domestica* VSSC. (Figure 47)

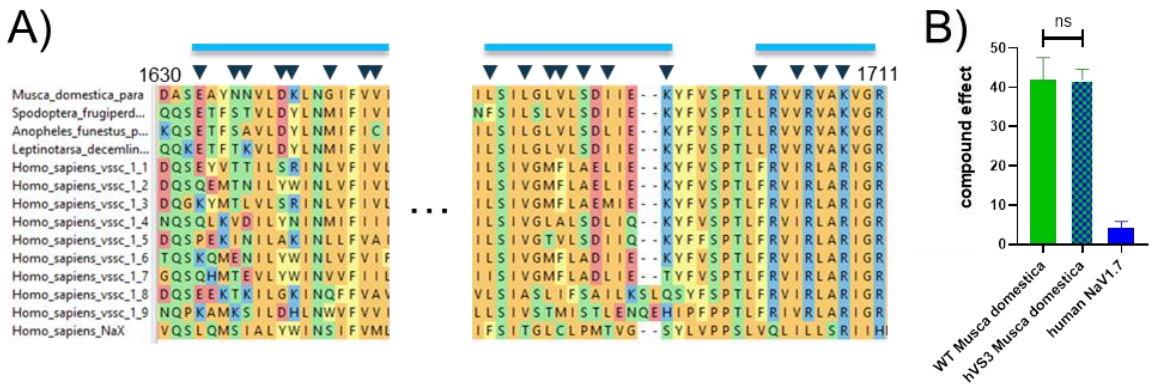

Figure 47 - Mutagenesis studies at the humanized voltage sensor 3 (VS3)
A) Alignment of the primary VSSC sequence from VS3 (upper funnel: blue bars) with the mutated sites indicated by arrows. Shown are four representatives of insect channels and all humans. B) Relative currents of transiently transfected HEK cells with the humanized channel. Measured were currents during the inactivated state after applying 10 µM reference compound for three different sodium channels. The data set consists of triplicates on all VSSC subtypes, statistical significance cannot be proven.

After excluding the whole voltage sensor three as the binding site, another area came into focus. For confidentiality reasons, the exact sequences remain secret in this thesis. In MPC experiments, it was shown that both mutants are functionally expressed. One mutant consisted of a point mutation and an amino acid depletion, while the other was just mutated once. The first mutant had a serine exchange by glutamine (alcohol to amid), featuring other steric properties besides the functional groups. The functional expression was successful and robust Na currents were measurable. The channel physiology, however, was altered, as the mutation caused a sub conductance during the fast inactivated state. The double point mutation shows no decline in response to the tool compound compared to the WT VSSC. The second mutation made with this approach was an exchange of glutamine to valine (polar to nonpolar), eliminating the functional amid reaching in the proclaimed cavity. The relative activity in the insect channel significantly dropped from 40 % at the WT channel to 25 % for the single point mutation Q > V after applying Bayer Cpd 33 (Figure 48). Even though this mutant did not create a loss of sensitivity, these results indicate the identification of the potential binding cavity.

Based on the Q > V mutant, a second mutation was introduced, exchanging methionine with an alanine (nonpolar to polar). The functional expression after chemical transfection of this mutant failed (out of 22 measured cells, none showed a significant Na^+ current).

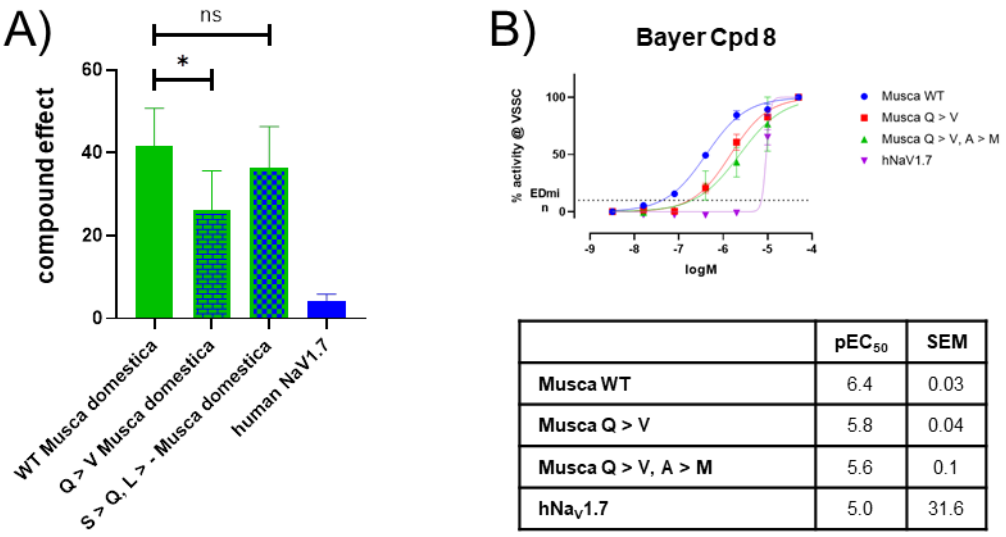

	pEC_{50}	SEM
Musca WT	6.4	0.03
Musca Q > V	5.8	0.04
Musca Q > V, A > M	5.6	0.1
$hNa_V1.7$	5.0	31.6

Figure 48 - response of different WT and humanized VSSCs to 10 µM Bayer Cpds
A) Relative currents of the VSSCs during the inactivated state after application of 10 µM Bayer Cpd 33 for four different sodium channels. The data set consists of triplicates on all 4 VSSC subtypes, statistical significance was proven by an unpaired two-tailed t-test (p 0.0278). **B)** Shown are CRCs and EC_{50} values of transiently transfected VSSCs for Bayer Cpd 8. The curves were normed to (their maximal response) fitted and calculated in GraphPad Prism using the commonly used variable slope fit.

Therefore, further experiments were conducted in the FLIPR Tetra after electroporation. Transfection was conducted in the MaxCyte®, having much higher transfection efficiencies as reported by Kim.[294] Tested was an insect-selective compound. It was measured at four cell lines in parallel after transfection. The selective compound (Bayer Cpd 8) exhibits the expected higher activity at the insect VSSC (pEC_{50} 6.38 ± 0.03) than the human homolog (pEC_{50} 5.03 ± 31.5). The high deviation results from an outlier at 10 µM, causing a too steep slope for curve fitting (Figure 48). At this concentration, just 1 out of 2 values showed a disproportionately higher effect than regular. A possible reason could be poor channel expression due to transient transfection. The concentration-response curve and the humanized channels' activity are located between both WT channels. The single point mutation (pEC_{50} 5.83 ± 0.04) features a slightly higher activity of Bayer Cpd 8 than the double point mutation (pEC_{50} 5.63 ± 0.1), resulting in an overall activity based order for reference compound: Musca VSSC < 1x humanized VSSC < 2x humanized VSSC < human $Na_V1.7$. These data align with the electrophysiological results of the single point mutation (Figure 48) and might help narrow down the binding cavity. However, those data are preliminary and require further investigation.

5.7 *Drosophila melanogaster* Slo

5.7.1 Electrophysiological characterization and cryo-EM structures

The physiological role of the Slo potassium channel makes it an exciting target for developing new insecticides. Therefore, two known modulators were electrophysiologically characterized. Emodepside is an anthelmintic market product in animal health, acting as an agonist. On the other hand, verruculogen, a mycotoxin, acts as an antagonist at the Slo channel. Parts of this thesis were published in Nature communications by Raisch,T., Brockmann, A., Ebbinghaus-Kintscher, U. et al.[295] The modulators were characterized in manual patch clamp experiments and supported by automated patch clamp (APC) experiments for statistical significance.

The traces in Figure 49 B revealed the characteristics of emodepside and verruculogen. Low intracellular Ca^{2+} concentrations were not able to activate Slo. After applying 3 µM emodepside, the channel opens, facilitating potassium influx at low potentials and outflux at high potentials. The measured currents for each pulse are equidistant, leading to the linear voltage-current relationship. As shown by the IV curve in Figure 49 C, the effect of emodepside at high Ca^{2+} concentrations is similar to those at low Ca^{2+} concentrations (Figure 49 B, upper panel and third panel). This indicates a loss of Ca^{2+} dependency, as already described by Crisford et al.[296] In this experiment, the reversal potential of -86 mV was measured, close to the equilibrium potential for potassium calculated by the Goldman-Hodkin-Katz equation, revealing the potassium ions as the driving force. The in and outflux at high and low membrane potentials were also shown in APC experiments (see Figure 52) with the cursor at -160 (light blue) and 100 mV (dark blue).

This effect's mechanics were resolved with the Max-Planck institute, which determined the cryo-EM structure. Figures 50 A and B show that the emodepside spans over all four subunits, and the side chains reach into the S6 segments within the central pore. Emodepside binding locks the channel in an open conformation. The ring structure with the central hole was shown to be wide enough to facilitate K^+ translocation despite binding. Even though an ion flux is still possible, it might be impaired by traveling across the ring structure. The cryo-EM structure furthermore revealed that coordination of dehydrated K^+ ions is possible but imperfect. The angles of the carbonyls are slightly diverging, leading to the observed lowered signals at high internal Ca^{2+} concentrations. The observed pore-like behavior is perfectly explained by the facilitated conductance through a permanently open and voltage and Ca^{2+} independent Slo channel.[295]

Verruculogen was measured under high internal Ca^{2+} concentrations, leading to a full block of potassium influx in MPC and APC, similar to the results of Crisford et al.[296]. In MPC and APC experiments, it was shown that verruculogen could not block emodepside-induced currents and *vice versa*.

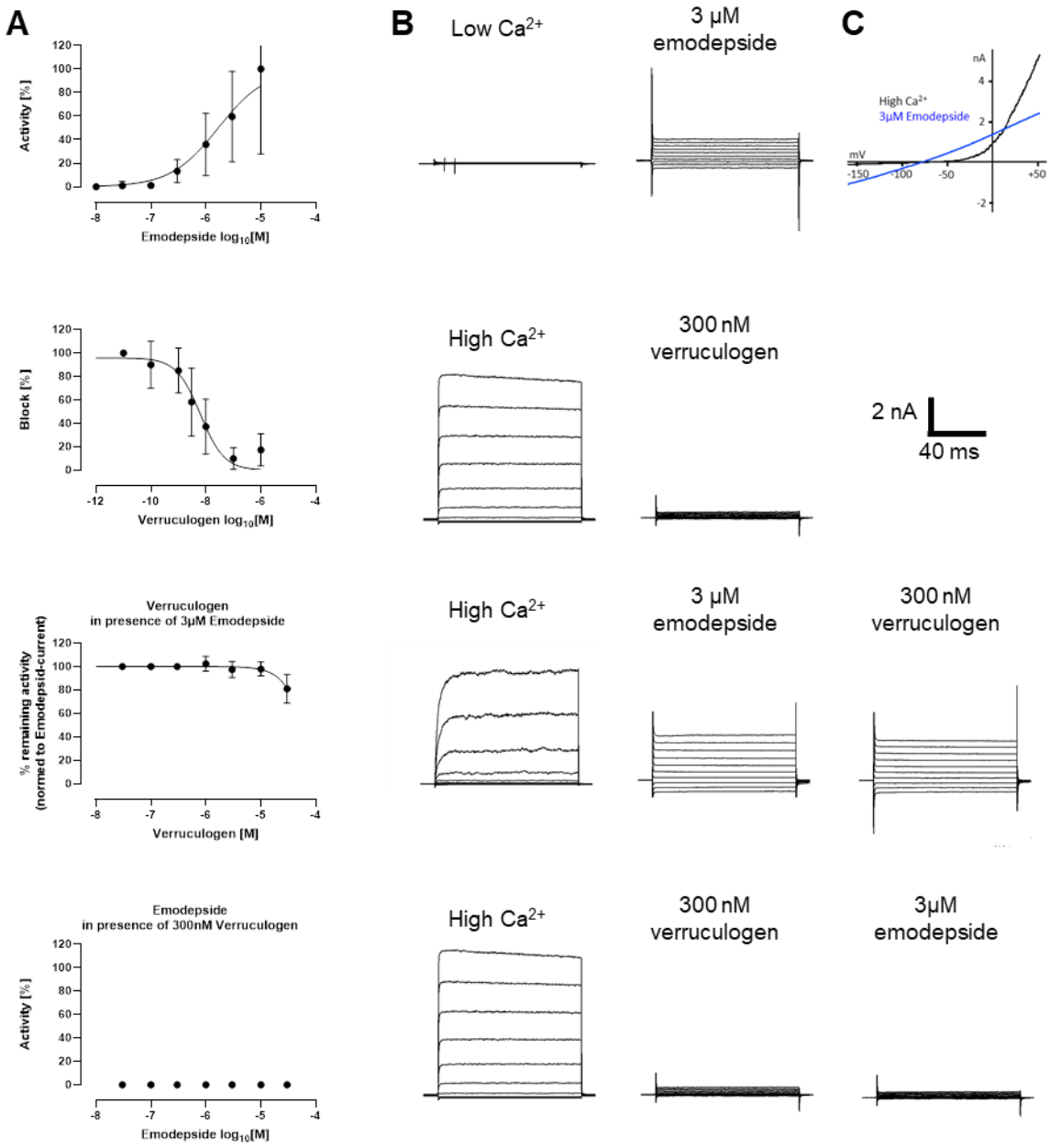

Figure 49 - Electrophysiological measurements on *Drosophila melanogaster* Slo channel with two tool compounds

A Shown are concentration-response curves of emodepside, verruculogen, and their interaction. Measured were cells stably expressing Slo at low (just first curve) and high internal Ca^{2+} in APC. **B** MPC data of the same cells were measured in ten voltage steps (Δ20 mV) starting at -120 mV and a holding potential of -70 mV. Measured were low (30 nM) and high (300 nM) internal Ca^{2+} conditions in the presence and absence of two tool compounds. **C** Emodepside effect (blue) on Slo channel at high intracellular Ca^{2+} levels measured in MPC with voltage ramps from -160 mV to 60 mV under control conditions (black).

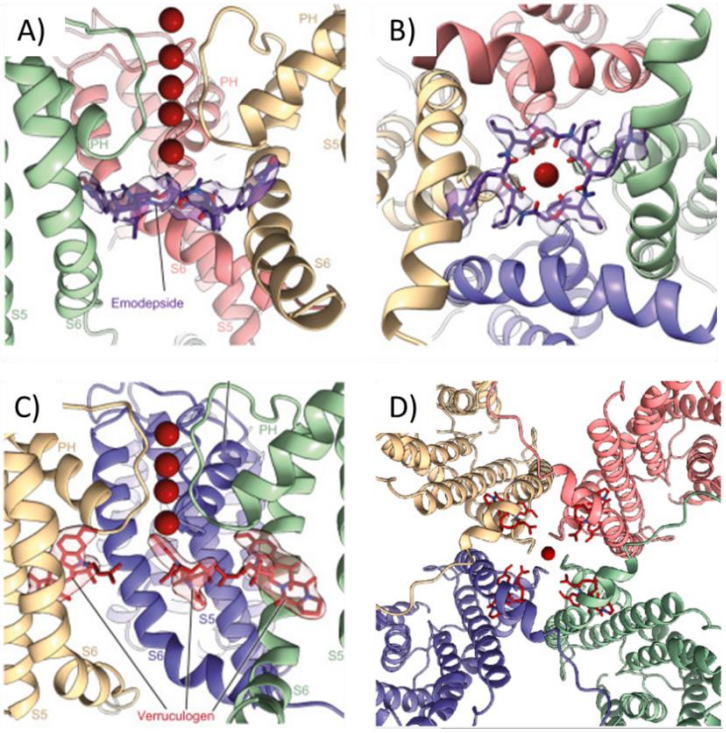

Figure 50 - cryo-EM structures of Slo bound to both tool-compounds[295]
The cryo-EM structure of Slo comprises all four macromolecular chains (color-labeled), the two modulators (violet and red) as well as potassium ions (red dots). A) Section of the cavity of emodepside bound Slo from the side. One of four macromolecular chains was removed to facilitate a view into the cavity B) Section of the cavity of emodepside bound Slo from the cytosol. C) Section of the cavity of verruculogen-bound Slo from the side. One of four macromolecular chains was removed to facilitate a view into the cavity. D) Section of the cavity of verruculogen-bound Slo from the cytosol.

The nature of the interaction for both compounds was solved by the already mentioned cryo-EM structure of verruculogen and emodepside bound *Drosophila* Slo. As a reason for the interference, we identified an overlap of the binding sites for both compounds, as seen in Figure 51. Two minor clashes between the morpholino of the cyclooctadepsipeptide and the isobutyl-group of two opposite verruculogen molecules prevent the binding of both modulators. Furthermore, two major clashes are between the verruculogen molecules binding at a 90° angle, the interaction of the isobutyl group and the emodepside heterocycle. Both compounds bind in the same cavity and have four clashes, preventing the other modulator from binding.

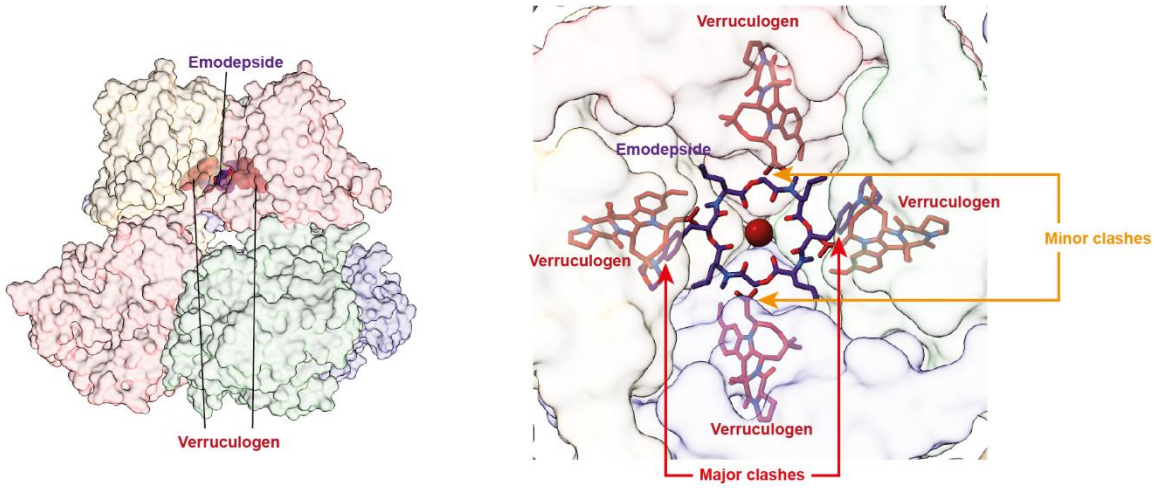

Figure 51 - An overlay of verruculogen and emodepside binding sites
Overlay of total CryoEM structure from *Drosophila melanogaster* Slo with either emodepside or verruculogen bound (left side) and overlay of the central pore region of verruculogen and emodepside bound Slo channel shown from the cytosol (right side).

The CRC quantification and calculations were made based on the APC experiments. The channel was activated by increased internal Ca^{2+} concentrations and measured by voltage ramps from -160 to 100mV. Control applications with DMSO revealed a decline in the signal at 100 mV. Rothberg et al. identified 1996 high Ca^{2+} concentrations to cause a desensitization of Slo channels in rat muscles, which could explain the measured effects.[297] These rundown effects were considered for calculations by applying the linear function depicted in Figure 52 (dotted green line).

The physiological agonistic effect of emodepside was quantified at low internal Ca^{2+}. Automated patch clamp experiments showed a pEC_{50} 5.76 ± 0.1 for emodepside. The upper panel of Figure 49 B and C MPC data describes the emodepside effect under low and high internal Ca^{2+}. A pEC_{50} is not published for the insect channel as emodepside is an anthelmintic market product. Kashyaop et al. published 2019 a sex-dependent EC_{50} of 0.72 and 0.29 µM for *Brugia malayi,* a tropical nematode.[298] Hübner et al. published 2021 EC_{50} values of emodepside for different nematode assays ranging from 0.01 – 0.35 µM.[299] Our measured pEC_{50} of 5.76 (EC_{50} of 2.14 µM) at the *Drosophila melanogaster* Slo in APC are approximately 10 - 100x fold higher.[295] This spectrum of selectivity has to be considered, as emodepside was optimized to target the nematode Slo and does not contradict but approves the measured insect values. Furthermore, Crisford et al. published 2015 data on emodepside use on drosophila Slo, which showed comparable activities, even though a complete concentration-response curve was not measured in 2015.[296]

The application of verruculogen leads to a reduced current, with complete inhibition at higher concentrations. The pIC_{50} value gained for verruculogen was measured in APC and calculated based on the described method. The measured pIC_{50} of 8.14 (IC_{50} of 7.24 nM) corresponds to the pIC_{50} value published in 2015 by Crisford et al. using MPC measurements.[296]

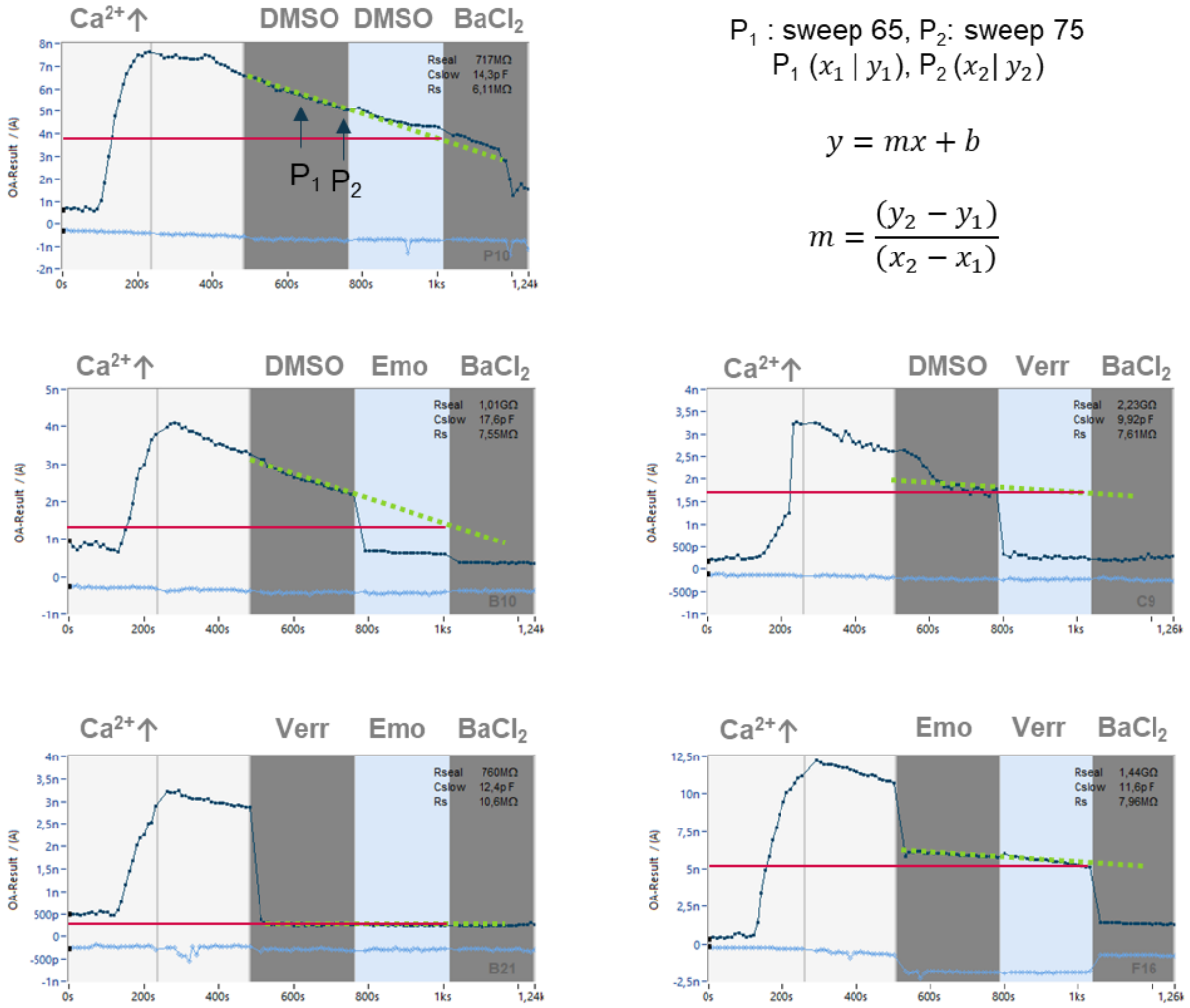

P_1 : sweep 65, P_2: sweep 75

$P_1\ (x_1 \mid y_1)$, $P_2\ (x_2 \mid y_2)$

$$y = mx + b$$

$$m = \frac{(y_2 - y_1)}{(x_2 - x_1)}$$

Figure 52 - Evaluation of automated patch clamp results on the Slo channel
Shown are Slo currents at potentials of -160 (light blue) and 100 mV (dark blue) in response to different changes (an increase of internal Ca^{2+}, application of 30 µM emodepside (Emo), 300 nM verruculogen (Verr) and 3 mM $BaCl_2$). The dotted green line describes the extrapolation of the rundown of potassium currents seen occasionally, with the assigned function used for calculation.

5.7.2 Mutagenesis studies

The mutagenesis studies were performed to identify the mechanics of the antagonist verruculogen. The cryo-EM structure discussed in the previous chapter revealed an unexpectedly large pore diameter of verrucologen-bound Slo, which is still capable of translocating potassium ions.[295] One reason verruculogen is nevertheless inhibiting ion flux might be the modification of gating physics. Gordon et al. published in 2010 the role of threonine 352 to the modulator (HMIMP) of the human Slo1.[300] The threonine was exchanged by a serine, maintaining the functional group without the methyl as a lever. The homolog mutation was performed in the *Drosophila melanogaster* Slo at position 301 and the mutant tested in MPC and APC. MPC data showed an altered channel behavior upon mutation under control conditions. While the WT channel requires membrane potentials of at

least +60 mV for measurable outward currents at 30 nM Ca^{2+}, the mutated channel is persistently open. The mutated channel remains pore-like for increased internal Ca2+, with higher currents than low internal Ca^{2+}. APC results indicate impaired verruculogen binding in two independent experiments. The effect of verruculogen on the mutant was investigated by applying a discriminating concentration of 100 nM. At this concentration, the WT channel was approximately 95 % blocked. The response of the T301S mutant to 100 nM verruculogen was significantly weaker (35%) than the inhibition at the WT channel. These findings were proven by concentration-response curves performed in APC. (Figure 53) The activity at the T301S mutant is reduced by one order of magnitude with a pIC_{50} of 7.52 ± 0.003 for the WT Slo and a pIC_{50} of 6.41 ± 0,067 for the mutant. Those findings are comparable to HMIMP at the human mutant as measured by Gordon et al.[300]

The channel behavior resembles an emodepside bound WT Slo, featuring:

- Reduction of Ca^{2+} sensitivity
- Linear current-voltage relation
- Reduction of verruculogen sensitivity

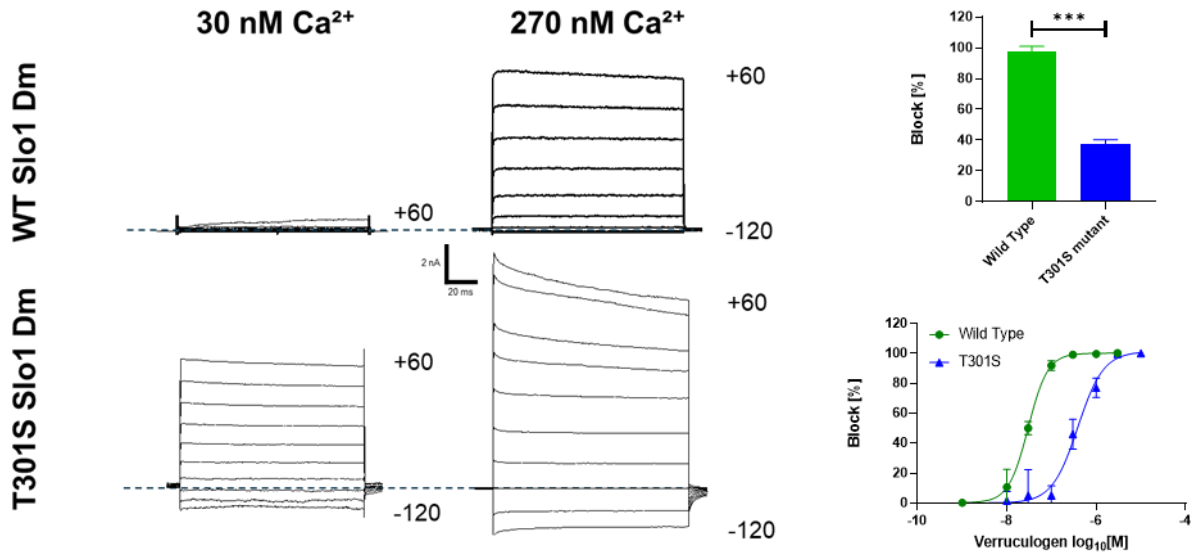

Figure 53 - Effect of T301S mutation on the insect Slo channel
A) Effect of the channel mutation on the calcium sensitivity shown based on two different calcium concentrations. The pulse protocol consisted of 10 voltage steps with 20 mV increments, starting at -120 mV. B) Block of Slo channels by a discriminating verruculogen concentration of 100 nM. C) Concentration-response curve of verruculogen on WT and T301S mutant.

These data are fitting to the results Gordon et al. published for HMIMP. Their reasoning is rotamer preference for the WT channel, as the required energy is 3.94 and 6.92 kcal/mol higher for the Ser352 mutant.[300] This theory does not consider that the pore diameter upon verruculogen binding remains wide enough for potassium translocation. Therefore, we proclaim an impaired dehydration or rehydration of potassium ions passing the selectivity filter. Instead of reducing verruculogen

affinity to the Slo channel, the exchange of threonine might lower the impact of verruculogen on the gating serine and, therefore, its function. On the other hand, the enhanced hydrophobicity in the verruculogen-bound Slo's central cavity prevents water molecules from entering the pore region.[301] This highly lipophilic environment impedes the transition of hydrated potassium ions to the pore domain, preventing ion transport across the channel.[302] Further analysis of the exact MoA requires further experiments investigating alterations in ion selectivity, radioligand binding studies or additional mutations. A better understanding would result in a targeted approach to identifying and synthesizing new Slo modulators.

6. Conclusion & future work

6.1 Optogenetic HTS for the voltage-sensitive sodium channel

In this thesis, an optogenetic HTS assay was developed and optimized and developed. Part of the work was the optimization of buffers on the requirements of a stable HTS assay. The new assay enhanced the response over baseline for different tool compounds covering various modes of action at the insect sodium Para-channel (VSSC). Weak tool compounds, including voltage shifter, not detectable in former HTS, are now measurable with the optogenetic screen. The ionophore facilitates the reduction of the resting potential resulting in a bigger measurement window. The interaction of ionophore and channelrhodopsin facilitated the frequent transition through all channel states.

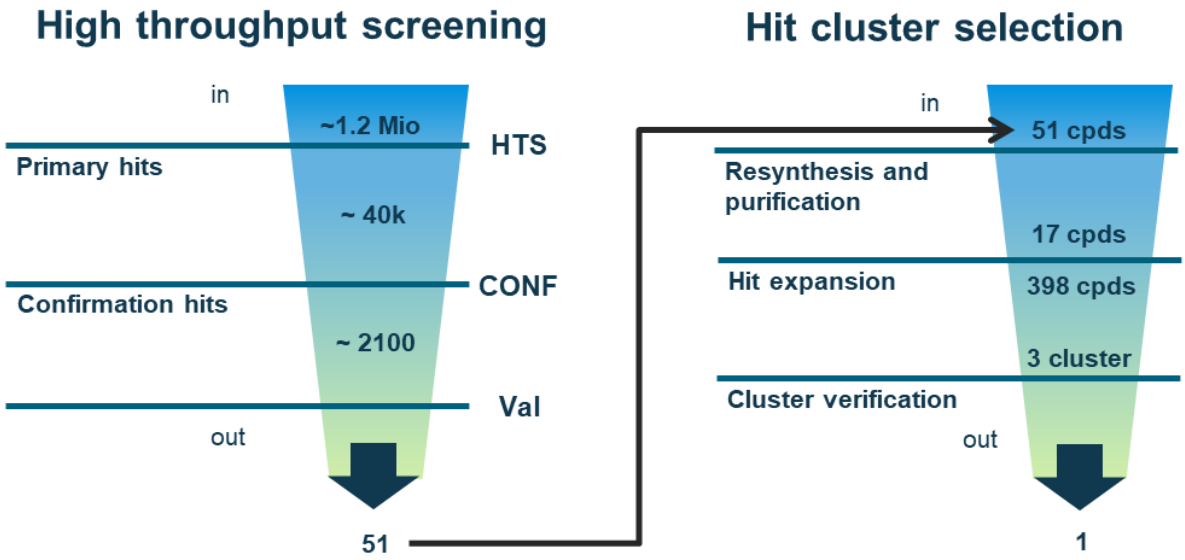

Figure 54 - Summary of VSSC high throughput screening campaign
Shown are the different sections the compounds had to pass until being considered a hit. Numbers indicate the number of compounds passing the stage and entering the next one.

In this HTS campaign, 1 200 000 compounds were tested in the Target Research department. After different selection steps, 2100 compounds were validated in parallel in the fluorescent readout and automated patch clamp (Figure 54). Different tool compounds covering voltage shifters, inhibitors of inactivation and tail currents were used to validate the pulse protocol. The decision of which compounds to choose for further biochemical validation was made on the primary basis of the patch clamp experiments. Additional aspects considered were the performance in the HTS fluorescent readout and the chemical attractiveness and accessibility of the compounds.

For biochemical validation, a testing cascade was established to identify the lead structures with the highest probability of success. Fifty-one compounds were tested in the analog fluorescent readout

(FLIPR), APC and symptomatology. One candidate, including its chemical analogs, showed the appropriate result profile (Figure 55). In electrophysiological experiments, the compound class was shown to shift the activation of the sodium channels towards more negative potentials. Besides, these experiments proved the resistance-breaking potential of this class by shifting the activation at the pyrethroid insensitive skdr mutant. The measured cluster of compounds had a consistent structure-activity relationship at the sodium channel. When comparing the fluorescence measurements with the injection studies, this class showed a good correlation between the in vitro and in vivo values.

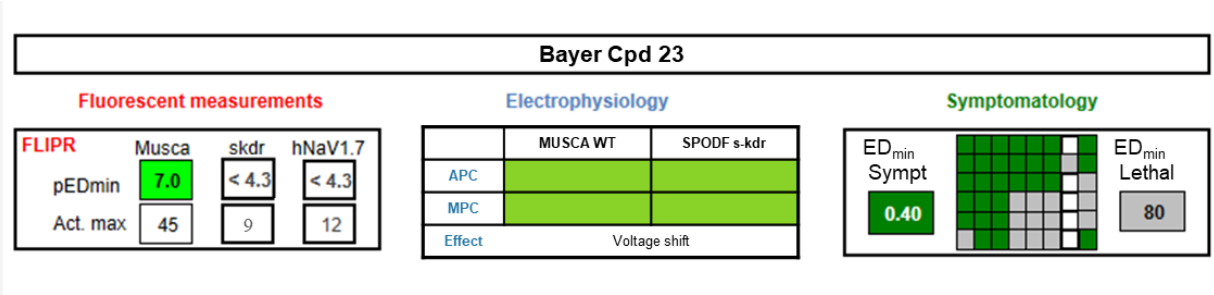

Figure 55 - Result profile of Bayer Cpd 23 as the most promising hit compound

In parallel binding studies for other VSSC modulators were implemented. In mutagenesis studies, different constructs were designed based on the selectivity profile of the compounds. All mutants were successfully functionally expressed and measured in either MPC or the FLIPR Tetra. The third voltage sensor of the VSSC was excluded as a binding site, while single point mutations close to an area of interest had a significant effect (Q > V). Based on these findings, a second single-point mutation was made, having a further mutation in this region (Q > V, A > M). In FLIPR experiments, the decline of efficacy for the first mutant was proven. Furthermore, the channel possessing the double-point (Q > V, A > M) mutation showed a slightly stronger decline than the single-point mutation. In follow-up studies, creating a mutant with a total loss of sensitivity would support these preliminary data. A cryo-EM structure would help to elucidate the exact binding mode.

6.2 Electrophysiological characterization of *Drosophila melanogaster* Slo

Mode of action and binding mode elucidation was performed for two different modulators, emodepside, a well-known anthelmintic and verruculogen, a mycotoxin. Both were applied in electrophysiological experiments and resolved in cryo-EM studies. The results of the linear current-voltage relation hinted towards a pore-like behavior. This mode of action was then validated by a cryo-EM structure, locating the cyclodepsipeptide in the pore region and facilitating an ion flux through the ring structure. Verruculogen binds in the same cavity as emodepside, explaining the interaction of both compounds observed in the electrophysiological experiments. Despite the cryo-EM structure, the antagonistic MoA is not fully understood. Therefore, mutagenesis studies on the

threonine, which is involved in gating, were performed. The mutation altered the channel physiology, mimicking an emodepside bound state of the Slo channel with a reduced verruculogen activity, an uncoupled Ca^{2+} dependency and linear current-voltage dependency. In further experiments, altered ion conductance and additional mutations must be investigated.

7. Material & Procedures

7.1 Material

7.1.1 Devices

Device	Model	Company
Amplifier	HEKA EPC10	HEKA Electronics
Analytical Balance	XS105 DualRange	Mettler Toledo
Assay Imager	Hamamatsu camera	Hamamatsu
Cell counter	LUNAII	Logos
	NucleoCounter SCC-100™	Chemometec
Centrifuges	5810 R	Eppendorf
	5417 C	
Fluorescent Reader	FLIPR Tetra	Molecular Devices
Heat plate with magnetic stirrer	RET	IKAMAG
	RCT	
Heat block	Thermomixer C	Eppendorf
Incubator	CCL 170 B	ESCO
	CB 170	Binder
Laminar Airflow Workbenches	SAFE2020	Thermo Scientific
Micromanipulator	MP-285	Sutter Instruments
Microscope	Axio	Zeiss
Multidrop	MultidropCombi	Thermo Scientific
Multipipettes	E1 ClipTip	Thermo Scientific
pE4000 CoolLED	pE4000	CoolLED
pH meter	pHMeter 766	Knick
Photometer		
Pipette robot	FELIX	Analytic Jena CyBio
Pipette robot	Biomeck	Flow Robotics
Pipettors	Pipetus	Hirschmann
Plate robot	Platebutler	LabServices
Puller	PC-10	Narishige
SyncroPatch384	SyncroPatch384 FX	Nanion Technologies
Ultrasonic Bath	TRAussonic460	FAUST
Water Bath	WNB	Memmet
Water purifier	Milliq QPOD	Merck

7.1.2 Software

Software	Company
PatchMaster	HEKA Electronic
Igor	WaveMetrics
Microsoft Office 365	Microsoft
GraphPad Prism9	Dotmatics
DNAStar Lasergene 16	DNAStar
MEGA6	MEGA Software

Screenworks4.0	MolecularDevices

5.1.3 Consumables

Hardware	Model	Company
Assay plates	96 well clear 384 well clear 384 read plates poly d Lysine treated	Greiner
Cellculture flask	75 cm² 175 cm² Triple 450 cm² 25 cm²	Sarstedt
Coverslips	12 mm	
Dispensing cassette	Volume 0.5 – 50 µL	Multidrop
Falcon tubes	15 and 50 mL	Sarstedt
Kits	QIAfilter™ Plasmid Midi Kit	Quiagen
Multiwell plates	Four well clear	Greiner
Pipette tips	Volume 1 – 50 mL	Eppendorf
Reaction tubes	0.5 – 5 mL	Eppendorf
Syncro Chip	384 high resistance 384 medium resistance	Nanion
Syringe	10µL	Hamilton

7.1.4 Chemicals

All chemicals mentioned in this thesis were purchased from Sigma-Aldrich. Otherwise, it is labeled in the text.

7.1.5 Solutions

Application	Buffer/Solutions	Component	MW [g/mol]	Molarity [mM] (or in %)	pH-value (used acid/base)
MPC general	Standard Ringer	NaCl	58.44	150	7.4 (NaOH)
		KCl	74.55	4	
		$CaCl_2$	95.21	2	
		$MgCl_2$	110.98	2	
		Hepes	238.30	10	
MPC VSSC	CsCl-Pip	CsCl	168.36	150	7.3 (CsOH)
		EGTA	380.35	10	
		Hepes	238.30	10	
	CsF-Pip	CsF	151.9	120	7.3 (CsOH)
		CsCl	168.36	30	
		EGTA	380.35	10	

		Hepes	238.30	10	
MPC Slo	KCl-Pip	KCl	74.56	150	7.3 (KOH)
		EGTA	380.35	10	
		Hepes	238.30	10	
APC general	External solution	NaCl	58.44	140	7.4 (NaOH)
		KCl	74.56	4	
		$CaCl_2$	147.02	2	
		$MgCl_2$	203.3	1	
		Glucose	180.16	9	
		HEPES	238.30	10	
	Seal enhancer	NaCl	58.44	80	7.4 (HCl)
		KCl	74.56	3	
		$CaCl_2$	147.02	35	
		$MgCl_2$	203.3	10	
		HEPES	238.30	10	
APC VSSC	Internal VSSC	CsCl	168.36	10	7.2 (CsOH)
		CSF	151.90	110	
		EGTA	380.35	20	
		HEPES	238.30	10	
	NMDG	NaCl	58.44	80	7.4 (HCl)
		KCl	74.56	4	
		$CaCl_2$	147.02	5	
		$MgCl_2$	203.3	1	
		NMDG	195.22	60	
		Glucose	180.16	5	
		HEPES	238.30	10	
APC Slo	Internal Slo 0nM Ca^{2+}	KF	58.1	60	7.2 (KOH)
		EGTA	380.35	2	
		HEPES	238.30	10	
		Na_2-ATP	551.14	2	
		KCl	74.56	75	
		$MgCl_2$	203.30	1	
	Internal Slo 30nM Ca^{2+}	KF	58.1	40	7.2 (KOH)
		EGTA	380.35	10	
		HEPES	238.30	10	
		Na_2-ATP	551.14	2	
		KCl	74.56	85	
		$CaCl_2$	147.02	3	
		$MgCl_2$	203.30	1	
	Internal Slo high Ca^{2+}	KF	58.10	50	7.2 (KOH)
		EGTA	380.35	2	
		HEPES	238.30	10	
		Na_2-ATP	551.14	2	
		KCl	74.56	83	
		$CaCl_2$	147.02	2	
		$MgCl_2$	203.30	1	
Nerve recording	Saline II	NaCl	58.44	28	6.5 (NaOH)
		KCl	74.56	16	
		$CaCl_2$	147.02	9	
		$MgCl_2$	203.3	18	
		Sucrose	342.3	175	
		NaH_2PO_4	119,98	1.5	
		Na_2HPO_4	141,96	1.5	
Fluorescence assay	K_0-Tyrode	NaCl	58.44	130	7.4 (NaOH)
		$NaHCO_3$	84.01	5	
		$MgCl_2$	203.3	1	
		$CaCl_2$	147.02	2	

	Glucose	180.16	10	
	HEPES	238.30	20	
K_{10}-Tyrode	KCl	74.56	10	7.4 (NaOH)
	NaCl	58.44	125	
	$NaHCO_3$	84.01	5	
	$MgCl_2$	203.3	1	
	$CaCl_2$	147.02	2	
	HEPES	238.30	20	
Loading buffer	dye		[0.75]	7.4 (NaOH)
	Retinal	284,44	5	
	Bayer Cpd 9		10	
	Pluronic		0,0015 %	
	K_0-Tyrode		ad	

A slider was used to calculate internal Ca2+ concentrations in APC Slo solutions. It calculated the concentrations based on the applied EGTA and Ca^{2+} concentrations.

For MPC Slo experiments, $CaCl_2$ was added to KCl-Pip, to reach the desired Ca^{2+} concentration.

7.1.6 Cell lines

Name	Host cell line	Origin
ßVSSC	HEK293	AXXAM
Musca VSSC ChR2	HEK293	AXXAM
Mock HTS (ChR2)	HEK293	AXXAM
hNaV1.7	HEK293	AXXAM
Musca VSSC	HEK293	AXXAM
Spo VSSC skdr	HEK293	AXXAM
DmSlo	CHO	Bayer Stock
Mock	CHO	Bayer Stock

7.1.6 Plasmids

Plasmid	Vector	Gene of Interest	Accession No.	Selection	Origin
pcDNA3.1Mut1	pcDNA3.1	Para Q>V		AMP/Puro	GeneArt
pcDNA3.1Mut2	pcDNA3.1	Para S>, L>Q		AMP/Puro	GeneArt
pcDNA3.1hVS3	pcDNA3.1	Para humanized in volt. sensor 3		AMP/Puro	GeneArt
pcDNA3.1Mut3	pcDNA3.1	Para A>M, Q>V		AMP/Puro	GeneArt
pEGFP-N1		eGFP		Kan	

7.2 Procedures

7.2.1 Computational analysis

Alignment was performed with a default MUSCLE alignment by DNAstar MegAlign Pro 16. Sequences analyzed were obtained by blasting the Musca domestica VSSC primary sequence among all organisms of interest by NCBI BLAST (*Link*) for all relevant sequences. Sequences of Musca domestica as a model organism were aligned, relevant pest species (*Spodoptera frugiperda*, *Anopheles funestus* and *Leptinotarsa decemlineata*) and all human VSSC subtypes. The amino acids were colored by chemistry.

Phylogenetic analysis was performed by the Maximum Likelihood method and a JTT matrix-based model (JONES D.T., Taylor W. R., and Thornton J.M. (1992) the rapid generation of mutation data matrices from protein sequences). Initial trees for the heuristic search were obtained automatically by applying Neighbor-Join and BioNJ algorithms to a matrix of a pairwise distance estimated using a JTT model, and then selecting the topology with superior log likelihood value. The tree with the highest log likelihood is shown. The tree is drawn to scale, with branch lengths measured in the number of substitutions per site. This analysis involved 31 amino acid sequences. There were a total of 2293 positions in the final dataset. Evolutionary analyses were conducted in MEGA X (Kumar S., Stecher G., Li M., Knyaz C and Tamura K. (2018). MEGA X: Molecular Evolutionary Genetics Analysis across computing platforms).

7.2.2 Cell culture

7.2.2.1 Culturing cells

Untransfected HEK293-cells were cultured in Minimum Essential Medium Eagle with Earle's Saltas (EMEM, BioWhittaker cat. No. BE12-125F), supplemented with 10 % (v/v) FBS and 2 mM Ultraglutamine 1 (BioWhittaker cat. No. BE17-605) at 37°C, 5 % CO2 and 95 % humidity.

Stably transfected HEK293 cells, expressing the human α NaV1.7 chain (Accession No. NP_002968.1), were cultured in the HEK293 medium with the addition of 200 µg/mL geneticin at 37°C, 5 % CO2 and 95 % humidity.

Stably transfected HEK293-cells expressing the *Musca domestica* Vssc1β (Accession No. AAD31018.1) were cultured in the HEK293 medium with the addition of 50 µg/mL zeocin.

Stably transfected HEK293-cells expressing the *Musca domestica* Vssc1α (Accession No. AAB47604.1) and *Musca domestica* Vssc1β (Accession No. AAD31018.1) were cultured in the HEK293 medium with the addition of two selection antibiotics (0.1 µg/mL puromycin and 50 µg/mL zeocin).

Stably transfected HEK293-cells expressing the *Musca domestica* Vssc1α (Accession No. AAB47604.1), *Musca domestica* Vssc1β (Accession No. AAD31018.1) and Channelrhodopsin 2 T159C (NCBI RefSeq. XM_001701673.1) were cultured in the HEK293 medium with the addition of three selection antibiotics (0.1 µg/mL puromycin, 50 µg/mL zeocin and 10 µg/mL hygromycin).

Stably transfected HEK293-cells expressing the *Spodoptera frugiperda* Vssc1α (Accession No. QRQ89298.1) and *Spodoptera frugiperda* Vssc1β (Accession No. XP_035453136.1) were cultured in the HEK293 medium with the addition of two selection antibiotics (0.25 µg/mL neomycin and 10 µg/mL hygromycin).

Stably transfected HEK293-cells expressing the *Spodoptera frugiperda* skdr Vssc1α (Accession No. QRQ89298.1 +introduced mutations) and *Spodoptera frugiperda* Vssc1β (Accession No. XP_035453136.1) were cultured in the HEK293 medium with the addition of two selection antibiotics (0.25 µg/mL puromycin and 10 µg/mL zeocin).

Untransfected CHOK1-cells were cultured in Minimum Essential Medium alpha Medium with GlutaMAX™ (MEM alpha medium, Gibco cat No. 32571-028), supplemented with 10 % (v/v) FBS at 37°C, 5 % CO2 and 95 % humidity.

Stably transfected CHOK1-cells expressing the *Drosophila melanogaster* Slo (Accession No. NP_001014658.1) were cultured in the CHOK1 medium supplemented with 200 µg/mL geneticin.

Stably transfected CHOK1-cells expressing the human Slo were cultured in the CHOK1 medium supplemented with 200 µg/mL geneticin.

PC3 cells were cultured in Opti-MEM Medium (Gibco cat No. 31985-047) supplemented with 10 % (v/v) FBS.

7.2.2.2 Thawing cells

Cell culture flasks (75 cm^2) were prepared by filling 13 mL of the respective medium without antibiotics. The cells were removed from the -80 °C or -150 °C freezer and thawed quickly. The cell solution was transferred into a 15 mL tube filled with 9 mL of selection medium and centrifuged (80 xg, 4 min). The supernatant was discarded, the cell pellet resuspended in 2 mL medium without antibiotics and then transferred into the prepared flask. The flask was incubated under conditions suitable for the respective cells (see above). After 1-2 days, the medium was exchanged by medium with a selection medium.

7.2.2.3 Passaging cells

The cells were passaged at a confluence rate of 70 - 80 %. All media and solutions were prepared, sterilized and placed in the clean benches in advance. The old medium was discarded, the cells were carefully washed with PBS and detached at 37 °C with 2 mL accutase solution to detach. Meanwhile, new flasks were prepared by labeling and adding the suitable medium (20 mL). During 2 - 5 min incubation, accutase digested the cells' adhesion molecules and detached them. Subsequently, 7.5 mL of the respective culture medium was added to stop the accutase reaction. The cells were then separated by pipetting the cells up and down against the bottom of the flask. A suitable fraction of

the cell suspension was then transferred to the prepared flasks. The remaining volume was used further or discarded. The new flasks were incubated under appropriate conditions.

7.2.2.4 Generation of Cryo-Cultures

Cells were frozen to keep backups in case re-culturing was necessary. The procedure is similar to the previously described passaging of the cells. After detachment, the cells were transferred into a 50 mL Falcon® tube and centrifuged for 5 min at 200 g. Afterwards, the supernatant was discarded and the pellet was resuspended in precooled FCS supplemented with 10 % DMSO. The cells were gently frozen in special containers with a reduction of 1°C/min.

7.2.2.5 Determination of Cell Number

To determine the exact cell number in the NucleoCounter™, 10 µL of cell suspension was diluted in 40 µL of the respective culture medium. After the addition of 50 µL reagent A100 (chemometic) and B (chemometic) with 1 min incubation time in between, the solution was imbibed air bubble free into the cassette (NucleoCassette™, Chemometec) by lowering the piston 8 mm. The cassette was then transferred into the NucleoCounter™ and analyzed. Dead-life discrimination was not performed. The resulting cell number was multiplied by 15 (dilution factor) to get the correct cell number per milliliter.

For cell number determination with the Luna Automated cell counter, 10 µL of cell suspension was diluted in 10 µL 0.4 % trypan blue stain (logosbiosystems, cat No. T13001) or Erythrosin B stain logosbiosystems, cat No. L13002). The mixture was then applied into the Luna™ Cell Counting Slide. The slide was inserted into the Luna Automated cell counter and the focus adjusted. A dead life discrimination was performed in the counter and the dilution factor was considered.

7.2.3 Molecular Biology

The midi plasmid preparation was performed using the QIAfilter™ Plasmid Midi Kit. All preparations were performed like in the producer's manual described. The dried plasmid was then eluted in 10 mM tris buffer and stored at -20°C. The dried plasmid was eluted in H2O for later electroporation experiments and stored at -80°C.

DNA measurements were performed in a photometer. 10 mM tris buffer was measured as blank in advance of the samples. Two microliters of each sample were diluted in 70 µL of 10 mM tris-buffer and measured at the excitation wavelengths of λ_{230}, λ_{260} and λ_{280}. Ratios 260/280 and 260/230 of approximately 1.8 and 2.0 – 2.2 were considered pure.

RNA isolation was performed on cell culture samples grown for 72 h at 37°C and 5 % CO_2 on 500 cm² tissue flasks. After washing with PBS, cells were detached with accutase solution at 37°C for 5 min. After incorporation with medium, cells were harvested by centrifugation (200 xg, 5 min, 4 °C) and

stored at -80°C until further processed.

RNA purification was performed with the RNeasy Mini Kit (QIAGEN) according to the manufacturer's manual disregarding the steps with the respective lysis buffer since this was already performed in Trizol. For isolation 1 mL Trizol was added and after vigorously mixing were the samples incubated 5 min at room temperature. After addition of 0.2 mL chloroform, sample was inverted 5-6 times and then centrifuged (12.000 xg, 15 min, 4°C). Samples should show a clear phase separation with a pink organic phase containing proteins, an interphase containing the DNA and a clear aqueous phase containing the RNA. 200 – 250 µL of the clear phase were transferred into a precooled 1.5 mL Eppendorf tube stored on ice. As RNA is no longer protected from degradation it was stored at -80°C until further processed.

Purified RNA was measured two times. First, a photometric measurement was performed with 2 µL RNA, diluted in 70 µL 10 mM Tris-buffer at wavelengths of 230 nm, 260 nm and 280nm. The 260/280 ratio should lay around 2. Differing numbers would indicate protein contamination. The 260/230 ratio should lay between 2.0 and 2.2. Lower values would indicate a phenol contamination.

If the photometric measurement was appropriate, samples were analyzed on the BioAnalyzer using the RNA 6000 Nano Kit to see whether the RNA was still intact. All steps were performed according to the manufacturer's manual.

7.2.3.1 Transient Transfection

Before **chemical transfection**, HEK 293 Mock cells were plated in the desired cell density onto Poly-D lysine-treated coverslips. The cells were incubated for 5-6 h under culture conditions to facilitate a sufficient cell attachment. One transfection approach (4 wells) consisted of 200 µL Opti-MEM™ (Cat-No.: 21985062 Gibco), 0.1 µg pEGFP-N1, 10 µg plasmid with nucleic acid of the respective sodium channel and 25 µg FuGENE® HD (Cat-No. E2311, Promega). In the case of co-transfections of α- and β-subunit, 5 µg of each was applied in the approach to reach a total of 10 µg of DNA. The approach was mixed and incubated for 10-15 min at 20 °C. Afterwards, 50 µL was transferred into each well. For human channels, the cells were stored under culture conditions of the HEK293 Mock cells, and cells expressing the insect channel were transferred to 26 °C after 12-16 h. After approximately 24 h, a GFP signal can be measured. However, electrophysiological measurements were performed after 36-72 h.

The day before **electroporation,** cells were passaged (HEK293: 1:2, CHO: 1:3) to obtain 80 – 90 % confluency on the day of the experiment. On the day of the experiment, 300 µg/mL f.c. DNA (start concentration >5µg/µL) was prepared in reaction tubes. The cells were detached with an accutase solution and the viability was determined. The required number of living cells was centrifuged (6 min at 120 xg) and washed with MaxCyte buffer. The cell pellet was then dissolved in 1/3 of the final

volume and filled to the reach a final concentration of 10^8 cells in MaxCyte buffer. The suitable amount was mixed with the DNA and transferred into the electroporation cuvette (max. volume/cuvette: 25/OC-3x25, 100/OC-100, 400/OC-400). The electroporation took place in the MaxCyteSTX using the suitable program (HEK293 or CHO) with the correct configuration. Cells were then transferred into sterile 6 well plates and mixed with 5 µL DNAse solution (1U/µL). After 30 min incubation at 37°C and 5 % CO_2, 1 mL Medium without antibiotics was added. After determining the viability and cell number, the cells were directly plated on 384 well plates (fluorescent measurements) or in 175 cm^2 flasks (for APC experiments) at the desired concentration. After 24 h – 48 h, the cells were measured or frozen for later experiments.

7.2.4 Whole-cell voltage clamp measurements

For all electrophysiological measurements, the electrodes were frequently chlorinated with Danklorix. After chlorination, the electrodes were rinsed in H2O. Manual patch clamp electrodes were chlorinated once in a month for 72h in the dark, while automated patch clamp electrodes were chlorinated for 10 min before each experiment.

7.2.4.1 Manual experiments

Whole-cell voltage-clamp recordings were performed as described elsewhere (Hamill et al. 1981).[303] The investigated cells were plated onto glass coverslips, previously coated with poly D-lysine (Kat-No.: A3890401, Gibco™). Cells expressing the Slo channel were incubated at 37 °C and 5 % CO_2 for at least 12 h to facilitate proper channel expression. Cells expressing the VSSC channel were incubated at 37 C and 5 % CO_2 for at least 12 h and then transferred to 26 °C and 5 % CO_2 for an additional 24 h to facilitate proper channel expression. The external bath contained Ringer's solution and the internal pipette solution KCl-Pip with defined Ca^{2+} concentrations for the Slo channel while containing a 2:1 mixture of CsF-Pip : CsCl-Pip for VSSC measurements. Compounds were applied using the U-tube reversed flow technique (Fenwick et al. 1982).[121] The test compounds were freshly diluted from a 10 mM stock solution in DMSO and diluted to the required concentrations in ringer's solution with 0.03 % pluronic and 0.05 % BSA. Currents were measured with the HEKA EPC 10 patch clamp amplifier (HEKA, Ludwigshafen, Germany). Current records were low-pass Bessel filtered at 3 kHz and digitized at a 10 kHz sample rate.

7.2.4.2 Automated experiments

Automated planar patch clamp measurements were performed with the SyncroPatch 384 (Nanion, Munich, Germany) in NPC-384 high-resistance chips (Nanion-Technologies, Cat-No. 221101). Before measurements, cells expressing the channel of interest were detached, incorporated in an external solution and transferred to the prechilled and shaking cell hotel (10°C and 200 rpm). Cell-catch was

performed with internal Slo 0 nM Ca^{2+} pipette solution for Slo measurements and internal VSSC pipette solution for VSSC measurements. Seal building was supported by applying a 40 µL Seal Enhancer externally. After 120 s, the Ca^{2+} concentration was adjusted to the desired concentration by changing the internal solution for Slo measurements, while the internal solution for VSSC experiments remained stable. The test compounds are freshly dissolved as a 10 mM stock solution in DMSO and diluted to the required concentrations in an external solution (f.c. DMSO 1%) with 0.03% Pluronic and 0.05% BSA (A9576-50ML) before the experiment. 60 s after the change of the internal solution, the compound is applied and evaluated 5 min at specific membrane potentials. Every 10 seconds, a ramp from -160 mV to 60 mV was recorded. The evaluation was done using the DataControl384 software (Nanion-Technologies, Munich). Discrimination of successful experiments was performed by adjustable quality control parameters (e.g., peak amplitude, seal resistance).

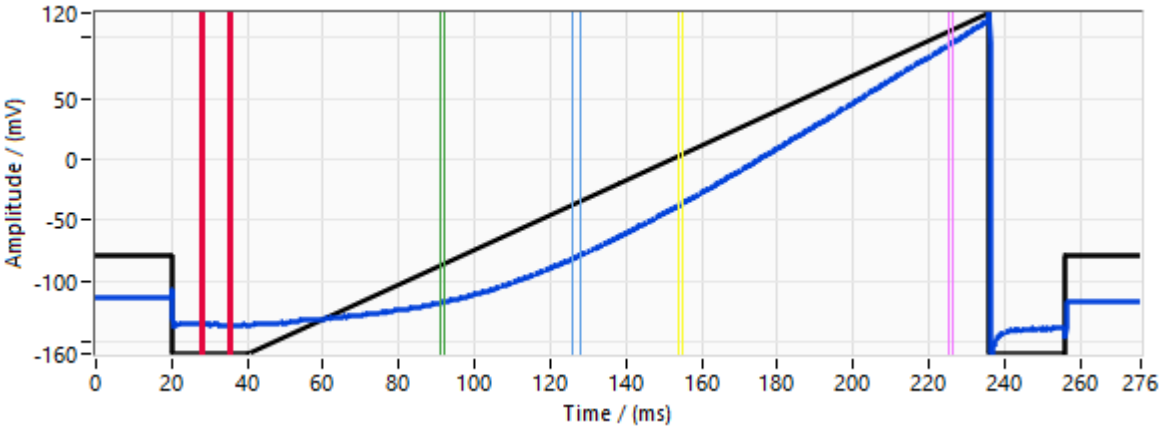

Figure 56 - Pulse protocol for automated patch clamp experiments at Slo channel
Pulse protocol for Slo measurement in automated patch clamp. The black graph shows the ramp from -160 mV to 60 mV recorded every 10 s. The blue trace shows a characteristic Slo control curve under high intracellular Ca^{2+}

7.2.5 High Throughput Fluorescence Measurements

7.2.5.1 FLIPR^{TETRA} Measurements

HEK cells stably expressing Musca VSSC and ChR2 T159C were plated on black-walled, poly-D-lysine, bottom µ-clear 384 well plates with a cell density of 40.000 cells/well (in assay medium: culture medium without selection markers). The plate stacks were cultured for 6 h at 37°C and 5 % CO_2 and then transferred for 18 h to 26 °C and 5% CO_2 for proper channel expression. The old medium was discarded and exchanged by loading buffer (20 µL/well). The plates were then for 1 h stored in the dark. On the one hand, ChR2 was excited (λ_{ex}: 470-495 nm; exp. time 0.4 s; intensity 30 %) and on the other hand, the fluorescence of the membrane potential sensitive dye was measured (λ_{ex}: 510-545 nm / λ_{em} 565-624 nm; exp. time 0.4 s; intensity 30 %) by the FLIPR^{TETRA} imager (Molecular Devices) every 5 s. Before compound application, the baseline was measured for 120 s. Subsequently, the

kinetic was measured for 10 min. All test compounds were diluted in DMSO from a 10 mM stock solution. In a second dilution step, the compounds dissolved in DMSO were transferred into the aqueous phase 2 : 80 (Dilution buffer: Tyrode, 0.03 % Pluronic). Finally, 5 µL was transferred onto the cells. The maximal response over baseline after seven minutes of compound application was normed to reference compound (*Musca domestica* VSSC and *Spodoptera* skdr VSSC) and Bayer Cpd 34 (human $Na_V1.7$) as 100 % and DMSO as 0 %. Curve fitting was calculated in either Excelfit or GraphPad Prism9.

7.2.5.2 HTS Measurements

The assay was performed on the plate butler system. HEK cells stably expressing Musca VSSC and ChR2 T159C were plated on black-walled, poly-D-lysine, bottom µ-clear 384 well plates with a cell density of 20.000 cells/well (in assay medium: culture medium without selection markers). The plate stacks were cultured for 6 h at 37°C and 5 % CO_2 and then transferred for 18 h to 26 °C and 5% CO_2 for proper channel expression. The medium was discarded in the BlueCat Washer (10 s, 800 rpm) and exchanged by 50 µL K_{10}-tyrode. After 120 min incubation at room temperature, the K_{10}-tyrode was removed and exchanged by 20 µL loading buffer. After 30 min incubation, the baseline fluorescence was measured over 120 s (λ_{ex}: 530 nm, λ_{em}: 575 nm, intensity 1 %; λ_{ex}: 530 nm, intensity 100 %, 90 ms, 0.1 Hz). The compound application was processed in the FELIX, where 5 µL compound diluted in K0-tyrode with 0.0015 % Pluronic (f.c. DMSO 1%) was transferred onto the cells. The final measurement was subsequently performed in the Assay Imager for 420 s (λ_{ex}: 530 nm, λ_{em}: 575 nm, intensity 1 %; λ_{ex}: 530 nm, intensity 100 %, 90 ms, 0.1 Hz). The area under the curve before and after the compound application was considered in relation to each other (main measurement / baseline measurement) and normed to reference compound (Musca domestica VSSC and Spodoptera skdr VSSC) as 200 % and DMSO as 100 %. Curve fitting was calculated in Tibco Spotfire.

7.2.6 Insect symptomatology

7.2.6.1 Injections Spodoptera frugiperda

For compound characterization, symptomatology and efficiency in *Spodoptera frugiperda* (strain Brasilia) were injected subcutaneously. The compounds were dissolved in either H_2O (toxins) or DMSO (small molecules), and 3 µL were injected laterally in the abdomen of L5 larvae with an approximate weight of 400mg (Hamilton 10 µL, 1701 RN, with a Gauge: 32, Length: 15-20mm needle). The symptoms were evaluated 1 h, 2 h, 4 h, 7 h, 24 h, 2 d, 3 d and 7d after injection by turning the larvae on their back under control conditions (DMSO) larvae turn back. The symptoms are characterized as follows:

7.2.6.2 In situ nerve recordings

An L5 larva of Spodoptera frugiperda was cut open lateral from the abdomen to the head for in situ nerve recording. The gut was carefully removed and the remaining tissue was stretched and fixated. The preparation is filled with saline II to prevent drying. The head and abdomen are cut off and a 2 cm long patch of the middle segment is fixated in the flow bath. The nerve, reaching from the ganglion over the trachea to the stretch receptor, is cleaned from the remaining tissues. The nerve is cut near the ganglion and sucked into the electrode. The preparation requires internal and external electrodes to reach the saline 2 solutions. As soon as a stable signal is recorded, the compound of interest is applied via the flow bath. Recorded are action potential amplitudes as well as action potential frequency.

8. References

(1) FAO, R. (Italy). P. P. and P. D. eng; (Italy), F. J. M. on the P. S. (JMPS) eng R.; WHO, G. (Switzerland) eng. Manual on Development and Use of FAO and WHO Specifications for Pesticides. Rome (Italy) FAO **2006**.

(2) Lowder, S. K.; Skoet, J.; Raney, T. The Number, Size, and Distribution of Farms, Smallholder Farms, and Family Farms Worldwide. *World Dev.* **2016**, *87*, 16–29. https://doi.org/https://doi.org/10.1016/j.worlddev.2015.10.041.

(3) OERKE, E.-C. Crop Losses to Pests. *J. Agric. Sci.* **2006**, *144* (1), 31–43. https://doi.org/DOI: 10.1017/S0021859605005708.

(4) Molden, D. A Comprehensive Assessment of Water Management in Agriculture. In *Water for Food Water for Life: A Comprehensive Assessment of Water Management in Agriculture*; **2007**; p 688. https://doi.org/https://doi.org/10.4324/9781849773799.

(5) Miflin, B. Crop Improvement in the 21st Century. *J. Exp. Bot.* **2000**, *51* (342), 1–8. https://doi.org/10.1093/jexbot/51.342.1.

(6) Insecticides Market Size, Share & Trends *Analysis Report By Type*; **2021**.

(7) Sparks, T. C.; Crossthwaite, A. J.; Nauen, R.; Banba, S.; Cordova, D.; Earley, F.; Ebbinghaus-Kintscher, U.; Fujioka, S.; Hirao, A.; Karmon, D.; et al. Insecticides, Biologics and Nematicides: Updates to IRAC's Mode of Action Classification - a Tool for Resistance Management. *Pestic. Biochem. Physiol.* **2020**, *167*, 104587. https://doi.org/https://doi.org/10.1016/j.pestbp.2020.104587.

(8) Sparks, T. C.; Nauen, R. IRAC: Mode of Action Classification and Insecticide Resistance Management. *Pestic. Biochem. Physiol.* **2015**, *121*, 122–128. https://doi.org/https://doi.org/10.1016/j.pestbp.2014.11.014.

(9) Melander, A. L. Can Insects Become Resistant to Sprays?1. *J. Econ. Entomol.* **1914**, *7* (2), 167–173. https://doi.org/10.1093/jee/7.2.167.

(10) Du, Y.; Garden, D. P.; Wang, L.; Zhorov, B. S.; Dong, K. Identification of New Batrachotoxin-Sensing Residues in Segment IIIS6 of the Sodium Channel. *J. Biol. Chem.* **2011**, *286* (15), 13151–13160. https://doi.org/10.1074/jbc.M110.208496.

(11) Rudy, B.; Iverson, L. E. *Ion Channels*; Ion Channels; Elsevier Science, **1997**.

(12) Zheng, J.; Trudeau, M. C. *Handbook of Ion Channels*; CRC Press, **2015**.

(13) Roux, B. Ion Channels and Ion Selectivity. *Essays Biochem.* **2017**, *61* (2), 201–209. https://doi.org/10.1042/EBC20160074.

(14) O'Rourke, B. Mitochondrial Ion Channels. *Annu. Rev. Physiol.* **2007**, *69* (1), 19–49. https://doi.org/10.1146/annurev.physiol.69.031905.163804.

(15) Gunner, M. R.; Amin, M.; Zhu, X.; Lu, J. Molecular Mechanisms for Generating Transmembrane Proton Gradients. *Biochim. Biophys. Acta* **2013**, *1827* (8–9), 892–913. https://doi.org/10.1016/j.bbabio.2013.03.001.

(16) Thakor, N. V. Biopotentials and Electrophysiology Measurement. In *Measurement, Instrumentation, and Sensors Handbook*; **2014**.

(17) Thompson, M. L.; Kateley, L. J. The Nernst Equation: Determination of Equilibrium Constants for Complex Ions of Silver. *J. Chem. Educ.* **1999**, *76* (1), 95. https://doi.org/10.1021/ed076p95.

(18) Feiner, A.-S.; McEvoy, A. J. The Nernst Equation. *J. Chem. Educ.* **1994**, *71* (6), 493. https://doi.org/10.1021/ed071p493.

(19) Hodkin, A. L.; Katz, B. The Effect of Sodium Ions on the Electrical Activity of Giant Axon of the Squid. *J. Physiol.* **1949**, *108* (1), 37–77. https://doi.org/10.1113/jphysiol.1949.sp004310.

(20) Goldman, D. E. Potential, Impedance, and Rectification in Membranes. *J. Gen. Physiol.* **1943**, *27* (1), 37–60. https://doi.org/10.1085/jgp.27.1.37.

(21) Eccles, J. C. The Ionic Mechanisms of Excitatory and Inhibitory Synaptic Action. *Ann. N. Y. Acad. Sci.* **1966**, *137* (2), 473–494. https://doi.org/10.1111/j.1749-6632.1966.tb50176.x.

(22) Barnett, M. W.; Larkman, P. M. The Action Potential. *Pract. Neurol.* **2007**, *7* (3), 192–197.

(23) Raghavan, M.; Fee, D.; Barkhaus, P. E. Generation and Propagation of the Action Potential. *Handb. Clin. Neurol.* **2019**, *160*, 3–22. https://doi.org/10.1016/B978-0-444-64032-1.00001-1.

(24) Frade, J. M.; Ovejero-Benito, M. C. Neuronal Cell Cycle: The Neuron Itself and Its Circumstances. *Cell Cycle* **2015**, *14* (5), 712–720. https://doi.org/10.1080/15384101.2015.1004937.

(25) Christensen, A. H.; Chatelain, F. C.; Huttner, I. G.; Olesen, M. S.; Soka, M.; Feliciangeli, S.; Horvat, C.; Santiago, C. F.; Vandenberg, J. I.; Schmitt, N.; et al. The Two-Pore Domain Potassium Channel, TWIK-1, Has a Role in the Regulation of Heart Rate and Atrial Size. *J. Mol. Cell. Cardiol.* **2016**, *97*, 24–35. https://doi.org/https://doi.org/10.1016/j.yjmcc.2016.04.006.

(26) Lesage, F.; Guillemare, E.; Fink, M.; Duprat, F.; Lazdunski, M.; Romey, G.; Barhanin, J. TWIK-1, a Ubiquitous Human Weakly Inward Rectifying K^+ Channel with a Novel Structure. *EMBO J.* **1996**, *15* (5), 1004–1011.

(27) Cosens, D. J.; Manning, A. Abnormal Electroretinogram from a Drosophila Mutant. *Nature* **1969**, *224* (5216), 285–287. https://doi.org/10.1038/224285a0.

(28) Walker, R. G.; Willingham, A. T.; Zuker, C. S. A Drosophila Mechanosensory Transduction Channel. *Science* **2000**,

287 (5461), 2229–2234. https://doi.org/10.1126/science.287.5461.2229.

(29) Caterina, M. J.; Rosen, T. A.; Tominaga, M.; Brake, A. J.; Julius, D. A Capsaicin-Receptor Homologue with a High Threshold for Noxious Heat. *Nature* **1999**, *398* (6726), 436–441. https://doi.org/10.1038/18906.

(30) Caterina, M. J.; Schumacher, M. A.; Tominaga, M.; Rosen, T. A.; Levine, J. D.; Julius, D. The Capsaicin Receptor: A Heat-Activated Ion Channel in the Pain Pathway. *Nature* **1997**, *389* (6653), 816–824. https://doi.org/10.1038/39807.

(31) Field, L. H.; Matheson, T. Chordotonal Organs of Insects. *Adv. In Insect Phys.* **1998**, *27*, 1–228.

(32) Unwin, N. Neurotransmitter Action: Opening of Ligand-Gated Ion Channels. *Cell* **1993**, *72*, 31–41. https://doi.org/https://doi.org/10.1016/S0092-8674(05)80026-1.

(33) Hucho, F.; Weise, C. Ligand-Gated Ion Channels. *Angew. Chemie Int. Ed.* **2001**, *40* (17), 3100–3116. https://doi.org/https://doi.org/10.1002/1521-3773(20010903)40:17<3100::AID-ANIE3100>3.0.CO;2-A.

(34) Hyman, S. E. Neurotransmitters. *Curr. Biol.* **2005**, *15* (5), R154–R158. https://doi.org/https://doi.org/10.1016/j.cub.2005.02.037.

(35) Simon-Delso, N.; Amaral-Rogers, V.; Belzunces, L. P.; Bonmatin, J. M.; Chagnon, M.; Downs, C.; Furlan, L.; Gibbons, D. W.; Giorio, C.; Girolami, V.; et al. Systemic Insecticides (Neonicotinoids and Fipronil): Trends, Uses, Mode of Action and Metabolites. *Environ. Sci. Pollut. Res.* **2015**, *22* (1), 5–34. https://doi.org/10.1007/s11356-014-3470-y.

(36) Strong, L.; Brown, T. A. Avermectins in Insect Control and Biology: A Review. *Bull. Entomol. Res.* **1987**, *77* (3), 357–389. https://doi.org/DOI: 10.1017/S0007485300011846.

(37) Lasota, J. A.; Dybas, R. A. Avermectins, A Novel Class of Compounds: Implications for Use in Arthropod Pest Control. *Annu. Rev. Entomol.* **1991**, *36* (1), 91–117. https://doi.org/10.1146/annurev.en.36.010191.000515.

(38) Matsuda, K.; Ihara, M.; Sattelle, D. B. Neonicotinoid Insecticides: Molecular Targets, Resistance, and Toxicity. *Annu. Rev. Pharmacol. Toxicol.* **2020**, *60* (1), 241–255. https://doi.org/10.1146/annurev-pharmtox-010818-021747.

(39) Catterall, W. A. Structure and Function of Voltage-Gated Ion Channels. *Annu. Rev. Biochem.* **1995**, *64* (1), 493–531. https://doi.org/10.1146/annurev.bi.64.070195.002425.

(40) Bezanilla, F. Voltage-Gated Ion Channels BT - Biological Membrane Ion Channels: Dynamics, Structure, and Applications; Chung, S.-H., Andersen, O. S., Krishnamurthy, V., Eds.; Springer New York: New York, NY, **2007**; pp 81–118. https://doi.org/10.1007/0-387-68919-2_3.

(41) de Lera Ruiz, M.; Kraus, R. L. Voltage-Gated Sodium Channels: Structure, Function, Pharmacology, and Clinical Indications. *J. Med. Chem.* **2015**, *58* (18), 7093–7118. https://doi.org/10.1021/jm501981g.

(42) Katz, E.; Stoler, O.; Scheller, A.; Khrapunsky, Y.; Goebbels, S.; Kirchhoff, F.; Gutnick, M. J.; Wolf, F.; Fleidervish, I. A. Role of Sodium Channel Subtype in Action Potential Generation by Neocortical Pyramidal Neurons. *Proc. Natl. Acad. Sci. U. S. A.* **2018**, *115* (30), E7184–E7192. https://doi.org/10.1073/pnas.1720493115.

(43) Jones, S. W. On the Resting Potential of Isolated Frog Sympathetic Neurons. *Neuron* **1989**, *3* (2), 153–161. https://doi.org/https://doi.org/10.1016/0896-6273(89)90028-7.

(44) Platkiewicz, J.; Brette, R. A Threshold Equation for Action Potential Initiation. *PLOS Comput. Biol.* **2010**, *6* (7), e1000850.

(45) Catterall, W. A. Forty Years of Sodium Channels: Structure, Function, Pharmacology, and Epilepsy. *Neurochem. Res.* **2017**, *42* (9), 2495–2504. https://doi.org/10.1007/s11064-017-2314-9.

(46) Noda, M.; Shimizu, S.; Tanabe, T.; Takai, T.; Kayano, T.; Ikeda, T.; Takahashi, H.; Nakayama, H.; Kanaoka, Y.; Minamino, N.; et al. Primary Structure of Electrophorus Electricus Sodium Channel Deduced from cDNA Sequence. *Nature* **1984**, *312* (5990), 121–127. https://doi.org/10.1038/312121a0.

(47) McCusker, E. C.; Bagnéris, C.; Naylor, C. E.; Cole, A. R.; D'Avanzo, N.; Nichols, C. G.; Wallace, B. A. Structure of a Bacterial Voltage-Gated Sodium Channel Pore Reveals Mechanisms of Opening and Closing. *Nat. Commun.* **2012**, *3*, 1102. https://doi.org/10.1038/ncomms2077.

(48) Shen, H.; Zhou, Q.; Pan, X.; Li, Z.; Wu, J.; Yan, N. Structure of a Eukaryotic Voltage-Gated Sodium Channel at near-Atomic Resolution. *Science* **2017**, *355* (6328). https://doi.org/10.1126/science.aal4326.

(49) Bosmans, F.; Swartz, K. J. Targeting Voltage Sensors in Sodium Channels with Spider Toxins. *Trends Pharmacol. Sci.* **2010**, *31* (4), 175–182. https://doi.org/https://doi.org/10.1016/j.tips.2009.12.007.

(50) Deuis, J.; Mueller, A.; Israel, M.; Vetter, I. The Pharmacology of Voltage-Gated Sodium Channel Activators. *Neuropharmacology* **2017**, *127*, 87–108. https://doi.org/10.1016/j.neuropharm.2017.04.014.

(51) Catterall, W. A. From Ionic Currents to Molecular Mechanisms: The Structure and Function of Voltage-Gated Sodium Channels. *Neuron* **2000**, *26* (1), 13–25. https://doi.org/10.1016/S0896-6273(00)81133-2.

(52) Meadows, L. S.; Isom, L. L. Sodium Channels as Macromolecular Complexes: Implications for Inherited Arrhythmia Syndromes. *Cardiovasc. Res.* **2005**, *67* (3), 448–458. https://doi.org/10.1016/j.cardiores.2005.04.003.

(53) O'Malley, H. A.; Isom, L. L. Sodium Channel β Subunits: Emerging Targets in Channelopathies. *Annu. Rev. Physiol.* **2015**, *77*, 481–504. https://doi.org/10.1146/annurev-physiol-021014-071846.

(54) Goldin, A. L.; Snutch, T.; Lübbert, H.; Dowsett, A.; Marshall, J.; Auld, V.; Downey, W.; Fritz, L. C.; Lester, H. A.; Dunn, R. Messenger RNA Coding for Only the Alpha Subunit of the Rat Brain Na Channel Is Sufficient for Expression of Functional Channels in Xenopus Oocytes. *Proc. Natl. Acad. Sci.* **1986**, *83* (19), 7503–7507. https://doi.org/10.1073/pnas.83.19.7503.

(55) Noda, M.; Ikeda, T.; Suzuki, H.; Takeshima, H.; Takahashi, T.; Kuno, M.; Numa, S. Expression of Functional Sodium Channels from Cloned cDNA. *Nature* **1986**, *322* (6082), 826–828. https://doi.org/10.1038/322826a0.

(56) Zybura, A.; Hudmon, A.; Cummins, T. R. Distinctive Properties and Powerful Neuromodulation of $Na_V1.6$ Sodium Channels Regulates Neuronal Excitability. *Cells*. **2021**. https://doi.org/10.3390/cells10071595.

(57) Schmalhofer, W. A.; Calhoun, J.; Burrows, R.; Bailey, T.; Kohler, M. G.; Weinglass, A. B.; Kaczorowski, G. J.; Garcia, M. L.; Koltzenburg, M.; Priest, B. T. ProTx-II, a Selective Inhibitor of $Na_V1.7$ Sodium Channels, Blocks Action Potential Propagation in Nociceptors. *Mol. Pharmacol.* **2008**, *74* (5), 1476 LP – 1484. https://doi.org/10.1124/mol.108.047670.

(58) Casida, J. E. Pyrethrum Flowers and Pyrethroid Insecticides. *Environ. Health Perspect.* **1980**, *34*, 189–202. https://doi.org/10.1289/ehp.8034189.

(59) Gordon, D.; Savarin, P.; Gurevitz, M.; Zinn-Justin, S. Functional Anatomy of Scorpion Toxins Affecting Sodium Channels. *J. Toxicol. Toxin Rev.* **1998**, *17* (2), 131–159. https://doi.org/10.3109/15569549809009247.

(60) Nicholson, G. M. Insect-Selective Spider Toxins Targeting Voltage-Gated Sodium Channels. *Toxicon* **2007**, *49* (4), 490–512. https://doi.org/10.1016/j.toxicon.2006.11.027.

(61) LaForge, F. B.; Barthel, W. F. Constituents of Pyrethrum Flowers; the Partial Synthesis of Pyrethrins and Cinerins and Their Relative Toxicities. *J. Org. Chem.* **1947**, *12* (1), 199–202. https://doi.org/10.1021/jo01165a024.

(62) Catterall, W. A. Structure and Function of Voltage-Sensitive Ion Channels. *Science (80-.).* **1988**, *242* (4875), 50–61. https://doi.org/10.1126/science.2459775.

(63) Soderlund, D. M.; Knipple, D. C. Actions of Insecticides on Sodium Channels. In *Molecular Action of Insecticides on Ion Channels*; ACS Symposium Series; American Chemical Society, **1995**; Vol. 591, pp 6–97. https://doi.org/doi:10.1021/bk-1995-0591.ch006.

(64) Lombet, A.; Mourre, C.; Lazdunski, M. Interaction of Insecticides of the Pyrethroid Family with Specific Binding Sites on the Voltage-Dependent Sodium Channel from Mammalian Brain. *Brain Res.* **1988**, *459* (1), 44–53. https://doi.org/10.1016/0006-8993(88)90284-3.

(65) Loughney, K.; Kreber, R.; Ganetzky, B. Molecular Analysis of the Para Locus, a Sodium Channel Gene in Drosophila. *Cell* **1989**, *58* (6), 1143–1154. https://doi.org/10.1016/0092-8674(89)90512-6.

(66) Thackeray, J. R.; Ganetzky, B. Developmentally Regulated Alternative Splicing Generates a Complex Array of Drosophila Para Sodium Channel Isoforms. *J. Neurosci. Off. J. Soc. Neurosci.* **1994**, *14* (5 Pt 1), 2569–2578. https://doi.org/10.1523/JNEUROSCI.14-05-02569.1994.

(67) Ganetzky, B. Neurogenetic Analysis of Drosophila Mutations Affecting Sodium Channels: Synergistic Effects on Viability and Nerve Conduction in Double Mutants Involving Tip-E. *J. Neurogenet.* **1986**, *3* (1), 19–31. https://doi.org/10.3109/01677068609106892.

(68) Feng, G.; Deák, P.; Chopra, M.; Hall, L. M. Cloning and Functional Analysis of TipE, a Novel Membrane Protein That Enhances Drosophila Para Sodium Channel Function. *Cell* **1995**, *82* (6), 1001–1011. https://doi.org/10.1016/0092-8674(95)90279-1.

(69) Olson, R. O.; Liu, Z.; Nomura, Y.; Song, W.; Dong, K. Molecular and Functional Characterization of Voltage-Gated Sodium Channel Variants from Drosophila Melanogaster. *Insect Biochem. Mol. Biol.* **2008**, *38* (5), 604–610. https://doi.org/https://doi.org/10.1016/j.ibmb.2008.01.003.

(70) Tan, J.; Liu, Z.; Nomura, Y.; Goldin, A. L.; Dong, K. Alternative Splicing of an Insect Sodium Channel Gene Generates Pharmacologically Distinct Sodium Channels. *J. Neurosci.* **2002**, *22* (13), 5300 LP – 5309. https://doi.org/10.1523/JNEUROSCI.22-13-05300.2002.

(71) Research, E. M. Global Pyrethroids Market Outlook. In *Global Pyrethroids Market*; **2022**.

(72) Davies, J. H. Pyrethroids: A Historical Introduction. *Pyrethroid insecticides / edited by John P. Leahey*. London : Taylor & Francis, c1985. **1985**.

(73) Narahashi, T. Mode of Action of Pyrethroids. *Bull. World Health Organ.* **1971**, *44* (1–3), 337–345.

(74) Davies, T. G. E.; Field, L. M.; Usherwood, P. N. R.; Williamson, M. S. DDT, Pyrethrins, Pyrethroids and Insect Sodium Channels. *IUBMB Life* **2007**, *59* (3), 151–162. https://doi.org/https://doi.org/10.1080/15216540701352042.

(75) Hu, Z.; Du, Y.; Nomura, Y.; Dong, K. A Sodium Channel Mutation Identified in Aedes Aegypti Selectively Reduces Cockroach Sodium Channel Sensitivity to Type I, but Not Type II Pyrethroids. *Insect Biochem. Mol. Biol.* **2011**, *41* (1), 9–13. https://doi.org/https://doi.org/10.1016/j.ibmb.2010.09.005.

(76) Soderlund, D. M. Molecular Mechanisms of Pyrethroid Insecticide Neurotoxicity: Recent Advances. *Arch. Toxicol.* **2012**, *86* (2), 165–181. https://doi.org/10.1007/s00204-011-0726-x.

(77) Domingues, L. N.; Guerrero, F. D.; Foil, L. D. Impacts of Long-Term Insecticide Treatment Regimes on Skdr and Kdr Pyrethroid Resistance Alleles in Horn Fly Field Populations. *Parasitol. Res.* **2019**, *118* (9), 2485–2497. https://doi.org/10.1007/s00436-019-06386-8.

(78) Comins, H. N. The Development of Insecticide Resistance in the Presence of Migration. *J. Theor. Biol.* **1977**, *64* (1), 177–197. https://doi.org/https://doi.org/10.1016/0022-5193(77)90119-9.

(79) Chang, C. P.; Plapp, F. W. DDT and Pyrethroids: Receptor Binding in Relation to Knockdown Resistance (Kdr) in the House Fly. *Pestic. Biochem. Physiol.* **1983**, *20* (1), 86–91. https://doi.org/https://doi.org/10.1016/0048-3575(83)90124-4.

(80) Milani, R. Mendelian Behavior of Resistance to the Knock-Down Action of DDT and Correlation between Knock-Down and Mortality in *Musca domestica* L. *Rend. Ist. Sup. Sanit.* **1956**, *19* (11), 1107–1143.

(81) Rinkevich, F. D.; Du, Y.; Dong, K. Diversity and Convergence of Sodium Channel Mutations Involved in Resistance to Pyrethroids. *Pestic. Biochem. Physiol.* **2013**, *106* (3), 93–100. https://doi.org/https://doi.org/10.1016/j.pestbp.2013.02.007.

(82) Burton, M. J.; Mellor, I. R.; Duce, I. R.; Davies, T. G. E.; Field, L. M.; Williamson, M. S. Differential Resistance of Insect Sodium Channels with Kdr Mutations to Deltamethrin, Permethrin and DDT. *Insect Biochem. Mol. Biol.* **2011**, *41* (9), 723–732. https://doi.org/https://doi.org/10.1016/j.ibmb.2011.05.004.

(83) Soderlund, D. M.; Knipple, D. C. The Molecular Biology of Knockdown Resistance to Pyrethroid Insecticides. *Insect Biochem. Mol. Biol.* **2003**, *33* (6), 563–577. https://doi.org/https://doi.org/10.1016/S0965-1748(03)00023-7.

(84) Soderlund, D. M.; Bloomquist, J. R.; Wong, F.; Payne, L. L.; Knipple, D. C. Molecular Neurobiology: Implications for Insecticide Action and Resistance. *Pestic. Sci.* **1989**, *26* (4), 359–374. https://doi.org/https://doi.org/10.1002/ps.2780260404.

(85) Williamson, M. S.; Martinez-Torres, D.; Hick, C. A.; Devonshire, A. L. Identification of Mutations in the Housefly Para-Type Sodium Channel Gene Associated with Knockdown Resistance (Kdr) to Pyrethroid Insecticides. *Mol. Gen. Genet.* **1996**, *252* (1–2), 51–60. https://doi.org/10.1007/BF02173204.

(86) Usherwood, P. N. R.; Vais, H.; Khambay, B. P. S.; Davies, T. G. E.; Williamson, M. S. Sensitivity of the Drosophila Para Sodium Channel to DDT Is Not Lowered by the Super-Kdr Mutation M918T on the IIS4–S5 Linker That Profoundly Reduces Sensitivity to Permethrin and Deltamethrin. *FEBS Lett.* **2005**, *579* (28), 6317–6325. https://doi.org/https://doi.org/10.1016/j.febslet.2005.09.096.

(87) Vais, H.; Williamson, M. S.; Goodson, S. J.; Devonshire, A. L.; Warmke, J. W.; Usherwood, P. N. R.; Cohen, C. J. Activation of Drosophila Sodium Channels Promotes Modification by Deltamethrin: Reductions in Affinity Caused by Knock-down Resistance Mutations. *J. Gen. Physiol.* **2000**, *115* (3), 305–318. https://doi.org/10.1085/jgp.115.3.305.

(88) Hyeock Lee, S.; Smith, T.; C. Knipple, D.; Soderlund, D. Mutations in the House Fly Vssc1 Sodium Channel Gene Associated with Super-Kdr Resistance Abolish the Pyrethroid Sensitivity of Vssc1/TipE Sodium Channels Expressed in Xenopus Oocytes. *Insect Biochem. Mol. Biol.* **1999**, *29* (2), 185–194. https://doi.org/https://doi.org/10.1016/S0965-1748(98)00122-2.

(89) Wing, K. D.; Sacher, M.; Kagaya, Y.; Tsurubuchi, Y.; Mulderig, L.; Connair, M.; Schnee, M. Bioactivation and Mode of Action of the Oxadiazine Indoxacarb in Insects. *Crop Prot.* **2000**, *19* (8), 537–545. https://doi.org/https://doi.org/10.1016/S0261-2194(00)00070-3.

(90) Gilbert, L. I.; Gill, S. S. *Insect Control: Biological and Synthetic Agents*; Elsevier Science, **2010**.

(91) Silver, K. S.; Song, W.; Nomura, Y.; Salgado, V. L.; Dong, K. Mechanism of Action of Sodium Channel Blocker Insecticides (SCBIs) on Insect Sodium Channels. *Pestic. Biochem. Physiol.* **2010**, *97* (2), 87–92. https://doi.org/https://doi.org/10.1016/j.pestbp.2009.09.001.

(92) Song, W.; Liu, Z.; Dong, K. Molecular Basis of Differential Sensitivity of Insect Sodium Channels to DCJW, a Bioactive Metabolite of the Oxadiazine Insecticide Indoxacarb. *Neurotoxicology* **2006**, *27* (2), 237–244. https://doi.org/https://doi.org/10.1016/j.neuro.2005.10.004.

(93) Wang, X.-L.; Su, W.; Zhang, J.-H.; Yang, Y.-H.; Dong, K.; Wu, Y.-D. Two Novel Sodium Channel Mutations Associated with Resistance to Indoxacarb and Metaflumizone in the Diamondback Moth, Plutella Xylostella. *Insect Sci.* **2016**, *23* (1), 50–58. https://doi.org/10.1111/1744-7917.12226.

(94) Shono, T.; Zhang, L.; Scott, J. G. Indoxacarb Resistance in the House Fly, Musca Domestica. *Pestic. Biochem. Physiol.* **2004**, *80* (2), 106–112. https://doi.org/https://doi.org/10.1016/j.pestbp.2004.06.004.

(95) Yu, F. H.; Catterall, W. A. Overview of the Voltage-Gated Sodium Channel Family. *Genome Biol.* **2003**, *4* (3), 207. https://doi.org/10.1186/gb-2003-4-3-207.

(96) Goldin, A. L. Resurgence of Sodium Channel Research. *Annu. Rev. Physiol.* **2001**, *63*, 871–894. https://doi.org/10.1146/annurev.physiol.63.1.871.

(97) Dib-Hajj, S.; Black, J. A.; Cummins, T. R.; Waxman, S. G. NaN/Na_V1.9: A Sodium Channel with Unique Properties. *Trends Neurosci.* **2002**, *25* (5), 253–259. https://doi.org/10.1016/s0166-2236(02)02150-1.

(98) Wang, D. W.; Yazawa, K.; Makita, N.; George Jr, A. L.; Bennett, P. B. Pharmacological Targeting of Long QT Mutant Sodium Channels. *J. Clin. Invest.* **1997**, *99* (7), 1714–1720. https://doi.org/10.1172/JCI119335.

(99) Emery, E. C.; Luiz, A. P.; Wood, J. N. Na_V1.7 and Other Voltage-Gated Sodium Channels as Drug Targets for Pain Relief. *Expert Opin. Ther. Targets* **2016**, *20* (8), 975–983. https://doi.org/10.1517/14728222.2016.1162295.

(100) Abdi, S.; Lee, D. H.; Chung, J. M. The Anti-Allodynic Effects of Amitriptyline, Gabapentin, and Lidocaine in a Rat Model of Neuropathic Pain. *Anesth. Analg.* **1998**, *87* (6).

(101) Ventham, N. T.; Kennedy, E. D.; Brady, R. R.; Paterson, H. M.; Speake, D.; Foo, I.; Fearon, K. C. H. Efficacy of Intravenous Lidocaine for Postoperative Analgesia Following Laparoscopic Surgery: A Meta-Analysis. *World J. Surg.* **2015**, *39* (9), 2220–2234. https://doi.org/10.1007/s00268-015-3105-6.

(102) Mao, J.; Chen, L. L. Systemic Lidocaine for Neuropathic Pain Relief. *Pain* **2000**, *87* (1), 7–17. https://doi.org/https://doi.org/10.1016/S0304-3959(00)00229-3.

(103) Dunn, L. K.; Durieux, M. E. Perioperative Use of Intravenous Lidocaine. *Anesthesiology* **2017**, *126* (4), 729–737. https://doi.org/10.1097/ALN.0000000000001527.

(104) Dailey, J. W.; Reith, M. E. A.; Yan, Q.-S.; Li, M.-Y.; Jobe, P. C. Anticonvulsant Doses of Carbamazepine Increase Hippocampal Extracellular Serotonin in Genetically Epilepsy-Prone Rats: Dose Response Relationships. *Neurosci. Lett.* **1997**, *227* (1), 13–16. https://doi.org/https://doi.org/10.1016/S0304-3940(97)00288-7.

(105) Bothe, S. N.; Lampert, A. The Insecticide Deltamethrin Enhances Sodium Channel Slow Inactivation of Human Na_V1.9, Na_V1.8 and Na_V1.7. *Toxicol. Appl. Pharmacol.* **2021**, *428*, 115676. https://doi.org/https://doi.org/10.1016/j.taap.2021.115676.

(106) Thull, S.; Neacsu, C.; O'Reilly, A. O.; Bothe, S.; Hausmann, R.; Huth, T.; Meents, J.; Lampert, A. Mechanism Underlying Hooked Resurgent-like Tail Currents Induced by an Insecticide in Human Cardiac Na_V1.5. *Toxicol. Appl. Pharmacol.* **2020**, *397*, 115010. https://doi.org/https://doi.org/10.1016/j.taap.2020.115010.

(107) Aldridge, W. N. An Assessment of the Toxicological Properties of Pyrethroids and Their Neurotoxicity. *Crit. Rev.*

Toxicol. **1990**, *21* (2), 89–104. https://doi.org/10.3109/10408449009089874.

(108) Soderlun, D. M.; Lee, S. H. Point Mutations in Homology Domain II Modify the Sensitivity of Rat Nav1.8 Sodium Channels to the Pyrethroid Insecticide Cismethrin. *Neurotoxicology* **2001**, *22* (6), 755–765. https://doi.org/10.1016/s0161-813x(01)00065-1.

(109) Smith, T. J.; Lee, S. H.; Ingles, P. J.; Knipple, D. C.; Soderlund, D. M. The L1014F Point Mutation in the House Fly VSSC1 Sodium Channel Confers Knockdown Resistance to Pyrethroids. *Insect Biochem. Mol. Biol.* **1997**, *27* (10), 807–812. https://doi.org/10.1016/s0965-1748(97)00065-9.

(110) Vais, H.; Williamson, M. S.; Devonshire, A. L.; Usherwood, P. N. The Molecular Interactions of Pyrethroid Insecticides with Insect and Mammalian Sodium Channels. *Pest Manag. Sci.* **2001**, *57* (10), 877–888. https://doi.org/10.1002/ps.392.

(111) Neher, E.; Sakmann, B. The Patch Clamp Technique. *Sci. Am.* **1992**, *266* (3), 44–51.

(112) Hodkin, A. L.; Huxley, A. F. Action Potentials Recorded from Inside a Nerve Fibre. *Nature* **1939**, *144* (3651), 710–711. https://doi.org/10.1038/144710a0.

(113) Hodgkin, A. L.; Huxley, A. F. Resting and Action Potentials in Single Nerve Fibres. *J. Physiol.* **1945**, *104* (2), 176–195. https://doi.org/10.1113/jphysiol.1945.sp004114.

(114) Hodkin, A. L.; Huxley, A. F. Propagation of Electrical Signals along Giant Nerve Fibers. *Proc. R. Soc. London. Ser. B, Biol. Sci.* **1952**, *140* (899), 177–183. https://doi.org/10.1098/rspb.1952.0054.

(115) Lynch, J. W.; Zhang, Y.; Talwar, S.; Estrada-Mondragon, A. Chapter Eight - Glycine Receptor Drug Discovery. In *Ion Channels DownUnder*; Geraghty, D. P., Rash, L. D. B. T.-A. in P., Eds.; Academic Press, 2017; Vol. 79, pp 225–253. https://doi.org/https://doi.org/10.1016/bs.apha.2017.01.003.

(116) Suchyna, T. M.; Markin, V. S.; Sachs, F. Biophysics and Structure of the Patch and the Gigaseal. *Biophys. J.* **2009**, *97* (3), 738–747. https://doi.org/https://doi.org/10.1016/j.bpj.2009.05.018.

(117) Cummins, T. R.; Rush, A. M.; Estacion, M.; Dib-Hajj, S. D.; Waxman, S. G. Voltage-Clamp and Current-Clamp Recordings from Mammalian DRG Neurons. *Nat. Protoc.* **2009**, *4* (8), 1103–1112. https://doi.org/10.1038/nprot.2009.91.

(118) Wood, C.; Williams, C.; Waldron, G. J. Patch Clamping by Numbers. *Drug Discov. Today* **2004**, *9* (10), 434–441. https://doi.org/https://doi.org/10.1016/S1359-6446(04)03064-8.

(119) Penner, R. A Practical Guide to Patch Clamping BT - Single-Channel Recording; Sakmann, B., Neher, E., Eds.; Springer US: Boston, MA, **1995**; pp 3–30. https://doi.org/10.1007/978-1-4419-1229-9_1.

(120) Levis, R. A.; Rae, J. L. B. T.-M. in E. [2] Constructing a Patch Clamp Setup. In *Ion Channels*; Academic Press, **1992,** Vol. 207, pp 14–66. https://doi.org/https://doi.org/10.1016/0076-6879(92)07004-8.

(121) Fenwick, E. M.; Marty, A.; Neher, E. A Patch-Clamp Study of Bovine Chromaffin Cells and of Their Sensitivity to Acetylcholine. *J. Physiol.* **1982**, *331*, 577–597. https://doi.org/10.1113/jphysiol.1982.sp014393.

(122) Kornreich, B. G. The Patch Clamp Technique: Principles and Technical Considerations. *J. Vet. Cardiol.* **2007**, *9* (1), 25–37. https://doi.org/https://doi.org/10.1016/j.jvc.2007.02.001.

(123) Perkins, K. L. Cell-Attached Voltage-Clamp and Current-Clamp Recording and Stimulation Techniques in Brain Slices. *J. Neurosci. Methods* **2006**, *154* (1), 1–18. https://doi.org/https://doi.org/10.1016/j.jneumeth.2006.02.010.

(124) Xiao, C.; Zhao, L.; Asada, T.; Odendaal, W. G.; Wyk, J. D. van. An Overview of Integratable Current Sensor Technologies. In *38th IAS Annual Meeting on Conference Record of the Industry Applications Conference, **2003**,* Vol. 2, pp 1251–1258 vol.2. https://doi.org/10.1109/IAS.2003.1257710.

(125) Halliwell, J. V; Plant, T. D.; Robbins, J.; Standen, N. B. Voltage Clamp Techniques. In *Microelectrode Techniques. The Plymouth Workshop Handbook*; The Company of Biologists, Ltd. Cambridge, **1994**; pp 17–35.

(126) Cahalan, M.; Neher, E. B. T.-M. in E. [1] Patch Clamp Techniques: An Overview. In *Ion Channels*; Academic Press, **1992**; Vol. 207, pp 3–14. https://doi.org/https://doi.org/10.1016/0076-6879(92)07003-7.

(127) Geiger, J.; Bischofberger, J.; Vida, I.; Fröbe, U.; Pfitzinger, S.; Weber, H.; Haverkampf, K.; Jonas, P. Patch-Clamp Recording in Brain Slices with Improved Slicer Technology. *Pflügers Arch.* **2002**, *443* (3), 491–501. https://doi.org/10.1007/s00424-001-0735-3.

(128) Sakmann, B. *Single-Channel Recording*; Springer Science & Business Media, **2013**.

(129) Hill, C. L.; Stephens, G. J. An Introduction to Patch Clamp Recording BT - Patch Clamp Electrophysiology: Methods and Protocols; Dallas, M., Bell, D., Eds.; Springer US: New York, NY, **2021**; pp 1–19. https://doi.org/10.1007/978-1-0716-0818-0_1.

(130) Aria, M. M. Chapter 2 - Principle of Whole-Cell Patch-Clamp and Its Applications in Neural Interface Studies; Aria, M. M. B. T.-E. M. for S. N. I., Ed.; Academic Press, **2020**; pp 25–63. https://doi.org/https://doi.org/10.1016/B978-0-12-817070-0.00002-6.

(131) Guan, B.; Chen, X.; Zhang, H. Two-Electrode Voltage Clamp BT - Ion Channels: Methods and Protocols; Gamper, N., Ed.; Humana Press: Totowa, NJ, **2013**; pp 79–89. https://doi.org/10.1007/978-1-62703-351-0_6.

(132) Mescon, H.; Grots, I. A. Fluorescence Microscopy in Dermatology. *J. Invest. Dermatol.* **1963**, *41*, 181–196. https://doi.org/10.1038/jid.1963.95.

(133) Stryer, L. Fluorescence Energy Transfer as a Spectroscopic Ruler. *Annu. Rev. Biochem.* **1978**, *47*, 819–846. https://doi.org/10.1146/annurev.bi.47.070178.004131.

(134) Gerdes, H.-H.; Kaether, C. Green Fluorescent Protein: Applications in Cell Biology. *FEBS Lett.* **1996**, *389* (1), 44–47. https://doi.org/https://doi.org/10.1016/0014-5793(96)00586-8.

(135) Eason, M. G.; Damry, A. M.; Chica, R. A. Structure-Guided Rational Design of Red Fluorescent Proteins: Towards Designer Genetically-Encoded Fluorophores. *Curr. Opin. Struct. Biol.* **2017**, *45*, 91–99.

https://doi.org/https://doi.org/10.1016/j.sbi.2016.12.001.

(136) Carlson, H. J.; Campbell, R. E. Genetically Encoded FRET-Based Biosensors for Multiparameter Fluorescence Imaging. *Curr. Opin. Biotechnol.* **2009**, *20* (1), 19–27. https://doi.org/https://doi.org/10.1016/j.copbio.2009.01.003.

(137) Ibrahim, S. F.; van den Engh, G. Flow Cytometry and Cell Sorting. *Adv. Biochem. Eng. Biotechnol.* **2007**, *106*, 19–39. https://doi.org/10.1007/10_2007_073.

(138) Weibrecht, I.; Leuchowius, K.-J.; Clausson, C.-M.; Conze, T.; Jarvius, M.; Howell, W. M.; Kamali-Moghaddam, M.; Söderberg, O. Proximity Ligation Assays: A Recent Addition to the Proteomics Toolbox. *Expert Rev. Proteomics* **2010**, *7* (3), 401–409. https://doi.org/10.1586/epr.10.10.

(139) Chilibeck, K. A.; Wu, T.; Liang, C.; Schellenberg, M. J.; Gesner, E. M.; Lynch, J. M.; MacMillan, A. M. FRET Analysis of *in Vivo* Dimerization by RNA-Editing Enzymes *. *J. Biol. Chem.* **2006**, *281* (24), 16530–16535. https://doi.org/10.1074/jbc.M511831200.

(140) Adams, G. A Beginner's Guide to RT-PCR, QPCR and RT-QPCR. *Biochem. (Lond).* **2020**, *42* (3), 48–53. https://doi.org/10.1042/BIO20200034.

(141) Shimada, Y.; Hirano, M.; Nishimura, Y.; Tanaka, T. A High-Throughput Fluorescence-Based Assay System for Appetite-Regulating Gene and Drug Screening. *PLoS One* **2012**, *7* (12), e52549.

(142) Martin, S.; Nongluk, S.; Xu, K. J.; Prapon, W.; Michael, R. Simple and Inexpensive Fluorescence-Based Technique for High-Throughput Antimalarial Drug Screening. *Antimicrob. Agents Chemother.* **2004**, *48* (5), 1803–1806. https://doi.org/10.1128/AAC.48.5.1803-1806.2004.

(143) Krutzik, P. O.; Nolan, G. P. Fluorescent Cell Barcoding in Flow Cytometry Allows High-Throughput Drug Screening and Signaling Profiling. *Nat. Methods* **2006**, *3* (5), 361–368. https://doi.org/10.1038/nmeth872.

(144) Gribbon, P.; Sewing, A. Fluorescence Readouts in HTS: No Gain without Pain? *Drug Discov. Today* **2003**, *8* (22), 1035–1043. https://doi.org/https://doi.org/10.1016/S1359-6446(03)02895-2.

(145) Griffiths, P. C.; Roe, J. A.; Bales, B. L.; Pitt, A. R.; Howe, A. M. Fluorescence Probe Studies of Gelatin−Sodium Dodecyl Sulfate Interactions. *Langmuir* **2000**, *16* (22), 8248–8254. https://doi.org/10.1021/la0001833.

(146) Gao, G.; Cao, Y.; Liu, W.; Li, D.; Zhou, W.; Liu, J. Fluorescent Sensors for Sodium Ions. *Anal. Methods* **2017**, *9* (38), 5570–5579. https://doi.org/10.1039/C7AY01708A.

(147) Tay, B.; Stewart, T. A.; Davis, F. M.; Deuis, J. R.; Vetter, I. Development of a High-Throughput Fluorescent No-Wash Sodium Influx Assay. *PLoS One* **2019**, *14* (3), e0213751.

(148) Wolff, C.; Fuks, B.; Chatelain, P. Comparative Study of Membrane Potential-Sensitive Fluorescent Probes and Their Use in Ion Channel Screening Assays. *J. Biomol. Screen.* **2003**, *8* (5), 533–543. https://doi.org/10.1177/1087057103257806.

(149) Baxter, D. F.; Kirk, M.; Garcia, A. F.; Raimondi, A.; Holmqvist, M. H.; Flint, K. K.; Bojanic, D.; Distefano, P. S.; Curtis, R.; Xie, Y. A Novel Membrane Potential-Sensitive Fluorescent Dye Improves Cell-Based Assays for Ion Channels. *J. Biomol. Screen.* **2002**, *7* (1), 79—85. https://doi.org/10.1177/108705710200700110.

(150) Agus, V.; Flak, T. A.; Picardi, P.; Pizzi, S.; Rutigliano, L.; Cainarca, S.; Redaelli, L.; Rolland, J.-F.; Scarabottolo, L. Parallel All-Optical Assay to Study Use-Dependent Functioning of Voltage-Gated Ion Channels in a Miniaturized Format. *SLAS Discov. Adv. Sci. Drug Discov.* **2021**, *26* (3), 460–469.

(151) Oviedo, N. J.; Nicolas, C. L.; Adams, D. S.; Levin, M. Live Imaging of Planarian Membrane Potential Using DiBAC4 (3). *Cold Spring Harb. Protoc.* **2008**, 2008 (10), pdb-prot5055.

(152) Whiteaker, K. L.; Gopalakrishnan, S. M.; Groebe, D.; Shieh, C. C.; Warrior, U.; Burns, D. J.; Coghlan, M. J.; Scott, V. E.; Gopalakrishnan, M. Validation of FLIPR Membrane Potential Dye for High Throughput Screening of Potassium Channel Modulators. *J. Biomol. Screen.* **2001**, *6* (5), 305–312. https://doi.org/10.1177/108705710100600504.

(153) Yu, H.; Li, M.; Wang, W.; Wang, X. High Throughput Screening Technologies for Ion Channels. *Acta Pharmacol. Sin.* **2016**, *37* (1), 34–43. https://doi.org/10.1038/aps.2015.108.

(154) Deisseroth, K.; Feng, G.; Majewska, A. K.; Miesenböck, G.; Ting, A.; Schnitzer, M. J. Next-Generation Optical Technologies for Illuminating Genetically Targeted Brain Circuits. In *Journal of Neuroscience*; **2006**. https://doi.org/10.1523/JNEUROSCI.3863-06.2006.

(155) Deisseroth, K. Optogenetics. *Nature Methods*. **2011**. https://doi.org/10.1038/nmeth.f.324.

(156) Miesenböck, G. The Optogenetic Catechism. *Science*. **2009**. https://doi.org/10.1126/science.1174520.

(157) Kaplan, J. H.; Somlyo, A. P. Flash Photolysis of Caged Compounds: New Tools for Cellular Physiology. *Trends Neurosci.* **1989**. https://doi.org/10.1016/0166-2236(89)90136-7.

(158) Ellis-Davies, G. C. R. Caged Compounds: Photorelease Technology for Control of Cellular Chemistry and Physiology. *Nature Methods*. **2007**. https://doi.org/10.1038/nmeth1072.

(159) Fishell, G.; Heintz, N. The Neuron Identity Problem: Form Meets Function. *Neuron*. **2013**. https://doi.org/10.1016/j.neuron.2013.10.035.

(160) Gong, S.; Zheng, C.; Doughty, M. L.; Losos, K.; Didkovsky, N.; Schambra, U. B.; Nowak, N. J.; Joyner, A.; Leblanc, G.; Hatten, M. E.; et al. A Gene Expression Atlas of the Central Nervous System Based on Bacterial Artificial Chromosomes. *Nature* **2003**. https://doi.org/10.1038/nature02033.

(161) Hawrylycz, M. J.; Lein, E. S.; Guillozet-Bongaarts, A. L.; Shen, E. H.; Ng, L.; Miller, J. A.; Van De Lagemaat, L. N.; Smith, K. A.; Ebbert, A.; Riley, Z. L.; et al. An Anatomically Comprehensive Atlas of the Adult Human Brain Transcriptome. *Nature* **2012**. https://doi.org/10.1038/nature11405.

(162) Boyden, E. S.; Zhang, F.; Bamberg, E.; Nagel, G.; Deisseroth, K. Millisecond-Timescale, Genetically Targeted Optical Control of Neural Activity. *Nat. Neurosci.* **2005**. https://doi.org/10.1038/nn1525.

(163) Schoenenberger, P.; Schärer, Y.-P. Z.; Oertner, T. G. Channelrhodopsin as a Tool to Investigate Synaptic

Transmission and Plasticity. *Exp. Physiol.* **2011**, *96* (1), 34–39. https://doi.org/https://doi.org/10.1113/expphysiol.2009.051219.

(164) Cardin, J. A.; Carlén, M.; Meletis, K.; Knoblich, U.; Zhang, F.; Deisseroth, K.; Tsai, L.-H.; Moore, C. I. Targeted Optogenetic Stimulation and Recording of Neurons in Vivo Using Cell-Type-Specific Expression of Channelrhodopsin-2. *Nat. Protoc.* **2010**, *5* (2), 247–254. https://doi.org/10.1038/nprot.2009.228.

(165) Madisen, L.; Mao, T.; Koch, H.; Zhuo, J.; Berenyi, A.; Fujisawa, S.; Hsu, Y.-W. A.; Garcia, A. J.; Gu, X.; Zanella, S.; et al. A Toolbox of Cre-Dependent Optogenetic Transgenic Mice for Light-Induced Activation and Silencing. *Nat. Neurosci.* **2012**, *15* (5), 793–802. https://doi.org/10.1038/nn.3078.

(166) Govorunova, E. G.; Sineshchekov, O. A.; Li, H.; Spudich, J. L. Microbial Rhodopsins: Diversity, Mechanisms, and Optogenetic Applications. *Annu. Rev. Biochem.* **2017**, *86* (1), 845–872. https://doi.org/10.1146/annurev-biochem-101910-144233.

(167) Boyden, E. S. A History of Optogenetics: The Development of Tools for Controlling Brain Circuits with Light. *F1000 Biology Reports*. **2011**. https://doi.org/10.3410/B3-11.

(168) Sharma, A. K.; Spudich, J. L.; Doolittle, W. F. Microbial Rhodopsins: Functional Versatility and Genetic Mobility. *Trends Microbiol.* **2006**, *14* (11), 463–469. https://doi.org/https://doi.org/10.1016/j.tim.2006.09.006.

(169) Hochbaum, D. R.; Zhao, Y.; Farhi, S. L.; Klapoetke, N.; Werley, C. A.; Kapoor, V.; Zou, P.; Kralj, J. M.; Maclaurin, D.; Smedemark-Margulies, N.; et al. All-Optical Electrophysiology in Mammalian Neurons Using Engineered Microbial Rhodopsins. *Nat. Methods* **2014**, *11* (8), 825–833. https://doi.org/10.1038/nmeth.3000.

(170) Spergel, D. J.; Krüth, U.; Hanley, D. F.; Sprengel, R.; Seeburg, P. H. GABA- and Glutamate-Activated Channels in Green Fluorescent Protein- Tagged Gonadotropin-Releasing Hormone Neurons in Transgenic Mice. *J. Neurosci.* **1999**. https://doi.org/10.1523/JNEUROSCI.19-06-02037.1999.

(171) Luo, L.; Callaway, E. M.; Svoboda, K. Genetic Dissection of Neural Circuits. *Neuron*. **2008**. https://doi.org/10.1016/j.neuron.2008.01.002.

(172) Zeng, H.; Madisen, L. Mouse Transgenic Approaches in Optogenetics. In *Progress in Brain Research*; **2012**. https://doi.org/10.1016/B978-0-444-59426-6.00010-0.

(173) Gong, S.; Doughty, M.; Harbaugh, C. R.; Cummins, A.; Hatten, M. E.; Heintz, N.; Gerfen, C. R. Targeting Cre Recombinase to Specific Neuron Populations with Bacterial Artificial Chromosome Constructs. *Journal of Neuroscience*. **2007**. https://doi.org/10.1523/JNEUROSCI.2707-07.2007.

(174) Madisen, L.; Garner, A. R.; Shimaoka, D.; Chuong, A. S.; Klapoetke, N. C.; Li, L.; van der Bourg, A.; Niino, Y.; Egolf, L.; Monetti, C.; et al. Transgenic Mice for Intersectional Targeting of Neural Sensors and Effectors with High Specificity and Performance. *Neuron* **2015**. https://doi.org/10.1016/j.neuron.2015.02.022.

(175) Li, Y. K. C. & D. Optogenetics: Basis Concepts and Their Development. In *Optogenetics Methods and Protocols*; **2016**; pp 1–17. https://doi.org/10.1007/978-1-4939-3512-3.

(176) Strotmann, R.; Schröck, K.; Böselt, I.; Stäubert, C.; Russ, A.; Schöneberg, T. Evolution of GPCR: Change and Continuity. *Mol. Cell. Endocrinol.* **2011**, *331* (2), 170–178. https://doi.org/10.1016/j.mce.2010.07.012.

(177) Möglich, A.; Yang, X.; Ayers, R. A.; Moffat, K. Structure and Function of Plant Photoreceptors. *Annu. Rev. Plant Biol.* **2010**, *61*, 21–47. https://doi.org/10.1146/annurev-arplant-042809-112259.

(178) Herrou, J.; Crosson, S. Function, Structure and Mechanism of Bacterial Photosensory LOV Proteins. *Nat. Rev. Microbiol.* **2011**, *9* (10), 713–723. https://doi.org/10.1038/nrmicro2622.

(179) Wu, Y. I.; Frey, D.; Lungu, O. I.; Jaehrig, A.; Schlichting, I.; Kuhlman, B.; Hahn, K. M. A Genetically Encoded Photoactivatable Rac Controls the Motility of Living Cells. *Nature* **2009**, *461* (7260), 104–108. https://doi.org/10.1038/nature08241.

(180) Möglich, A.; Ayers, R. A.; Moffat, K. Design and Signaling Mechanism of Light-Regulated Histidine Kinases. *J. Mol. Biol.* **2009**, *385* (5), 1433–1444. https://doi.org/10.1016/j.jmb.2008.12.017.

(181) Nagel, G.; Szellas, T.; Huhn, W.; Kateriya, S.; Adeishvili, N.; Berthold, P.; Ollig, D.; Hegemann, P.; Bamberg, E. Channelrhodopsin-2, a Directly Light-Gated Cation-Selective Membrane Channel. *Proc. Natl. Acad. Sci. U. S. A.* **2003**. https://doi.org/10.1073/pnas.1936192100.

(182) Gerwert, K. Channelrhodopsin Reveals Its Dark Secrets. *Science*. **2017**. https://doi.org/10.1126/science.aar2299.

(183) Volkov, O.; Kovalev, K.; Polovinkin, V.; Borshchevskiy, V.; Bamann, C.; Astashkin, R.; Marin, E.; Popov, A.; Balandin, T.; Willbold, D.; et al. Structural Insights into Ion Conduction by Channelrhodopsin 2. *Science (80-.).* **2017**, *358* (6366), eaan8862. https://doi.org/10.1126/science.aan8862.

(184) Pan, Z. H.; Ganjawala, T. H.; Lu, Q.; Ivanova, E.; Zhang, Z. ChR2 Mutants at L132 and T159 with Improved Operational Light Sensitivity for Vision Restoration. *PLoS One* **2014**. https://doi.org/10.1371/journal.pone.0098924.

(185) Fraietta, I.; Gasparri, F. The Development of High-Content Screening (HCS) Technology and Its Importance to Drug Discovery. *Expert Opin. Drug Discov.* **2016**, *11* (5), 501–514. https://doi.org/10.1517/17460441.2016.1165203.

(186) Hodkin, A. L.; Huxley, A. F. A Quantitative Description of Membrane Current and Its Application to Conduction and Excitation in Nerve. *J. Physiol.* **1952**, *117* (4), 500–544. https://doi.org/10.1113/jphysiol.1952.sp004764.

(187) Agnew, W. S.; Levinson, S. R.; Brabson, J. S.; Raftery, M. A. Purification of the Tetrodotoxin-Binding Component Associated with the Voltage-Sensitive Sodium Channel from Electrophorus Electricus Electroplax Membranes. *Proc. Natl. Acad. Sci. U. S. A.* **1978**, *75* (6), 2606–2610. https://doi.org/10.1073/pnas.75.6.2606.

(188) Rasmussen, L.; Tigabu, B.; White, E. L.; Bostwick, R.; Tower, N.; Bukreyev, A.; Rockx, B.; LeDuc, J. W.; Noah, J. W. Adapting High-Throughput Screening Methods and Assays for Biocontainment Laboratories. *Assay Drug Dev. Technol.* **2015**, *13* (1), 44–54. https://doi.org/10.1089/adt.2014.617.

(189) Riniker, S.; Wang, Y.; Jenkins, J. L.; Landrum, G. A. Using Information from Historical High-Throughput Screens to

Predict Active Compounds. *J. Chem. Inf. Model.* **2014**, *54* (7), 1880–1891. https://doi.org/10.1021/ci500190p.
(190) Zhang, Z.; Guan, N.; Li, T.; Mais, D. E.; Wang, M. Quality Control of Cell-Based High-Throughput Drug Screening. *Acta Pharm. Sin. B* **2012**, *2* (5), 429–438. https://doi.org/https://doi.org/10.1016/j.apsb.2012.03.006.
(191) Lipinski, C. A. Lead- and Drug-like Compounds: The Rule-of-Five Revolution. *Drug Discov. Today Technol.* **2004**, *1* (4), 337–341. https://doi.org/https://doi.org/10.1016/j.ddtec.2004.11.007.
(192) Chen, X.; Li, H.; Tian, L.; Li, Q.; Luo, J.; Zhang, Y. Analysis of the Physicochemical Properties of Acaricides Based on Lipinski's Rule of Five. *J. Comput. Biol.* **2020**, *27* (9), 1397–1406. https://doi.org/10.1089/cmb.2019.0323.
(193) Walters, W. P.; Namchuk, M. Designing Screens: How to Make Your Hits a Hit. *Nat. Rev. Drug Discov.* **2003**, *2* (4), 259–266. https://doi.org/10.1038/nrd1063.
(194) Soderlund, D. M. Pyrethroids, Knockdown Resistance and Sodium Channels. *Pest Manag. Sci.* **2008**, *64* (6), 610–616. https://doi.org/https://doi.org/10.1002/ps.1574.
(195) Brueggemann, A.; George, M.; Klau, M.; Beckler, M.; Steindl, J.; Behrends, J. C.; Fertig, N. Ion Channel Drug Discovery and Research: The Automated Nano-Patch-Clamp Technology. *Curr. Drug Discov. Technol.* **2004**, *1* (1), 91–96. https://doi.org/10.2174/1570163043484833.
(196) Sigworth, F. J. The Patch Clamp Is More Useful than Anyone Had Expected. *Fed. Proc.* **1986**, *45* (12), 2673–2677.
(197) Gilly, W. F.; Armstrong, C. M. Threshold Channels—a Novel Type of Sodium Channel in Squid Giant Axon. *Nature* **1984**, *309* (5967), 448–450. https://doi.org/10.1038/309448a0.
(198) Nirenberg, M. W. The Genetic Code. *Sci. Am.* **1963**, *208* (3), 80–95.
(199) Czech, A.; Fedyunin, I.; Zhang, G.; Ignatova, Z. Silent Mutations in Sight: Co-Variations in TRNA Abundance as a Key to Unravel Consequences of Silent Mutations. *Mol. BioSyst.* **2010**, *6* (10), 1767–1772. https://doi.org/10.1039/C004796C.
(200) Strauss, B. S. Hypermutability and Silent Mutations in Human Carcinogenesis. *Semin. Cancer Biol.* **1998**, *8* (6), 431–438. https://doi.org/10.1006/scbi.1998.0092.
(201) Stefl, S.; Nishi, H.; Petukh, M.; Panchenko, A. R.; Alexov, E. Molecular Mechanisms of Disease-Causing Missense Mutations. *J. Mol. Biol.* **2013**, *425* (21), 3919–3936. https://doi.org/https://doi.org/10.1016/j.jmb.2013.07.014.
(202) Blakeslee, A. F. Types of Mutations and Their Possible Significance in Evolution. *Am. Nat.* **1921**, *55* (638), 254–267.
(203) Auerbach, C. *Mutation Research: Problems, Results and Perspectives*; Springer, 2013.
(204) Bibb, J. A.; da Cruz e Silva F., E. Identification of Posttranslational Modification Sites by Site-Directed Mutagenesis BT - Regulatory Protein Modification: Techniques and Protocols; Hemmings, H. C., Ed.; Humana Press: Totowa, NJ, **1997**; pp 275–307. https://doi.org/10.1385/0-89603-415-1:275.
(205) Cane, D. E.; Shim, J. H.; Xue, Q.; Fitzsimons, B. C.; Hohn, T. M. Trichodiene Synthase. Identification of Active Site Residues by Site-Directed Mutagenesis. *Biochemistry* **1995**, *34* (8), 2480–2488. https://doi.org/10.1021/bi00008a011.
(206) Brodie, A.; Jelovac, D.; Sabnis, G.; Long, B.; Macedo, L.; Goloubeva, O. Model Systems: Mechanisms Involved in the Loss of Sensitivity to Letrozole. *J. Steroid Biochem. Mol. Biol.* **2005**, *95* (1), 41–48. https://doi.org/https://doi.org/10.1016/j.jsbmb.2005.04.026.
(207) Jacobson, K. A.; Hoffmann, C.; Kim, Y.-C.; Camaioni, E.; Nandanan, E.; Jang, S. Y.; Guo, D.; Ji, X.; Kügelgen, I. von; Moro, S.; et al. Chapter 10 Molecular Recognition in P2 Receptors: Ligand Development Aided by Molecular Modeling and Mutagenesis. In *Nucleotides and their Receptors in the Nervous System*; Illes, P., Zimmermann, H. B. T.-P. in B. R., Eds.; Elsevier, **1999**; Vol. 120, pp 119–132. https://doi.org/https://doi.org/10.1016/S0079-6123(08)63550-5.
(208) Betts, M. J.; Russell, R. B. Amino Acid Properties and Consequences of Substitutions. In *Bioinformatics for Geneticists*; **2003**; pp 289–316. https://doi.org/https://doi.org/10.1002/0470867302.ch14.
(209) White, M. M. Designer Channels: Site-Directed Mutagenesis as a Probe for Structural Features of Channels and Receptors. *Trends Neurosci.* **1985**, *8*, 364–368. https://doi.org/https://doi.org/10.1016/0166-2236(85)90124-9.
(210) Ahuja, S.; Mukund, S.; Deng, L.; Khakh, K.; Chang, E.; Ho, H.; Shriver, S.; Young, C.; Lin, S.; Johnson, J. P.; et al. Structural Basis of Nav1.7 Inhibition by an Isoform-Selective Small-Molecule Antagonist. *Science (80-.).* **2015**, *350* (6267), aac5464. https://doi.org/10.1126/science.aac5464.
(211) Göldel, B.; Lemic, D.; Bažok, R. Alternatives to Synthetic Insecticides in the Control of the Colorado Potato Beetle (*Leptinotarsa Decemlineata* Say) and Their Environmental Benefits. *Agriculture*. **2020**. https://doi.org/10.3390/agriculture10120611.
(212) Coetzee, M.; Fontenille, D. Advances in the Study of Anopheles Funestus, a Major Vector of Malaria in Africa. *Insect Biochem. Mol. Biol.* **2004**, *34* (7), 599–605. https://doi.org/https://doi.org/10.1016/j.ibmb.2004.03.012.
(213) Tay, W. T.; Meagher, R. L.; Czepak, C.; Groot, A. T. Spodoptera Frugiperda: Ecology, Evolution, and Management Options of an Invasive Species. *Annu. Rev. Entomol.* **2023**, *68* (1), 299–317. https://doi.org/10.1146/annurev-ento-120220-102548.
(214) Martinez-Torres, D.; Devonshire, A. L.; Williamson, M. S. Molecular Studies of Knockdown Resistance to Pyrethroids: Cloning of Domain II Sodium Channel Gene Sequences from Insects. *Pestic. Sci.* **1997**, *51* (3), 265–270. https://doi.org/https://doi.org/10.1002/(SICI)1096-9063(199711)51:3<265::AID-PS626>3.0.CO;2-P.
(215) Renaud, J.-P.; Chari, A.; Ciferri, C.; Liu, W.; Rémigy, H.-W.; Stark, H.; Wiesmann, C. Cryo-EM in Drug Discovery: Achievements, Limitations and Prospects. *Nat. Rev. Drug Discov.* **2018**, *17* (7), 471–492. https://doi.org/10.1038/nrd.2018.77.
(216) Cheng, Y. Single-Particle Cryo-EM—How Did It Get Here and Where Will It Go. *Science (80-.).* **2018**, *361* (6405), 876–880. https://doi.org/10.1126/science.aat4346.

(217) Gonoi, T.; Hille, B.; Catterall, W. A. Voltage Clamp Analysis of Sodium Channels in Normal and Scorpion Toxin-Resistant Neuroblastoma Cells. *J. Neurosci.* **1984**, *4* (11), 2836 LP – 2842. https://doi.org/10.1523/JNEUROSCI.04-11-02836.1984.

(218) Stühmer, W.; Conti, F.; Suzuki, H.; Wang, X.; Noda, M.; Yahagi, N.; Kubo, H.; Numa, S. Structural Parts Involved in Activation and Inactivation of the Sodium Channel. *Nature* **1989**, *339* (6226), 597–603.

(219) Berndt, A.; Schoenenberger, P.; Mattis, J.; Tye, K. M.; Deisseroth, K.; Hegemann, P.; Oertner, T. G. High-Efficiency Channelrhodopsins for Fast Neuronal Stimulation at Low Light Levels. *Proc. Natl. Acad. Sci. U. S. A.* **2011**, *108* (18), 7595–7600. https://doi.org/10.1073/pnas.1017210108.

(220) Zhu, G.; Zhang, Y.; Xu, H.; Jiang, C. Identification of Endogenous Outward Currents in the Human Embryonic Kidney (HEK 293) Cell Line. *J. Neurosci. Methods* **1998**, *81* (1), 73–83. https://doi.org/https://doi.org/10.1016/S0165-0270(98)00019-3.

(221) Agus, V.; Janovjak, H. Optogenetic Methods in Drug Screening: Technologies and Applications. *Curr. Opin. Biotechnol.* **2017**, *48*, 8–14. https://doi.org/https://doi.org/10.1016/j.copbio.2017.02.006.

(222) Zhang, H.; Cohen, A. E. Optogenetic Approaches to Drug Discovery in Neuroscience and Beyond. *Trends Biotechnol.* **2017**, *35* (7), 625–639. https://doi.org/https://doi.org/10.1016/j.tibtech.2017.04.002.

(223) Sawicki, R. M. Resistance to Pyrethroid Insecticides in Arthropods. *Prog. Pestic. Biochem. Toxicol.* **1985**.

(224) Martinez-Torres, D.; Chandre, F.; Williamson, M. S.; Darriet, F.; Bergé, J. B.; Devonshire, A. L.; Guillet, P.; Pasteur, N.; Pauron, D. Molecular Characterization of Pyrethroid Knockdown Resistance (Kdr) in the Major Malaria Vector Anopheles Gambiae s.S. *Insect Mol. Biol.* **1998**, *7* (2), 179–184. https://doi.org/10.1046/j.1365-2583.1998.72062.x.

(225) Li, G.; Woltz, R. L.; Wang, C.; Ren, L.; He, P.; Yu, S.; Liu, X.; Yarov-Yarovoy, V.; Hu, D.; Chiamvimonvat, N. Gating Properties of Mutant Sodium Channels and Responses to Sodium Current Inhibitors Predict Mexiletine-Sensitive Mutations of Long QT Syndrome 3. *Front. Pharmacol.* **2020**, *11*, 1182.

(226) Leipold, E.; Hansel, A.; Olivera, B. M.; Terlau, H.; Heinemann, S. H. Molecular Interaction of δ-Conotoxins with Voltage-Gated Sodium Channels. *FEBS Lett.* **2005**, *579* (18), 3881–3884. https://doi.org/https://doi.org/10.1016/j.febslet.2005.05.077.

(227) Benoit, E. [Mechanism of action of neurotoxins acting on the inactivation of voltage-gated sodium channels]. *C. R. Seances Soc. Biol. Fil.* **1998**, *192* (3), 409–436.

(228) Kirsch, G. E.; Skattebøl, A.; Possani, L. D.; Brown, A. M. Modification of Na Channel Gating by an Alpha Scorpion Toxin from Tityus Serrulatus. *J. Gen. Physiol.* **1989**, *93* (1), 67–83. https://doi.org/10.1085/jgp.93.1.67.

(229) Clairfeuille, T.; Cloake, A.; Infield, D. T.; Llongueras, J. P.; Arthur, C. P.; Li, Z. R.; Jian, Y.; Martin-Eauclaire, M.-F.; Bougis, P. E.; Ciferri, C.; et al. Structural Basis of α-Scorpion Toxin Action on Na(v) Channels. *Science* **2019**, *363* (6433). https://doi.org/10.1126/science.aav8573.

(230) Ekberg, J.; Craik, D. J.; Adams, D. J. Conotoxin Modulation of Voltage-Gated Sodium Channels. *Int. J. Biochem. Cell Biol.* **2008**, *40* (11), 2363–2368. https://doi.org/10.1016/j.biocel.2007.08.017.

(231) Wouters, W.; van den Bercken, J. Action of Pyrethroids. *Gen. Pharmacol.* **1978**, *9* (6), 387–398. https://doi.org/10.1016/0306-3623(78)90023-x.

(232) McCavera, S. J.; Soderlund, D. M. Differential State-Dependent Modification of Inactivation-Deficient Nav1.6 Sodium Channels by the Pyrethroid Insecticides S-Bioallethrin, Tefluthrin and Deltamethrin. *Neurotoxicology* **2012**, *33* (3), 384–390. https://doi.org/10.1016/j.neuro.2012.03.007.

(233) Soderlund, D. M. State-Dependent Modification of Voltage-Gated Sodium Channels by Pyrethroids. *Pestic. Biochem. Physiol.* **2010**, *97* (2), 78–86. https://doi.org/10.1016/j.pestbp.2009.06.010.

(234) Vijverberg, H. P.; van den Bercken, J. Frequency-Dependent Effects of the Pyrethroid Insecticide Decamethrin in Frog Myelinated Nerve Fibres. *Eur. J. Pharmacol.* **1979**, *58* (4), 501–504. https://doi.org/10.1016/0014-2999(79)90325-x.

(235) Zhorov, B. S.; Dong, K. Pyrethroids in an AlphaFold2 Model of the Insect Sodium Channel. *Insects* **2022**, *13* (8). https://doi.org/10.3390/insects13080745.

(236) Casida, J. E.; Gammon, D. W.; Glickman, A. H.; Lawrence, L. J. Mechanisms of Selective Action of Pyrethroid Insecticides. *Annu. Rev. Pharmacol. Toxicol.* **1983**, *23* (1), 413–438. https://doi.org/10.1146/annurev.pa.23.040183.002213.

(237) Smith, T. M.; Stratton, G. W. Effects of Synthetic Pyrethroid Insecticides on Nontarget Organisms BT - Residue Reviews; Gunther, F. A., Ed.; Springer New York: New York, NY, 1986; pp 93–120.

(238) Morandi, P.; Valzasina, B.; Colombo, C.; Curti, B.; Vanoni, M. A. Glutamate Synthase: Identification of the NADPH-Binding Site by Site-Directed Mutagenesis. *Biochemistry* **2000**, *39* (4), 727–735. https://doi.org/10.1021/bi9920329.

(239) Jamieson, K. V; Hubbard, S. R.; Meruelo, D. Structure-Guided Identification of a Laminin Binding Site on the Laminin Receptor Precursor. *J. Mol. Biol.* **2011**, *405* (1), 24–32. https://doi.org/10.1016/j.jmb.2010.10.028.

(240) Kuhlman, P. A.; Hemmings, L.; Critchley, D. R. The Identification and Characterisation of an Actin-Binding Site in Alpha-Actinin by Mutagenesis. *FEBS Lett.* **1992**, *304* (2–3), 201–206. https://doi.org/10.1016/0014-5793(92)80619-r.

(241) Ambert-Balay, K.; Fuchs, S. M.; Tien, M. Identification of the Veratryl Alcohol Binding Site in Lignin Peroxidase by Site-Directed Mutagenesis. *Biochem. Biophys. Res. Commun.* **1998**, *251* (1), 283–286. https://doi.org/10.1006/bbrc.1998.9454.

(242) Catterall, W. A.; Risk, M. Toxin T4(6) from Ptychodiscus Brevis (Formerly Gymnodinium Breve) Enhances Activation of Voltage-Sensitive Sodium Channels by Veratridine. *Mol. Pharmacol.* **1981**, *19* (2), 345–348.

(243) Campos, F. V; Chanda, B.; Beirão, P. S. L.; Bezanilla, F. Beta-Scorpion Toxin Modifies Gating Transitions in All Four Voltage Sensors of the Sodium Channel. *J. Gen. Physiol.* **2007**, *130* (3), 257–268. https://doi.org/10.1085/jgp.200609719.

(244) Zhang, J. H.; Chung, T. D.; Oldenburg, K. R. A Simple Statistical Parameter for Use in Evaluation and Validation of High Throughput Screening Assays. *J. Biomol. Screen.* **1999**, *4* (2), 67–73. https://doi.org/10.1177/108705719900400206.

(245) Srinivasan, S.; Schelhaas, B.; Maimon, B.; Song, H.; Herr, H. Retinal Supplementation Augments Optogenetic Stimulation Efficacy in Vivo. *J. Neural Eng.* **2019**, *16* (5), 54002. https://doi.org/10.1088/1741-2552/ab1e22.

(246) Nakanishi, K. Why 11-Cis-Retinal? *Am. Zool.* **1991**, *31* (3), 479–489.

(247) Granit, R.; Munsterhjelm, A.; Zewi, M. The Relation between Concentration of Visual Purple and Retinal Sensitivity to Light during Dark Adaptation. *J. Physiol.* **1939**, *96* (1), 31–44. https://doi.org/10.1113/jphysiol.1939.sp003755.

(248) An, W. F.; Tolliday, N. Cell-Based Assays for High-Throughput Screening. *Mol. Biotechnol.* **2010**, *45* (2), 180–186. https://doi.org/10.1007/s12033-010-9251-z.

(249) Bourque, K.; Jones-Tabah, J.; Mnasri, N.; Martin, R. D.; Hébert, T. E. Combining Optical Approaches with Human Inducible Pluripotent Stem Cells in G Protein-Coupled Receptor Drug Screening and Development. *Biomolecules* **2018**, *8* (4). https://doi.org/10.3390/biom8040180.

(250) Chunduri, V.; Maddi, S. Role of in Vitro Two-Dimensional (2D) and Three-Dimensional (3D) Cell Culture Systems for ADME-Tox Screening in Drug Discovery and Development: A Comprehensive Review. *ADMET DMPK* **2023**, *11* (1), 1–32. https://doi.org/10.5599/admet.1513.

(251) Potekhina, E. S.; Bass, D. Y.; Kelmanson, I. V; Fetisova, E. S.; Ivanenko, A. V; Belousov, V. V; Bilan, D. S. Drug Screening with Genetically Encoded Fluorescent Sensors: Today and Tomorrow. *Int. J. Mol. Sci.* **2020**, *22* (1). https://doi.org/10.3390/ijms22010148.

(252) Miller, C. An Overview of the Potassium Channel Family. *Genome Biol.* **2000**, *1* (4), reviews0004.1. https://doi.org/10.1186/gb-2000-1-4-reviews0004.

(253) Wiedmann, F.; Frey, N.; Schmidt, C. Two-Pore-Domain Potassium (K2P-) Channels: Cardiac Expression Patterns and Disease-Specific Remodelling Processes. *Cells*. 2021. https://doi.org/10.3390/cells10112914.

(254) Palti, Y.; Adelman, W. J. J. Measurement of Axonal Membrane Conductances and Capacity by Means of a Varying Potential Control Voltage Clamp. *J. Membr. Biol.* **1969**, *1* (1), 431–458. https://doi.org/10.1007/BF01869791.

(255) Chandler, W. K.; Meves, H. Slow Changes in Membrane Permeability and Long-Lasting Action Potentials in Axons Perfused with Fluoride Solutions. *J. Physiol.* **1970**, *211* (3), 707–728. https://doi.org/https://doi.org/10.1113/jphysiol.1970.sp009300.

(256) Sundberg, S. A. High-Throughput and Ultra-High-Throughput Screening: Solution- and Cell-Based Approaches. *Curr. Opin. Biotechnol.* **2000**, *11* (1), 47–53. https://doi.org/10.1016/s0958-1669(99)00051-8.

(257) Jager, S.; Brand, L.; Eggeling, C. New Fluorescence Techniques for High-Throughput Drug Discovery. *Current Pharmaceutical Biotechnology*. **2003**, pp 463–476. https://doi.org/http://dx.doi.org/10.2174/1389201033377382.

(258) Sun, Y.; Yu, H.; Zheng, D.; Cao, Q.; Wang, Y.; Harris, D.; Wang, Y. Sudan Black B Reduces Autofluorescence in Murine Renal Tissue. *Arch. Pathol. Lab. Med.* **2011**, *135* (10), 1335–1342. https://doi.org/10.5858/arpa.2010-0549-OA.

(259) Grimm, F.; Iwata, Y.; Sirenko, O.; Bittner, M.; Rusyn, I. High-Content Assay Multiplexing for Toxicity Screening in Induced Pluripotent Stem Cell-Derived Cardiomyocytes and Hepatocytes. *Assay Drug Dev. Technol.* **2015**, *13*. https://doi.org/10.1089/adt.2015.659.

(260) Billen, B.; Vassilevski, A.; Nikolsky, A.; Debaveye, S.; Tytgat, J.; Grishin, E. Unique Bell-Shaped Voltage-Dependent Modulation of Na^+ Channel Gating by Novel Insect-Selective Toxins from the Spider Agelena Orientalis. *J. Biol. Chem.* **2010**, *285* (24), 18545–18554. https://doi.org/10.1074/jbc.M110.125211.

(261) Katsuda, Y. Progress and Future of Pyrethroids. *Top. Curr. Chem.* **2012**, *314*, 1–30. https://doi.org/10.1007/128_2011_252.

(262) Coats, J. R. Structure-Activity Relationships among DDT Derivatives. *J. Environ. Sci. Heal. Part. B, Pestic. food Contam. Agric. wastes* **1983**, *18* (1), 173–188. https://doi.org/10.1080/03601238309372362.

(263) Matsuo, N. Discovery and Development of Pyrethroid Insecticides. *Proc. Jpn. Acad. Ser. B. Phys. Biol. Sci.* **2019**, *95* (7), 378–400. https://doi.org/10.2183/pjab.95.027.

(264) Wheeler, K. P.; Watt, D. D.; Lazdunski, M. Classification of Na Channel Receptors Specific for Various Scorpion Toxins. *Pflugers Arch.* **1983**, *397* (2), 164–165. https://doi.org/10.1007/BF00582058.

(265) Leipold, E.; Borges, A.; Heinemann, S. H. Scorpion β-Toxin Interference with NaV Channel Voltage Sensor Gives Rise to Excitatory and Depressant Modes. *J. Gen. Physiol.* **2012**, *139* (4), 305–319. https://doi.org/10.1085/jgp.201110720.

(266) González, C.; Baez-Nieto, D.; Valencia, I.; Oyarzún, I.; Rojas, P.; Naranjo, D.; Latorre, R. K^+ Channels: Function-Structural Overview. *Compr. Physiol.* **2012**, *2* (3), 2087–2149. https://doi.org/10.1002/cphy.c110047.

(267) Marmor, M. F. The Membrane of Giant Molluscan Neurons: Electrophysiologic Properties and the Origin of the Resting Potential. *Prog. Neurobiol.* **1975**, *5* (2), 167–195. https://doi.org/10.1016/0301-0082(75)90018-0.

(268) Bamann, C.; Kirsch, T.; Nagel, G.; Bamberg, E. Spectral Characteristics of the Photocycle of Channelrhodopsin-2 and Its Implication for Channel Function. *J. Mol. Biol.* **2008**, *375* (3), 686–694. https://doi.org/10.1016/j.jmb.2007.10.072.

(269) Atchison, W. D.; Luke, V. S.; Narahashi, T.; Vogel, S. M. Nerve Membrane Sodium Channels as the Target Site of Brevetoxins at Neuromuscular Junctions. *Br. J. Pharmacol.* **1986**, *89* (4), 731–738. https://doi.org/10.1111/j.1476-5381.1986.tb11177.x.

(270) Seitz, P. M.; Cooper, R.; Gatto, G. J. J.; Ramon, F.; Sweitzer, T. D.; Johns, D. G.; Davenport, E. A.; Ames, R. S.; Kallal, L. A. Development of a High-Throughput Cell-Based Assay for Superoxide Production in HL-60 Cells. *J. Biomol. Screen.* **2010**, *15* (4), 388–397. https://doi.org/10.1177/1087057109359687.

(271) Rotordam, M. G.; Obergrussberger, A.; Brinkwirth, N.; Takasuna, K.; Becker, N.; Horváth, A.; Goetze, T. A.; Rapedius, M.; Furukawa, H.; Hasegawa, Y.; et al. Reliable Identification of Cardiac Conduction Abnormalities in Drug Discovery Using Automated Patch Clamp II: Best Practices for Nav1.5 Peak Current in a High Throughput Screening Environment. *J. Pharmacol. Toxicol. Methods* **2021**, *112*, 107125. https://doi.org/10.1016/j.vascn.2021.107125.

(272) Smilkstein, M.; Sriwilaijaroen, N.; Kelly, J. X.; Wilairat, P.; Riscoe, M. Simple and Inexpensive Fluorescence-Based Technique for High-Throughput Antimalarial Drug Screening. *Antimicrob. Agents Chemother.* **2004**, *48* (5), 1803–1806. https://doi.org/10.1128/AAC.48.5.1803-1806.2004.

(273) Kaur, R.; Jain, R.; Budholiya, N.; Rathore, A. S. Long Term Culturing of CHO Cells: Phenotypic Drift and Quality Attributes of the Expressed Monoclonal Antibody. *Biotechnol. Lett.* **2023**, *45* (3), 357–370. https://doi.org/10.1007/s10529-023-03346-2.

(274) Yasumura, D.; Oshima, Y.; Yasumoto, T.; Alcala, A. C.; Alcala, L. C. Tetrodotoxin and Paralytic Shellfish Toxins in Philippine Crabs. *Agric. Biol. Chem.* **1986**, *50* (3), 593–598. https://doi.org/10.1080/00021369.1986.10867447.

(275) Zhang, H.; Reichert, E.; Cohen, A. E. Optical Electrophysiology for Probing Function and Pharmacology of Voltage-Gated Ion Channels. *Elife* **2016**, *5*, e15202. https://doi.org/10.7554/eLife.15202.

(276) Pavlov, E.; Bladen, C.; Winkfein, R.; Diao, C.; Dhaliwal, P.; French, R. J. The Pore, Not Cytoplasmic Domains, Underlies Inactivation in a Prokaryotic Sodium Channel. *Biophys. J.* **2005**, *89* (1), 232–242. https://doi.org/10.1529/biophysj.104.056994.

(277) Kadala, A.; Charreton, M.; Jakob, I.; Le Conte, Y.; Collet, C. A Use-Dependent Sodium Current Modification Induced by Type I Pyrethroid Insecticides in Honeybee Antennal Olfactory Receptor Neurons. *Neurotoxicology* **2011**, *32* (3), 320–330. https://doi.org/10.1016/j.neuro.2011.02.007.

(278) Ranson, H.; Jensen, B.; Vulule, J. M.; Wang, X.; Hemingway, J.; Collins, F. H. Identification of a Point Mutation in the Voltage-Gated Sodium Channel Gene of Kenyan Anopheles Gambiae Associated with Resistance to DDT and Pyrethroids. *Insect Mol. Biol.* **2000**, *9* (5), 491–497. https://doi.org/https://doi.org/10.1046/j.1365-2583.2000.00209.x.

(279) Silver, K. S.; Du, Y.; Nomura, Y.; Oliveira, E. E.; Salgado, V. L.; Zhorov, B. S.; Dong, K. Voltage-Gated Sodium Channels as Insecticide Targets. *Adv. In Insect Phys.* **2014**, *46*, 389–433. https://doi.org/10.1016/B978-0-12-417010-0.00005-7.

(280) Buczek, O.; Wei, D.; Babon, J. J.; Yang, X.; Fiedler, B.; Chen, P.; Yoshikami, D.; Olivera, B. M.; Bulaj, G.; Norton, R. S. Structure and Sodium Channel Activity of an Excitatory I1-Superfamily Conotoxin,. *Biochemistry* **2007**, *46* (35), 9929–9940. https://doi.org/10.1021/bi700797f.

(281) Zhang, J. Z.; Yarov-Yarovoy, V.; Scheuer, T.; Karbat, I.; Cohen, L.; Gordon, D.; Gurevitz, M.; Catterall, W. A. Structure-Function Map of the Receptor Site for β-Scorpion Toxins in Domain II of Voltage-Gated Sodium Channels. *J. Biol. Chem.* **2011**, *286* (38), 33641–33651. https://doi.org/10.1074/jbc.M111.282509.

(282) Yang, Z.-Y.; He, J.-H.; Lu, A.-P.; Hou, T.-J.; Cao, D.-S. Frequent Hitters: Nuisance Artifacts in High-Throughput Screening. *Drug Discov. Today* **2020**, *25* (4), 657–667. https://doi.org/https://doi.org/10.1016/j.drudis.2020.01.014.

(283) Carroll, S. S.; Inglese, J.; Mao, S.-S.; Olsen, D. B. Drug Screening: Assay Development Issues. In *Molecular Cancer Therapeutics*; **2004**; pp 119–140. https://doi.org/https://doi.org/10.1002/047165616X.ch7.

(284) Ramakrishna Seethala, L. Z. *Handbook of Drug Screening*, 2nd ed.; CRC Press, **2009**. https://doi.org/https://doi.org/10.3109/9781420061697.

(285) Zhang, J.; Yuan, H.; Yao, X.; Chen, S. Endogenous Ion Channels Expressed in Human Embryonic Kidney (HEK-293) Cells. *Pflugers Arch.* **2022**, *474* (7), 665–680. https://doi.org/10.1007/s00424-022-02700-z.

(286) Amar, M.; Pichon, Y.; Inoue, I. Patch-Clamp Analysis of the Effects of the Insecticide Deltamethrin on Insect Neurones. *J. Exp. Biol.* **1992**, *163*, 65–84. https://doi.org/10.1242/jeb.163.1.65.

(287) Ishibashi, H.; Moorhouse, A. J.; Nabekura, J. Perforated Whole-Cell Patch-Clamp Technique: A User's Guide. In *Patch Clamp Techniques: From Beginning to Advanced Protocols*; Okada, Y., Ed.; Springer Japan: Tokyo, **2012**; pp 71–83. https://doi.org/10.1007/978-4-431-53993-3_4.

(288) Linley, J. E. Perforated Whole-Cell Patch-Clamp Recording. In *Ion Channels: Methods and Protocols*; Gamper, N., Ed.; Humana Press: Totowa, NJ, **2013**; pp 149–157. https://doi.org/10.1007/978-1-62703-351-0_11.

(289) Gammon, D. W.; Brown, M. A.; Casida, J. E. Two Classes of Pyrethroid Action in the Cockroach. *Pestic. Biochem. Physiol.* **1981**, *15* (2), 181–191. https://doi.org/https://doi.org/10.1016/0048-3575(81)90084-5.

(290) Yamamoto, I. Mode of Action of Pyrethroids, Nicotinoids, and Rotenoids. *Annu. Rev. Entomol.* **1970**, *15* (1), 257–272. https://doi.org/10.1146/annurev.en.15.010170.001353.

(291) Couraud, F.; Jover, E.; Dubois, J. M.; Rochat, H. Two Types of Scorpion Toxin Receptor Sites, One Related to the Activation, the Other to the Inactivation of the Action Potential Sodium Channel. *Toxicon* **1982**, *20* (1), 9–16. https://doi.org/https://doi.org/10.1016/0041-0101(82)90138-6.

(292) Stankiewicz, M.; Dąbrowski, M.; de Lima, M. E. Nervous System of *Periplaneta Americana* Cockroach as a Model in Toxinological Studies: A Short Historical and Actual View. *J. Toxicol.* **2012**, 143740. https://doi.org/10.1155/2012/143740.

(293) Ayon, N. J. Features, Roles and Chiral Analyses of Proteinogenic Amino Acids. *AIMS Mol. Sci.* **2020**, *7* (3), 229–268.

https://doi.org/10.3934/molsci.2020011.

(294) Kim, T. K.; Eberwine, J. H. Mammalian Cell Transfection: The Present and the Future. *Anal. Bioanal. Chem.* **2010**, *397* (8), 3173–3178. https://doi.org/10.1007/s00216-010-3821-6.

(295) Raisch, T.; Brockmann, A.; Ebbinghaus-Kintscher, U.; Freigang, J.; Gutbrod, O.; Kubicek, J.; Maertens, B.; Hofnagel, O.; Raunser, S. Small Molecule Modulation of the Drosophila Slo Channel Elucidated by Cryo-EM. *Nat. Commun.* **2021**, *12* (1), 7164. https://doi.org/10.1038/s41467-021-27435-w.

(296) Crisford, A.; Ebbinghaus-Kintscher, U.; Schoenhense, E.; Harder, A.; Raming, K.; O'Kelly, I.; Ndukwe, K.; O'Connor, V.; Walker, R. J.; Holden-Dye, L. The Cyclooctadepsipeptide Anthelmintic Emodepside Differentially Modulates Nematode, Insect and Human Calcium-Activated Potassium (SLO) Channel Alpha Subunits. *PLoS Negl. Trop. Dis.* **2015**, *9* (10), e0004062. https://doi.org/10.1371/journal.pntd.0004062.

(297) Rothberg, B. S.; Bello, R. A.; Song, L.; Magleby, K. L. High Ca^{2+} Concentrations Induce a Low Activity Mode and Reveal Ca^{2+}-Independent Long Shut Intervals in BK Channels from Rat Muscle. *J. Physiol.* **1996**, *493* (3), 673–689. https://doi.org/https://doi.org/10.1113/jphysiol.1996.sp021414.

(298) Kashyap, S. S.; Verma, S.; Voronin, D.; Lustigman, S.; Kulke, D.; Robertson, A. P.; Martin, R. J. Emodepside Has Sex-Dependent Immobilizing Effects on Adult Brugia Malayi Due to a Differentially Spliced Binding Pocket in the RCK1 Region of the SLO-1 K Channel. *PLoS Pathog.* **2019**, *15* (9), e1008041. https://doi.org/10.1371/journal.ppat.1008041.

(299) Hübner, M. P.; Townson, S.; Gokool, S.; Tagboto, S.; Maclean, M. J.; Verocai, G. G.; Wolstenholme, A. J.; Frohberger, S. J.; Hoerauf, A.; Specht, S.; et al. Evaluation of the in Vitro Susceptibility of Various Filarial Nematodes to Emodepside. *Int. J. Parasitol. Drugs Drug Resist.* **2021**, *17*, 27–35. https://doi.org/https://doi.org/10.1016/j.ijpddr.2021.07.005.

(300) Gordon, E.; Semus, S. F.; Lozinskaya, I. M.; Lin, Z.; Xu, X. Characterizing the Role of T352 in the Inhibition of the Large Conductance Ca^{2+}-Activated (BK) Channels by 1-[1-Hexyl-6-(Methyloxy)-1H-Indazol-3-Yl]-2-Methyl-1-Propanone (HMIMP). *J. Pharmacol. Exp. Ther.* **2010**, jpet.110.166017. https://doi.org/10.1124/jpet.110.166017.

(301) Sansom, M. S. P.; Bond, P.; Beckstein, O.; Biggin, P. C.; Faraldo-Gómez, J.; Law, R. J.; Patargias, G.; Tieleman, D. P. Water in Ion Channels and Pores—Simulation Studies. In *Ion Channels: From Atomic Resolution Physiology to Functional Genomics*; Novartis Foundation Symposia; **2002**; pp 66–83. https://doi.org/https://doi.org/10.1002/0470868759.ch6.

(302) Corry, B.; Chung, S.-H. Mechanisms of Valence Selectivity in Biological Ion Channels. *Cell. Mol. Life Sci. C.* **2006**, *63* (3), 301–315. https://doi.org/10.1007/s00018-005-5405-8.

(303) Hamill, O.; Marty, A.; Neher, E.; Sakmann, B.; Sigworth, F. Hamill, O.P., Marty, A., Neher, E., Sakmann, B. & Sigworth, F.J. Improved Patch-Clamp Technique for High-Resolution Current Recording from Cells and Cell-Free Membrane Patches. Pfl??Gers Arch. Eur. J. Physiol. 391, 85-100. *Pflugers Arch.* **1981**, *391*, 85–100. https://doi.org/10.1007/BF00656997.

9. Acknowledgement

For a young researcher, the decision to write a Ph.D. thesis is very important and influences not just their life but also friends, colleagues and family. In the following, I want to thank all my supporters and those who shared this important time of my life.

First, I would like to thank Bayer AG for sponsoring my research. Besides my salary, they provided me with all the cutting-edge technologies and tools required for my thesis. Furthermore, they shared their knowledge and expertise with me.

I would like to thank Ulrich (Bayer AG) for the opportunity to do my Ph.D. in his lab and for his project engagement. Under his supervision, we tackled the important questions on VSSC pesticides. Besides his background knowledge of insecticides and drug discovery, he shared his insights into industrial research with me. Furthermore, I would like to thank Anke for taking the same position on the academic side. The uncomplicated interaction and her engagement in the organizational hurdles facilitated me to concentrate on my research thoroughly.

I want to thank my colleagues from Bayer AG for supporting me during my work in the lab of MoA classification. Annette introduced me to the manual patch clamp experiments, Tanja for the introduction to automated patch clamp, Claudia for supporting the FLIPR measurements and Edith for showing and supporting me with the symptomatology. Finally, I would like to thank all four for the friendly and welcoming team environment and the stimulating lunch breaks.

Several people contributed to the success of this thesis. I want to thank Tobias and Stefan from the MPI and Jörg and Oliver from Bayer Crop Science for supporting us with the Slo cryo-EM structure. Melanie and Alexander supported this thesis with their expertise in high throughput screenings and chemistry. Their contribution made a well-functioning team for our screening campaign. Furthermore, I want to thank Katharina, Jürgen and Klaus for allowing me to write my thesis at Bayer Crop Science.

Special thanks go to my family, not just for my Ph.D. or academic career but also for supporting me through the whole 27 years. My mother, father, brother and sister always listened to the numerous complaints and problems throughout the whole time and my nieces gave me the energy and made me aware of what is essential in life.

I want to thank my friends for balancing my free time and showing understanding in rough times. Carsten, Dominik, Flora, Hanna, Jana, Jil, Karen, Leon, Lucas, Max, Simon and Steffen nevertheless let me step back from work when I recognized I was getting lost in work. A special thanks go to Suse for supporting me during the rough time and helping me to stay focused.

10. Abbreviations

ADME – acronym for the pharmacokinetic parameters: absorption, distribution, metabolism and excretion
Cpd – Compound

CRC – concentration response curve

Cryo-EM – cryogenic electron microscopy
DRC – dose response curve

Effect – the impact a certain modulator has on a channel (e.g. voltage shift, tail current and inhibition of inactivation)
FCS – fetal calf serum

HPLC – High pressure liguid chromatograpy

KI – potassium ionophor

MoA – Mode of action, as characterized by the IRAC. Mediated by a certain compound class, at a distinct binding site.
MPDye – membrane potential sensitive dye

Na_V/VSSC – voltage sensitive sodium channel
PD – pore-domain
RoB – Response over baseline

SPA – single particle analysis
VSD – voltage sensor domain
VSSC – voltage sensitive sodium channel